KAPOSI'S SARCOMA-ASSOCIATED HERPESVIRUS PROTEIN, KAPOSIN B INDUCES THE SELECTIVE CATABOLISM OF PROCESSING BODIES

by

Gillian K. Singh

Submitted in partial fulfilment of the requirements
for the degree of Master of Science

at

Dalhousie University
Halifax, Nova Scotia
August 2019

Table of Contents

List of Tables

List of Figures

Abstract

Kaposi's sarcoma-associated herpesvirus (KSHV) is the causative agent of the inflammatory endothelial cell (EC) cancer, Kaposi's Sarcoma (KS). Many inflammatory mRNAs (ARE-mRNAs) are subject to constitutive decay in cytoplasmic ribonucleoprotein granules called processing bodies (PB). The viral protein KapB contributes to this inflammatory phenotype by inducing PB disassembly and a correlative increase in ARE-mRNA stabilization. However, the precise molecular mechanism governing KapB-mediated PB disassembly is unclear. My research uncovered a novel link between selective autophagy (SA) and PB disassembly. During SA, molecular-adaptor proteins, such as NDP52, selectively bind and target cargo for degradation. I found that KapB-mediated PB disassembly and stabilization of a reporter ARE-mRNA requires NDP52. Moreover, overexpression of authentic NDP52, but not mutated NDP52, rescued KapB-mediated PB disassembly in the context of NDP52 knockdown. Collectively, these data suggest KapB hijacks SA machinery to disassemble PBs, thus contributing to the proinflammatory environment beneficial for tumourigenesis.

.

List of Abbreviations Used

3’-UTR	3’ Untranslated region
AIDS	Acquired Immunodeficiency Syndrome
ANOVA	Analysis of variance
AP1	Activator protein 1
ARE	AU-rich element
Atg	Autophagy-related
Bp	Base pairs
Bsd	Blasticidin
cART	Combined antiretroviral therapy
CCL	CC-Chemokine ligand
CDS	Coding sequence
CLIR	Non-canonical LC3-interacting regions
COX-2	Cyclooxygenase-2
CXCL8	C-X-C Motif Chemokine Ligand 8
DAPI	4',6-diamidino-2-phenylindole, dihydrochloride
DMEM	Dulbecco’s minimal essential medium
DOX	Doxycycline
DR	Direct repeats
DTT	1,4-Dithiothreitol
EBM-2	Endothelial Cell Growth Basal Medium-2
EC	Endothelial cell
EDTA	Ethylenediaminetetraacetic acid
eGFP	Enhanced green fluorescent protein

EGM-2	Endothelial Cell Growth Medium-2
em.	Emission
ER	Endoplasmic reticulum
ex.	Excitation
FBS	Fetal bovine serum
FLICE	Fas-associated protein with death domain-like interleukin-1β-converting enzyme
FLIP	FLICE inhibitory protein
FRAP	Fluorescence recovery after photobleaching
FSC	Forward Scatter
GALB	Galectin-8 binding domain
GFP	Green fluorescent protein
GM-CSF	Granulocyte-macrophage colony-stimulating factor
GTPase	Guanosine triphosphatase
HEK	Human embryonic kidney
HEPES	4-(2-hydroxyethyl)-1-piperazineethanesulfonic acid
HI-FBS	Heat-inactivated FBS
HIV	Human immunodeficiency virus
HRP	Horseradish peroxidase
HSP27	Heat shock protein 27
HUR	Human antigen R
HUVEC	Human umbilical vein endothelial cells
IE	Immediate Early
IFN-γ	Interferon-gamma

IL-1α, β, -6	Interleukin-1 alpha, -1 beta, -6
JAK-STAT	Janus Kinase-Signal Transducer and Activator of Transcription
Kap	Kaposin
KS	Kaposi's sarcoma
KSHV	Kaposi's sarcoma-associated herpesvirus
LANA	Latency-associated nuclear antigen
LC3	Microtubule-associated protein 1A/1B-light chain 3
LIR	LC3-interacting region
LPS	Lipopolysaccharide
LTR	Long terminal repeat
MAPK	Mitogen-activated protein kinase
MCD	Multicentric Castleman's disease
mCh	Monomeric Cherry
MCP-1	Monocyte chemotactic protein-1
miRNA	MicroRNA
MK2	MAPK-associated protein kinase 2
NBR1	Next to BRCA1 gene 1 protein
NDP52	Nuclear dot protein 52
NFAT	Nuclear factor of activated T-cells
NF-κβ	Nuclear factor kappa-light-chain-enhancer of activated B cells
NRF2	Nuclear factor erythroid 2-related factor 2
O/N	Over night
OPTN	Optineurin

ORF	Open reading frame
PAGE	Polyacrylamide gel electrophoresis
PB	Processing body
PB1	Phox and Bem1
PBS	Phosphate-buffered saline
PCR	Polymerase chain reaction
PE	Phosphatidylethanolamine
PEI	Polyethylenimine
PEL	Primary effusion lymphoma
PES	Polyethersulfone
PI3K	Phosphoinositide 3-kinase
PIP3	Phosphatidylinositol (3,4,5)-trisphosphate
PKC	Protein kinase C
PSQ	Penicillin/streptomycin/glutamine
Puro	Puromycin
qPCR	Quantitative PCR
RFP	Red fluorescent protein
RhoA	Ras homolog gene family, member A
RNP	Ribonucleoprotein
ROCK	Rho-associated protein kinase
RT	Room temperature
RTA	Replication and transcription activator
SDS	Sodium dodecyl sulfate

SG	Stress granule
shRNA	Short hairpin RNA
SKICH	SKI-interacting protein (SKIP) carboxyl homology
SSC	Side scatter
TBS-T	Tris-buffered saline/Tween-20
TFEB	Transcription factor EB
TGF-β	Transforming growth factor-beta
TGN	*Trans*-Golgi network
TNF	Tumour necrosis factor
TRE	Tetracycline-responsive element
TTP	Tristetraprolin
UBD	Ubiquitin binding domain
ULK	Unc-51 Like Autophagy Activating Kinase 1
VCP	Valosin containing protein
vCyclin	Viral cyclin
VEGF	Vascular endothelial growth factor
vFLIP	Viral FLICE-inhibitory protein
vGPCR	Viral G protein-coupled receptors
vIL-6	Viral IL-6
WGA	Wheat germ agglutinin

Acknowledgements

I have been very fortunate to be surrounded by many friends, colleagues, and mentors, who have made my time at Dalhousie University so enjoyable and supported me through the highs and lows of completing my master's degree. Words cannot adequately express my gratitude to these individuals.

I could not have asked for a better mentor than Dr. Jennifer Corcoran. She has set a high and perhaps unsurmountable bar for all my future supervisors. Her unwavering commitment to the betterment of her students from near or far has taught me to turn challenges into opportunities and to have confidence in my abilities. Thank you for teaching me to appreciate the puzzle despite not having all the pieces.

I would like to express my great appreciation for my co-supervisor, Dr. Craig McCormick. Thank you for the support, opportunities, inclusion and infectious passion for science you and your lab members have provided, especially over the past year.

To my committee members; Dr. Jean Marshall and Dr. Thomas Pulinilkunnil, I would like to offer my special thanks for your guidance and knowledge. I have been lucky to have such a thoughtful and astute committee throughout my degree.

My sincere thank you to all members of the Corcoran-Weeks lab group and Microbiology Department members, especially Kathleen, Grant, Jamie, Chris, Beth, Eric and Carolyn for your friendship, advice and many laughs.

Lastly, I would like to thank my family and Jonnie for their endless encouragement and love. You have always inspired me to dream big, work hard and enjoy life to the fullest.

.

Chapter 1 Introduction

1.1 Kaposi's Sarcoma

Kaposi's sarcoma-associated herpesvirus (KSHV) is a γ-herpesvirus that causes rare neoplastic disease. KSHV is the etiological agent of the endothelial cell cancer, Kaposi's sarcoma (KS) (Ethel Cesarman, Chang, Moore, Said, & Knowles, 1995; Y. Chang et al., 1994; Soulier et al., 1995). KS is not a true sarcoma (derived from mesenchymal tissues), but is instead a highly complex endothelial cell-derived tumour that manifests on the skin, mucosal membranes and visceral linings as red, purple and brown lesions. (Beckstead, Wood, & Fletcher, 1985; Ganem, 2010; Wang et al., 2004). Notably, KSHV infection alone is not sufficient to cause KS, as immunodeficiency is generally a prerequisite for disease manifestation (Klepp, Dahl, & Stenwig, 1978).

There are 4 main epidemiological forms of KS: classical, endemic, iatrogenic and Acquired Immunodeficiency Syndrome (AIDs)-associated. Each KS form exhibits differences in lesion appearance and location; despite this, KS lesions are histopathologically similar (Ethel Cesarman et al., 2019; Wen & Damania, 2010). The primary cells comprising KS tumours are called spindle cells due to their abnormally elongated shape (Wen & Damania, 2010). Despite poor differentiation, spindle cells are believed to be of blood and lymphatic endothelial origin and are highly proliferative (Kahn, Bailey, & Marks, 2002; Pyakurel et al., 2006; Wang et al., 2004). KSHV infected spindle cells are reprogrammed to produce high levels of pro-inflammatory cytokines and angiogenic factors such as tumour necrosis factor (TNF), interleukins -1alpha, -1beta and -6 (IL-1α, IL-1β, IL-6), C-X-C Motif Chemokine Ligand 8 (CXCL8), interferon-gamma

(INF-γ), vascular endothelial growth factor (VEGF), cyclooxygenase-2 (COX-2) and granulocyte-macrophage colony-stimulating factor (GM-CSF) (Barbara Ensoli et al., 2010; Barbara Ensoli & Stürzl, 1998; Lane et al., 2002; Miles et al., 1990; Riva, Barozzi, Torelli, & Luppi, 2010; Sadagopan et al., 2007; Salahuddin et al., 1988). KS lesions feature widespread erythrocyte extravasation and lesion infiltration by diverse immune cells including lymphocytes, plasma cells and tissue macrophages (Ablashi, Chatlynne, Whitman, Cesarman, & Cesarman, 2002; Ethel Cesarman et al., 2019; Chung, Means, Choi, Lee, & Jung, 2002). KSHV also encodes homologues of cytokines such as viral IL-6 (vIL-6) and chemokine ligands (vCCL-1, -2, and -3), indicating the virus requires specific immunomodulatory signals for KS development (Chen et al., 2009; Choi & Nicholas, 2008). Unlike many cancers, advanced KS lesions are predominantly polyclonal and spindle cells have an exaggerated dependence on exogenous growth factors for proliferation (Duprez et al., 2007; Barbara Ensoli & Stürzl, 1998; Ganem, 2010). This dependence and the inflammatory nature of KS suggests that it is a paracrine and autocrine signaling disorder, whereby the production of inflammatory and angiogenic factors by spindle cells recruits specific inflammatory-responsive immune cells to the lesion (Ganem, 2010). These recruited cells contribute to the production of growth factors and cytokines necessary to promote transformation, cell survival and maintenance of KSHV-infection (Ganem, 2010).

1.2 Kaposi's Sarcoma-Associated Herpesvirus

KSHV is one of eight human herpesviruses and is a member of the lymphotrophic γ-herpesvirinae subfamily. KSHV is an enveloped virus with an icosahedral capsid and a linear dsDNA genome that is approximately 165kB (Renne et al., 1996). More than 80

open reading frames (ORFs) are encoded by KSHV (Russo et al., 1996). Many of these genes are conserved between the herpesviruses and are involved in essential processes like viral DNA replication and virus particle assembly. However, KSHV also encodes unique open-reading frames (ORFS) that are denoted as unique to KSHV by the letter 'K' preceding the ORF number (Russo et al., 1996; Wen & Damania, 2010).

1.*2.1 Viral Life Cycle*

KSHV has a broad tropism *in vivo*; infecting many cell types including epithelial cells, monocytes, macrophages, B-cells and endothelial cells (Chakraborty, Veettil, & Chandran, 2012; Ganem, 2010). KSHV, like all *Herpesviridae* family members, can establish a biphasic lytic or latent infection cycle in these cells. In KS patients, endothelial cells predominantly harbor latent KSHV infection (Ganem, 2010). *In vitro*, lytic reactivation is induced using phorbol esters or histone deacetylase inhibitors (sodium butyrate or trichostatin) however, the physiological stimuli required for reactivation is not well understood(Lukac & Yuan, 2007). Notably, over 95% of cells in KS lesions are latently infected and less than 3% of cells express lytic transcripts (Decker et al., 1996; Staskus et al., 1997) (Figure 1.1). Accordingly, KSHV latency is believed to be the major contributor to cell survival, proliferation and inflammatory phenotypes seen in KS tumours, however several lytic genes also have oncogenic properties and provide paracrine signals to promote inflammation and angiogenesis (Figure 1.1)(Wen & Damania, 2010).

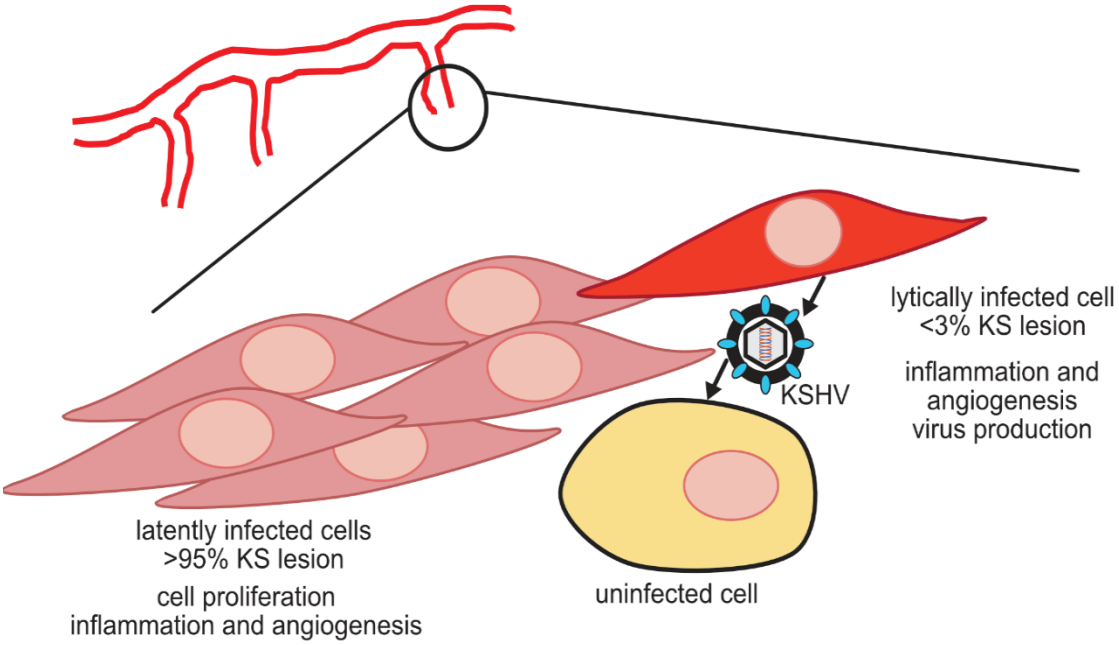

Figure 1.1: KS lesions are predominantly composed of latently infected spindle cells. Schematic of KS lesion. Greater than 95% of spindle cells within a KS lesion are latently infected with KSHV while less than 3% of cells in the lesion express lytic transcripts. As the predominant constituent of KS lesions, latently infected cells contribute to cell survival and proliferation and to the establishment of the highly inflammatory and vascularized nature of the KS lesion (Ganem, 2010). Lytic KSHV infected cells produce virus critical for tumour propagation, however several lytic genes also contribute to the inflammatory and angiogenetic environment required for KS.

1.2.2 Lytic Replication

During lytic replication, virus particles are produced and released from host cells. Over 80 transcripts are expressed in a tightly controlled, temporal fashion, which proceeds in an order of immediate early (IE), early and late genes (Ganem, 2010). IE genes are transcribed immediately following viral entry and do not require *de novo* viral protein translation, unlike early and late genes (R. Sun et al., 1998). Several IE genes are transcription regulators and factors important for controlling subsequent gene transcription and viral DNA replication initiation (Ethel Cesarman et al., 2019; Ganem, 2010). Replication and transcription activator (RTA) is an IE gene that acts as a molecular switch between latent and lytic infection cycles (Jha, Banerjee, & Robertson, 2016; Lukac, Renne, Kirshner, & Ganem, 1998; R. Sun et al., 1998). RTA induces a cascade of early gene transcription, including the viral DNA polymerase, processivity factors and DNA binding proteins which contribute to viral genome replication and cellular reprogramming (Gradoville et al., 2000; Lukac et al., 1998; R. Sun et al., 1998). Following genome replication, late genes are transcribed including structural proteins for virus particle assembly, maturation and egress (Mesri, Cesarman, & Boshoff, 2010). Viral genomes are encapsidated, capsids undergo nuclear egress and acquire the tegument and final envelope at the *trans*-Golgi network (TGN) (Johnston & Baines, 2011). Exocytic machinery facilitates the budding of progeny virus particles into the extracellular space (Mesri et al., 2010).

A handful of lytic genes, such as vIL-6 and viral G-protein-coupled receptor (vGPCR), are important for oncogenic transformation and inflammatory phenotypes. vIL-6 activates the Janus Kinase (JAK)-Signal Transducer and Activator of Transcription

(STAT) pathway causing increases in VEGF production and paracrine and autocrine signaling (J. An et al., 2002). Inoculation of vIL-6 expressing cells in athymic mice also increased hematopoiesis and tumour formation (J. An et al., 2002). vGPCR is a viral homologue to cellular CXCL8 receptor that is constitutively active and signals in the absence of ligand binding (E Cesarman et al., 1996; Nicholas et al., 1997). vGPCR expression immortalizes HUVECs and vGPCR transgenic mice can develop angio-proliferative lesions which express similar cell surface markers and cytokines to that detected in KS lesions (Bais et al., 2003; H.-G. Guo et al., 2003; Montaner et al., 2003; T.-Y. Yang et al., 2000). These studies establish a role for lytic genes in promoting tumourigenesis.

1.2.3 Establishment of Latency

KSHV establishes life-long latent infection in B-cells and endothelial cells. During latency the viral genome is circularized to form an episome, which is tethered to host chromatin (Ballestas, Chatis, & Kaye, 1999; Renne et al., 1996). A small subset of viral genes are expressed during latency including latency-associated nuclear antigen (LANA), viral cyclin (vCyclin), viral FLICE-inhibitory protein (vFLIP), Kaposins A, B and C and 12 pre-micro-RNAs (miRNAs) that are processed to form 24 miRNAs (Ethel Cesarman et al., 2019; Qin, Li, Gao, & Lu, 2017). Latency-specific promotors control the transcription of LANA, vFLIP and vCyclin and Kaposins A, B and C (Pearce, Matsumura, & Wilson, 2005; Sadler et al., 1999). LANA is a multifunctional protein that tethers the KSHV episome to host chromatin proteins, ensuring the genome is replicated during normal cell division; LANA also participates in immune and cell cycle

dysregulation (Ballestas et al., 1999; Purushothaman, Uppal, Sarkar, & Verma, 2016; Renne et al., 1996).

Several latent genes including LANA vCyclin, vFLIP and the Kaposins also display transformative and oncogenic phenotypes. vCyclin is a cellular D-type cyclin homolog that promotes cell cycle progression by constitutively activating cellular cyclin-dependent kinase 6 (Jones et al., 2014; Van Dross et al., 2005). Mice inoculated with ΔvCyclin-KSHV-infected cells have decreased tumour incidences relative to mice inoculated with wild-type (WT) virus-infected cells (Jones et al., 2014). vFLIP is a homolog of cellular FLICE inhibitory protein (FLIP) and activates the Nuclear Factor kappa-light-chain-enhancer of activated B cells (NF-κβ) pathway by directly binding Iκβ kinase thus, promoting cell survival, proliferation and inflammatory cytokine production (Ballon, Akar, & Cesarman, 2015; Chaudhary, Jasmin, Eby, & Hood, 1999; Field et al., 2003; Guasparri, Keller, & Cesarman, 2004; Grossman, Podgrabinska, Skobe & Ganem, 2006). vFLIP ectopic expression also induces spindle cell morphology in endothelial cells (Grossmann, Podgrabinska, Skobe, & Ganem, 2006; Guasparri et al., 2004). Latent viral proteins primarily comprise KS lesions; these proteins alters cell morphology, promotes cell survival and inflammatory phenotypes that contribute to KS tumourigenesis.

1.3 The Kaposin Locus

The Kaposin locus encodes three unique KSHV proteins expressed during the lytic and latent cycle: Kaposins (Kap) A, B and C (Sadler et al., 1999). The Kaposin locus transcript was first identified by Zhong et al., (1996) via northern blot hybridization of total RNA from KS pulmonary tissue. Using a canonical AUG start codon, a short

open reading frame with a transmembrane domain and hydrophobicity was identified as KapA (Figure 1.2). Sadler et al., (1999) identified an upstream portion of the transcript containing two sets of GC-rich, 23 nucleotide repeats called direct repeat 1 and 2 (DR1 and DR2) (Figure 1.2). Two proteins, KapB and KapC are translated from non-canonical CUG or GUG start codons upstream of KapA (Sadler et al., 1999) (Figure 1.2). KapC is translated in the same frame as KapA and is derived from the DR1, DR2 and K12 region translation (Sadler et al., 1999) (Figure 1.2). KapB is translated from a different frame than KapA or KapC and is derived from DR1 and DR2 translation (Sadler et al., 1999) (Figure 1.2). All three ORFs of the DR1 and DR2 produce the same polypeptide sequence suggesting the importance of its conservation (Sadler et al., 1999) (Figure 1.2). In different KSHV strains, the kDa size of KapB and C varies due to inconsistency in the number of 23 amino acid repeats maintained in DR1 and DR2; the significance of the expansion or contraction of DR repeats in this region is not understood (Li, Komatsu, Dezube, & Kaye, 2002; Sadler et al., 1999). Furthermore, there are multiple non-canonical initiation codons that can be used for translation (Li et al., 2002; Sadler et al., 1999). To date, the Kaposins have no known homology to other proteins and KapB is predicted to have an intrinsically disordered structure (Corcoran, unpublished). The Kaposin transcript is one of the most highly expressed transcripts during latency but is also expressed at higher levels during lytic reactivation (P.-J. Chang et al., 2002; Sadler et al., 1999). These features suggest the Kaposins play a significant role in KSHV latency and tumourigenesis. To date, no function has been ascribed to KapC. By contrast, KapB is the most widely investigated Kaposin locus product and ectopic KapB expression in primary ECs recapitulates several phenotypes of KSHV infection and KS lesions.

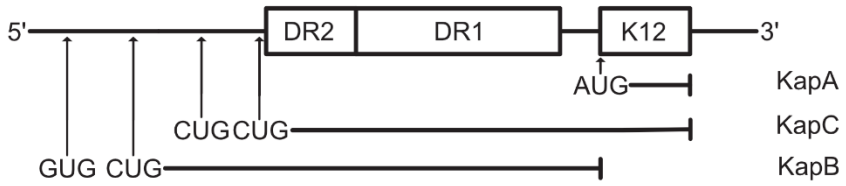

Figure 1.2: Kaposin locus translation. Adapted from McCormick & Ganem (2005). KapA is a short protein expressed from an AUG start codon denoted K12. Upstream is two sets of 23 amino acid direct repeats (DR1 and DR2). KapC is translated in the same frame as KapA from CUG non-canonical initiation codons, through the DR2, DR1 and K12 regions. KapB is translated in a different frame than KapA and KapC from CUG or GUG non-canonical start codons.

1.3.1 Kaposin B

1.3.1.1 KapB Activates MK2-RhoA Signaling Axis

KapB ectopic expression in primary ECs recapitulates several important phenotypes observed in KS lesions and KSHV infection. One of the ways KapB exerts these effects is by modulating regulatory cell signalling pathways. McCormick & Ganem (2005) identified that KapB directly binds the catalytic domain of mitogen-activated protein kinase (MAPK)-associated protein kinase 2 (MK2). MK2 is a p38 MAPK downstream effector that is activated in response to cellular stress such as oxidative stress or DNA damage (Gurgis, Ziaziaris, & Munoz, 2014). Upon activation, p38 translocates to the nucleus where it phosphorylates MK2 (Gurgis et al., 2014). Phosphorylated MK2 and p38 are exported to the cytoplasm where MK2 can phosphorylate and influence the activation of several stress-response pathway proteins (Gurgis et al., 2014). KapB activates MK2 as indicated by immunoblotting for phospho-MK2 and the phosphorylated form of the down-stream effector, Heat Shock Protein 27 (HSP27) (Corcoran, Johnston, & McCormick, 2015; McCormick & Ganem, 2005).

Corcoran et al. (2015) identified that KapB activates the cytoskeletal regulator, Rho guanosine triphosphatase (GTPase), via a non-canonical signaling axis induced by MK2 activation. Upon HSP27 phosphorylation, p115RhoGEF is recruited to signaling complexes and activates the cytoskeletal regulator RhoA GTPase (RhoA) (Corcoran et al., 2015; Garcia et al., 2009). RhoA binds downstream effectors; Rho-associated kinase (ROCK) 1 and ROCK 2 (Corcoran et al., 2015; Garcia et al., 2009; Leung, Chen, Manser, & Lim, 1996). KapB elicits several phenotypes that depend on MK2 axis activation

KapB-mediated activation of cytoskeletal regulator RhoA and downstream effectors, ROCK 1 and ROCK 2 induce actin cytoskeleton rearrangement (Corcoran et al., 2015). Stress fibers are bundles of actin filaments held together by cross-linking proteins; the activation of ROCK1 and ROCK2 causes stress fiber formation and cell spindling (Corcoran et al., 2015; Leung et al., 1996; Sin, Chen, Leung, & Lim, 1998). Furthermore, KapB-expression increases endothelial cell migration and angiogenesis as determined by a tubule formation assay which model the reorganization stage of angiogenesis (Corcoran et al., 2015). These data indicate ectopic KapB expression induces changes in cell morphology, migration and angiogenesis that could contribute to latent tumourigenesis.

In addition to cytoskeletal modification, Corcoran et al., (2015) also identified that KapB induced the disassembly of a small RNA granules called processing bodies (PBs). PB disassembly depends on MK2, RhoA and ROCK activation and is significant because PBs are a major site of cytokine RNA post-transcriptional control (Corcoran et al., 2015; Corocran, unpublished).

1.4 Processing Bodies

1.4.1 Processing Body Components and Structure

PBs are non-membrane bound ribonucleoprotein (RNP) granules that are conserved among eukaryotes and are important sites for post-transcriptional gene regulation (Parker & Sheth, 2007). PBs contribute to translational repression, nonsense-mediated decay and labile mRNA decay (Fenger-Grøn, Fillman, Norrild, & Lykke-Andersen, 2005; Palanisamy, Jakymiw, Van Tubergen, D'Silva, & Kirkwood, 2012; Parker & Sheth, 2007). PB foci are on average 100-500 nm in diameter depending on cell

type (Cougot, Cavalier, Thomas, & Gillet, 2012; Eulalio, Behm-Ansmant, Schweizer, & Izaurralde, 2007; Z. Yang et al., 2004). PB formation is thought to be initiated through RNA-protein interactions and liquid-liquid phase separation, which allows the rapid and reversible recruitment of PB proteins into organized, membrane-less foci (Luo, Na, & Slavoff, 2018). Electron microscopy and immunogold labelling reveal PBs are organized into two compartments comprising; "a dense core on which peripheral protrusions are anchored" (Cougot et al., 2012).

The complete composition of PBs has not been elucidated; however, PBs contain enzymes and cofactors required for mRNA decay, several RNA binding proteins and translational repressors (Cougot, Babajko, & Séraphin, 2004; Cougot et al., 2012; Eulalio, Behm-Ansmant, & Izaurralde, 2007; Eulalio, Behm-Ansmant, Schweizer, et al., 2007; Sheth & Parker, 2003). Many diverse PB components have been identified through mass-spectrometry proteomics studies and validated by electron microscopy and immunofluorescence microscopy (Ayache et al., 2015; Bish et al., 2015; Eulalio, Behm-Ansmant, Schweizer, et al., 2007; Hubstenberger et al., 2017; Parker & Sheth, 2007). PBs components include several RNA binding proteins such as Human antigen R (HuR) and Tristetraprolin (TTP) and cytoskeleton regulators including Myosin 6 (Hubstenberger et al., 2017). Some of the best characterized PB proteins are involved in eukaryotic mRNA degradation. More specifically, the deadenylation complex (Ccr4p/Pop2p/Not complex), decapping complex (DCP1A, DCP1B, DCP2), several decapping activators and co-factors (Hedls, DDX6, Pat1B and LSM1-7) and the 5'-to-3' exonuclease, XRN1 are all PB components (Parker & Sheth, 2007b; Sheth & Parker, 2003). Many PB components are also important for the structural organization of the granule as electron microscopy

studies indicate that PB resident protein, DDX6 is localized to the periphery of PBs while XRN1 and DCP1A are localized to the interior of the electron dense granule (Cougot et al., 2012). Due to the dynamic nature of PBs, it is likely that many PB-associated factors remain unidentified (Kedersha et al., 2005b).

PBs are distinct from the better characterized RNA granule, stress granules (SGs). Normal cells typically have PBs, while SGs form in response to translational inhibition (Stoecklin & Kedersha, 2013). Although PBs and SGs have overlap in protein constituents, there are numerous proteins specific for each structure (Fujimura, Kano, & Murata, 2008; Gallouzi et al., 2000; Wilczynska, Aigueperse, Kress, Dautry, & Weil, 2005). DCP1A, DCP2 and Hedls are reliable markers that are only found in PBs (Kedersha et al., 2005b; Ozgur, Chekulaeva, & Stoecklin, 2010; van Dijk et al., 2002). PB component diversity provides incite into the several functions attributed to the RNA granules.

1.4.2 Processing Body Function

Several functions are attributed to PBs including mRNA decay and translational repression; however, research surrounding this area is controversial. Some evidence suggests PBs act as reservoirs for translationally repressed RNAs and not as sites of mRNA decay (Franks & Lykke-Andersen, 2008; Parker & Sheth, 2007. This model is supported by data showing mRNA decay occurs in the absence of PBs and that mRNAs can be exchanged from PBs to translating polysomes (Brengues, Teixeira, & Parker, 2005; Eulalio, Behm-Ansmant, Schweizer, et al., 2007). Moreover, Horvathova et al., (2017) developed a single-molecule reporter of 5'-to-3' mRNA decay. Imaging of this probe in live cells showed RNA decay products throughout the cytoplasm showing that

mRNA decay was not exclusive to PBs (Horvathova et al., 2017). Hubstenberger et al., (2017) sequenced PB-associated RNAs and detected as many as 1/5 of cellular RNAs, many of these RNAs were intact. Altogether these data indicate that PBs can store translationally repressed mRNAs and that mRNA does not exclusively occur in PBs.

Contrary to above, evidence supporting the theory that PBs are important sites of 5'-to-3' mRNA decay also exists. The presence of many enzymes (XRN1), co-factors and activators (DCP1A, DDX6, Hedls, LSM1-7) that are required for mRNA decay suggests that PBs may be sites of 5'-to-3' mRNA decay (Parker & Sheth, 2007b). Contrary to Hubstenberger et al., (2017) a publication by Aizer et al., (2014) described mRNA without poly-A tails accumulating and localizing to PBs, indicating that the transcripts are targeted for mRNA decay. Moreover, mRNAs trapped in the process of decay (through the insertion of strong secondary structure in the 3'-UTR of the transcript) were localized to PBs providing evidence for PBs as sites of mRNA decay (Parker and Sheth, 2003). PB size is also proportional to mRNA decay flux such that inhibition of mRNA decapping causes increases in PB size, suggesting the accumulation of transcripts destined for decay within PBs (Parker & Sheth, 2007; Sheth & Parker, 2003).

PB function is difficult to experimentally investigate as it is challenging to image RNA decay in real time and to isolate a non-membranous granule (Luo et al., 2018). Consequently, there are differing, but not mutually exclusive, models to describe PB function. At this time, it is clear that PBs play a multifunctional role in post-transcriptional gene regulation, especially for the group of cellular messages subject to constitutive decay, as is discussed below (Franks & Lykke-Andersen, 2008; Parker & Sheth, 2007).

1.4.2.1 Processing Bodies and AU-rich Element mRNAs

There is strong correlative evidence that PBs play an important role in the decay of a specific class of cellular mRNAs called AU-rich element mRNAs (ARE-mRNAs). ARE-mRNAs are a group of inherently labile genes that contain an ARE in their 3'-untranslated region (3'-UTR). Between 5-8% of mRNAs contain AREs and the presence of AREs targets these transcripts for constitutive decay in PBs (Bakheet, Williams, & Khabar, 2006; Franks & Lykke-Andersen, 2007; Kedersha et al., 2005b; Palanisamy et al., 2012). The vast number of transcripts containing AREs indicates the *cis*-element is important for regulating eukaryotic gene expression (Bakheet, Williams, & Khabar, 2006; Palanisamy et al., 2012). Moreover, many of the ARE-mRNAs degraded in PBs; such as IL-6, CXCL8, TNF, GM-CSF and VEGF play important roles as immune modulators and inflammatory mediators and are also upregulated with KSHV infection (Palanisamy, et al., 2012; Palanisamy, Park, Wang, & Wong, 2008).

The mechanism of ARE-mRNA delivery to PBs appears to be through RNA binding proteins. RNA binding proteins bind target transcripts by recognizing *cis*-elements like AREs and promote ARE-mRNA stabilization or destabilization (Palanisamy, et al., 2012). Several ARE-mRNA binding proteins like TTP and HuR have been detected as PB components (Franks & Lykke-Andersen, 2007; Kedersha et al., 2005a). Furthermore, *in situ* hybridization assays show the delivery of ARE-mRNAs that encode TNF and GM-CSF to PBs and that RNA binding proteins tether ARE-mRNAs to PBs (Franks & Lykke-Andersen, 2007). Correlative data linking PB dynamics to ARE-mRNA levels include a study where tumour growth factor-β (TGF-β) induced PB assembly correlated to a decrease in ARE-mRNA expression (Blanco, Sanduja, Deane,

Blackshear, & Dixon, 2014). Notably, the disassembly of PBs induced by MK2-activating viral protein, KapB, correlates to an increase in ARE-mRNA stabilization, as determined by luciferase assays containing an ARE from GM-CSF or IL-6 (Corcoran et al., 2012; Corcoran, Khaperskyy, & McCormick, 2011; McCormick & Ganem, 2005, 2006). KapB also stabilized an ARE-mRNA that encodes PROX-1, the master regulator of lymphatic endothelium differentiation. Altogether this evidence asserts PBs are a site of mRNA decay for immunomodulatory and inflammatory ARE-mRNAs. The characteristic immunomodulatory nature of many ARE-mRNAs highlights the importance of understanding ARE-mRNA regulation in PBs.

1.4.3 Processing Body Dynamics

PBs are important regulators of eukaryotic gene expression, yet little is known about PB assembly and disassembly. Although PBs are present in most cells, they vary in size and number (Eulalio, Behm-Ansmant, & Izaurralde, 2007). Cellular stress such as glucose deprivation or translation inhibition causes PBs to increase in size and/or number, highlighting the dynamic nature of the RNP granules (Decker & Parker, 2012; Eulalio, Behm-Ansmant, Schweizer, et al., 2007). This dynamic characterization was also confirmed by fluorescence recovery after photobleaching (FRAP) studies, which showed the rapid exchange of PB-associated proteins between the cytoplasm and PBs.

At a molecular level, the *de novo* assembly of PBs under normal conditions appears to require several PB proteins including EDC3, LSM4 and DDX6 (Ayache et al., 2015; Cougot et al., 2012; C. J. Decker, Teixeira, & Parker, 2007; Kedersha et al., 2005a) However, PB assembly under stress conditions such as arsenite treatment is not dependent on the expression of LSM4 or DDX6, suggesting PB assembly conditions

differ between homeostasis and stress (Ayache et al., 2015; Cougot et al., 2012; Kedersha et al., 2005a). Depletion of several key PB factors including Hedls and Pat1B decrease the number of cells with PBs, indicating some PB components are integral for PB structure. Similarly, DDX6 (found in the outer ring of PB organization) leads to PB disassembly as determined by electron microscopy (Cougot et al., 2012; Eulalio, Behm-Ansmant, Schweizer, et al., 2007; Marnef et al., 2010). The maintenance of PBs is also dependent on a pool of translationally repressed mRNAs, as cycloheximide treatment (which inhibits translation elongation thus trapping mRNAs in polysomes) causes loss of PBs (Brengues et al., 2005). These studies implicate the importance of specific PB proteins in promoting or maintaining PB structure and show that changes in the levels of key PB proteins causes PB disassembly.

Notably, several PB protein post translational modifications are important for PB assembly and function. Phosphorylation of DCP2 is required for its localization to PBs in yeast (Yoon, Choi, & Parker, 2010). In humans, DCP1A has several phosphorylation sites (Aizer, Kafri, Kalo, & Shav-Tal, 2013). DCP1A phosphorylation stabilized interactions with PB component DCP2; however DCP1A hyper phosphorylation coincided with PB loss during mitosis and cell division, thus showing phosphorylation can affect PB function and localization (Aizer et al., 2013). K63-ubiquitination knockdown impairs DCP1A phosphorylation and subsequently prevents interactions between DCP1A and Hedls (Tenekeci et al., 2016). Furthermore, many PB proteins including Hedls and DDX6, which are important for PB assembly and maintenance, have phosphorylation sites; however, the functional consequences of phosphorylation for these proteins is not well understood (Bish et al., 2015; Gustafson & Wessel, 2010; Rahman,

Qasim, Oellerich, & Asif, 2014). In summary, diverse post-translational modifications of several PB proteins are important regulatory events for PB function and dynamics. However, the precise signals regulating PB dynamics and turnover remain unclear.

1.5 Autophagy

Autophagy is a homeostatic, catabolic process by which cellular cargo, like RNA granules, can be degraded to maintain homeostasis or respond to cellular stress (Glick et al., 2010). Although autophagy is a ubiquitous process, autophagic flux is upregulated during certain developmental phases and cellular stresses such as hypoxia, starvation and pathogen infection(Anding & Baehrecke, 2017; Galluzzi, Baehrecke, et al., 2017; Glick et al., 2010). There are 3 main types of autophagy; chaperone-mediated autophagy, microautophagy and macroautophagy (Glick et al., 2010). In chaperone-mediated autophagy, chaperone proteins facilitate the transport of cargo targeted for degradation across the lysosomal membrane (Glick et al., 2010). Conversely, in microautophagy, cargo is internalized in the lysosome via invagination of the lysosomal membrane into small vesicles (Glick et al., 2010). Lastly, macroautophagy is characterized by the formation of cytosolic double-membraned vesicles called autophagosomes that fuse with lysosomes to form autolysosomes (Galluzzi, Baehrecke, et al., 2017; Kaur & Debnath, 2015). Macroautophagy is the best characterized type of autophagy and is a focus of this thesis. Accordingly, macroautophagy will hereafter be referred to as autophagy.

There are more than 32 autophagy-related genes (Atg) identified in mammalian cells (Glick et al., 2010; Kaur & Debnath, 2015). Many of them are conserved in yeast emphasizing the importance of autophagy in cellular function (Glick et al., 2010). The autophagic process is separated into several important stages; initiation, phagophore

nucleation, phagophore expansion, autophagosome formation and autolysosome formation. Several signals including amino acid starvation and hypoxia induce autophagy by causing Unc-51-like kinase 1 (ULK) complex assembly and activation (Dikic & Elazar, 2018). The ULK complex phosphorylates class III phosphoinositide 3-kinases (PI3K) components, causing ULK complex localization to an intracellular membrane source such as the endoplasmic reticulum (ER) (Dikic & Elazar, 2018). The membrane localization of these complexes promotes phosphatidylinositol 3,4,5- triphosphate (PIP3) production (Dikic & Elazar, 2018). The increasing PIP3 concentration (1) initiates phagophore nucleation (the isolated lipid bilayer derivation) and (2) recruits other Atg proteins including the cysteine protease, Atg4 and the Atg16-Atg12-Atg5 complex (Dikic & Elazar, 2018; Galluzzi, Baehrecke, et al., 2017) (Figure 1.3). Atg4 cleaves cytoplasmic microtubule-associated protein 1 light chain 3 (MAP1LC3; also known as LC3) exposing a glycine residue (LC3-I) that is subsequently conjugated phosphatidylethanolamine (PE) to form LC3-II by the Atg16-Atg12-Atg5 complex (Galluzzi, Baehrecke, et al., 2017) (Figure 1.3). The conversion of LC3-I to LC3-II is a hallmark of autophagosome biogenesis as LC3-II levels correlate with autophagosome number (Kabeya, 2000; Mizushima, Yoshimori, & Levine, 2010). The lipidated LC3-II is anchored in the phagophore membrane and promotes membrane expansion around cytosolic cargo until a double-membraned mature autophagosome

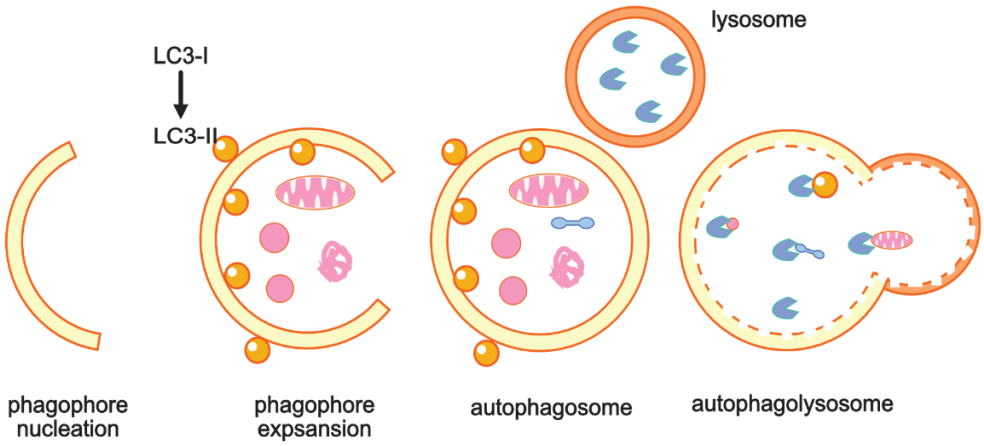

Figure 1.3: Bulk autophagy facilitates non-selective cytosolic degradation of cargo. Schematic representation of autophagosome biogenesis and autolysosome formation. An isolated lipid bilayer called a phagophore is derived from existing membrane sources. Phagophore expansion is mediated in part by the conversion of cytoplasmic LC3 to lipidated, membrane-bound LC3-II. The phagophore expands and fuses forming a mature, double-membraned autophagosome. The mature autophagosome fuses with a lysosome forming an autolysosome. Lysosomal enzymes degrade the content of the autolysosome allowing the component metabolites to be recycled in the cell.

forms (Dikic & Elazar, 2018; Olsvik et al., 2015) (Figure 1.3). At this point, most of the proteins involved in autophagosome formation and expansion (ULK complex, Atg5, Atg12, Atg4, Atg16) are no longer associated with the autophagosome, excluding LC3-II, which remains embedded in the autophagosome membranes (Dikic & Elazar, 2018). Following autophagosome biogenesis, the autophagosome fuses with a lysosome forming an autolysosome (Figure 1.3) (Galluzzi et al., 2017). Within the acidic autolysosome, proteases and hydrolases catabolize and degrade the autolysosome contents (Galluzzi et al., 2017). The autolysosome degradation products and metabolites are released into the cytoplasm, allowing them to be recycled and used in other anabolic cellular processes.

1.6 Selective Autophagy

Autophagy was originally thought to be a non-selective, bulk catabolic process. However, over the past decade, it has become evident that cargo can be selectively targeted to autophagosomes in a process known as selective autophagy. Thus far, the selective degradation of protein aggregates (aggrephagy), mitochondria (mitophagy), endoplasmic reticulum (ERphagy), stress granules (granulophagy), peroxisomes (pexophagy) and pathogens (xenophagy) have been reported (Rogov, Dötsch, Johansen, & Kirkin, 2014) (Figure 1.4).

1.6.1 Molecular Mechanism of Selective Autophagy

Cytosolic constituents can be targeted for autophagic degradation by direct binding to LC3 or indirect targeting to LC3 via molecular bridges termed selective autophagy receptors. Proteins that interact with LC3 do so via an LC3-interacting region (LIR) that consist of a W/F/Y-X-X-L/I/V motif (Ichimura et al., 2008; Noda et al., 2008; Noda, Ohsumi, & Inagaki, 2010; Birgisdottir et al., 2013). Some proteins such as PEX14

during pexophagy and the cell-cell adhesion regulator β-catenin have LIRs and bind LC3 directly facilitating their autophagic degradation, but most incidences of selective autophagy rely on selective autophagy receptors to confer specificity (Hara-Kuge & Fujiki, 2008; Petherick et al., 2013; Xie et al., 2015b).

Selective autophagy receptors bind cargo and LC3 (via LIR interactions) on growing autophagosomes to target cargo for autophagic degradation (Zaffagnini & Martens, 2016). Some of the best characterized receptors include p62, valosin containing protein (VCP), optineurin (OPTN), neighbor of BRCA1 gene 1 (NBR1) and nuclear dot protein 52 (NDP52) (Zaffagnini & Martens, 2016). OPTN, p62, NDP52, and NBR1 are members of the sequestosome-like family and contain several conserved motifs including a LIR motif, a domain that permits receptor multimerization and a ubiquitin binding domain (UBD) (Birgisdottir, Lamark, & Johansen, 2013). All three of these features are important for efficient cargo binding, targeting and degradation.

Selective autophagy receptor interactions with LC3 tend to be low affinity. Some cargo receptors, like OPTN, contain multiple LIRs, thus establishing high-avidity binding to LC3 (Zaffagnini & Martens, 2016). OPTN phosphorylation also increases its binding affinity for LC3 (Wild et al., 2011). Other cargo receptors, such as p62 and NDP52 contain few functional LIRs, but these receptors oligomerize via their Phox and Bem1 (PB1) and SKI-interacting protein (SKIP) carboxyl homology (SKICH) domains, respectively, to stabilize LC3 binding and cargo binding (Lu, den Brave, & Jentsch, 2017; Zaffagnini & Martens, 2016).

Recent publications also reveal that ubiquitination can target substrates for autophagic degradation in addition to proteasomal degradation

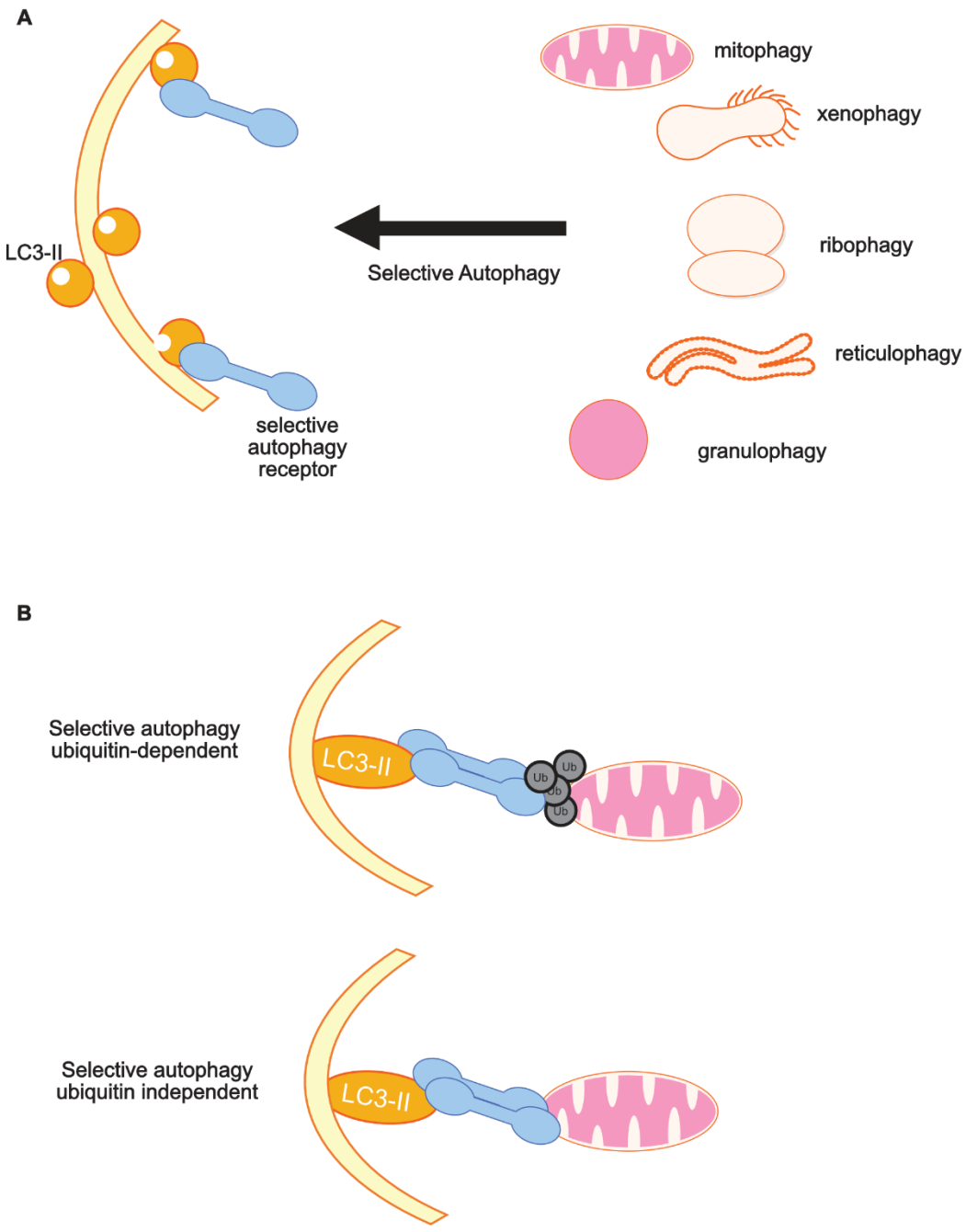

Figure 1.4: Selective autophagy facilitates targeted cargo degradation
(A) The turnover of diverse cargos including mitochondria (mitophagy), pathogens (xenophagy), ribosomes (ribophagy), ER (reticulophagy) and stress granules (granulophagy) are regulated by selective autophagy. (B) Selective autophagy receptors can bind cargo in a ubiquitin-dependent or independent manner. Receptors also contain LC3-interacting regions (LIRs) that allow targeting of the bound cargo to phagophore membranes via LC3 binding.

(Ichimura et al., 2008; Padman et al., 2019; Pankiv et al., 2007; Verlhac, Gregoire, et al., 2015). Accordingly, selective autophagy can occur in a ubiquitin-dependent or -independent manner (Rogov & Kirkin, 2014). During ubiquitin-dependent selective autophagy, cargo is ubiquitinated and this modification facilitates selective autophagy receptor binding (Rogov & Kirkin, 2014). Zaffagnini & Martens (2016) suggested that cargo tagged with high concentrations of ubiquitin will be more efficiently recruited to autophagosomes due to increased cargo recognition by selective autophagy receptors. Furthermore, the type of ubiquitin linkage e.g. K63-linked ubiquitination, is believed to confer a preference for cargo to be degraded by autophagy rather than the proteasome (Liu et al., 2017; Zaffagnini & Martens, 2016). This was contested by Lu et al., (2017), who showed that during yeast aggrephagy, the determining factor for whether a specific target was degraded via autophagy or the proteasome was the extent of selective autophagy receptor oligomerization, and not ubiquitin quantity or linkage. Ubiquitin-independent selective autophagy can also occur via selective autophagy receptors directly binding cargo; in this case, it is believed that the oligomerization of selective autophagy receptors is important for the efficiency of ubiquitin-independent selective autophagy (Khaminets, Behl, & Dikic, 2016; Lu et al., 2017; Padman et al., 2019). Some types of mitophagy are ubiquitin-independent (Padman et al., 2019). Selective autophagy receptors are implicated in the degradation of a wide variety of cargos; therefore, the activity of these receptors must be tightly regulated through several mechanisms that are not well understood.

1.7 Methods to Study Bulk and Selective Autophagy *In Vitro*

Autophagic flux is a dynamic process, yet we study its activation and regulation using static approaches. This necessitates careful sampling over time. For example, because autophagosomes are an intermediate in the autophagic process, to count their numbers at one specific time point in an experiment is not always representative of autophagic activity. This is because autophagosome number does not account for autolysosome formation and degradation of autophagic cargo (Glick et al., 2010). An increase in autophagosome number can indicate increased autophagy induction or a block in autophagy, downstream of autophagosome formation (Mizushima et al., 2010). Due to the complicated interpretation of autophagy-related results, researchers must use several methods, and interpret all these data together, to pinpoint how autophagy is changing in their system.

Many assays developed to study autophagy aim to determine autophagic flux, a term that encompasses the entire process, from autophagosome initiation and maturation, to autolysosome formation and the degradation of autophagic substrates (Mizushima et al., 2010). Autophagic flux is the best indicator of autophagic activity, but assessing autophagic flux requires combinational approaches (Mizushima et al., 2010)**.** Many common assays for autophagic flux rely on LC3-II as a measure of autophagy, as this is one of very few proteins that remain associated with autophagosomes after their formation. For example, other autophagy regulators like Atg5 or Atg12 cannot be used to assess changes in autophagy (Dikic & Elazar, 2018). Most of the methods that investigate autophagy, including those that measure LC3 levels, also cannot distinguish between bulk and selective autophagy. Because I use LC3-based assays in this thesis, their method and correct interpretation is described below.

1.7.1 Methods to Determine Autophagosome Number

Once believed to be the gold standard in the measurement of the autophagic process, electron microscopy can be used to identify autophagosomes. In transmission electron microscopy sections, these structures appear as double-membraned vesicles present in the cytosol (Mizushima et al., 2010). It is not possible to distinguish between bulk and selective autophagy by visualizing autophagosomes by electron microscopy (Mizushima et al., 2010). Furthermore, it is difficult to differentiate between autolysosomes, which contain a single membrane and may be undergoing partial degradation, and autophagosomes (Mizushima et al., 2010). Fluorescence microscopy can also be used to enumerate membrane-associated LC3-II puncta (Mizushima et al., 2010) . The overexpression of GFP-LC3 serves the same function, but reports of GFP-LC3 aggregations not associated with autophagosomes make this a less reliable method (Kuma, Matsui, & Mizushima, 2007). However, none of these methods can be used to evaluate changes in autophagic flux or selective autophagy without further validation, as no information about autolysosome formation or cargo degradation is gained from these assays.

1.7.2 Methods to Determine Autophagic Flux

Four of the main methods employed to investigate autophagic flux are LC3 or p62 turnover assays, overexpression of the mRFP-GFP-LC3 tandem reporter or the GFP-cleavage assay. These assays allow researchers to distinguish whether increased autophagosomes represent true increased autophagic flux (that culminates in cargo degradation and recycling) or a late-stage block in autophagosome maturation (Klionsky et al., 2012).

The LC3 turnover assay capitalizes on the fact that LC3-II, as it traffics through the autophagy pathway, is also degraded in autolysosomes along with cargo. Therefore, the addition of late-stage autolysosome formation inhibitors like bafilomycin and chloroquine block the LC3-II degradation (Mizushima et al., 2010). Under basal conditions some level of LC3-I and LC3-II are present (Figure 1.5A). If a treatment increases LC3-II levels, this increase could be due to increased autophagic flux or to a downstream block in autolysosome formation. Therefore, a third cell condition consisting of the treatment and late-stage autophagy inhibitor is required to differentiate between these two options(Barth, Glick, & Macleod, 2010). If the treatment-mediated increases in LC3-II are due to increased autophagic flux, there will be an even larger increase in LC3-II with the late-stage autophagy inhibitor addition, but if the increase in LC3-II was due to a degradation block there would be no increase in LC3-II in this condition (Barth et al., 2010). Therefore, increases or decreases in autophagic flux can be identified with the LC3 turnover assay.

Immunoblotting for autophagy-related protein p62 can also be used to determine autophagic flux (Mizushima et al., 2010). Although p62 is a selective autophagy receptor it is fairly ubiquitously included in autophagosomes and is degraded in autolysosomes like LC3-II. Consequently, p62 levels are inversely correlated with autophagic activity (Klionsky et al., 2012; Mizushima et al., 2010). If a treatment induces autophagy, p62 levels will decrease, whereas if a treatment inhibits autolysosome formation, p62 steady-state levels will increase (Figure 1.5A). Treatment with an autophagy inducer and late-stage autophagy inhibitor will cause a greater increase in p62 accumulation than seen with the inducer alone (Mizushima et al., 2010).

Figure 1.4: Methods to investigate autophagic flux. A-B are adapted from Yoshii & Mizushima (2017). (A) LC3 and p62 turnover assay schematic if cells are treated with an inducer of autophagic flux. Some level of LC3-II is present in a no treatment control. The addition of a treatment or late-stage autophagy inhibitor increases LC3-II levels; these results could be to increased autophagy initiation or a downstream block in autolysosome formation and cargo degradation. Concomitant use of the treatment and a late-stage autophagy inhibitor causes increases in LC3-II greater than that seen with the inhibitor indicating increased autophagic flux. p62 levels are inversely correlated with autophagic flux. Decreased levels of p62 with a treatment indicate increased autophagic flux and increased levels of p62 with a late stage inhibitor or simultaneous treatment with an inducer and inhibitor indicate increased autophagic flux. (B) mRFP-GFP-LC3 tandem reporter assay. When the reporter is in the autophagosome or cytosol it will appear as yellow puncta due to the expression of GFP and mRFP fluorescence. When the reporter enters the autolysosome the GFP will be quenched and only RFP signal is visible. Increases in yellow and red puncta indicate increases in autophagic flux. (C) GFP Fragmentation assay. GFP-LC3 in the autophagosome or cytosol remains intact. When the construct enters the autolysosome, it becomes partially degraded and free GFP becomes detectable by immunoblotting. Increased free GFP-relative to the intact construct signifies increased autophagic flux.

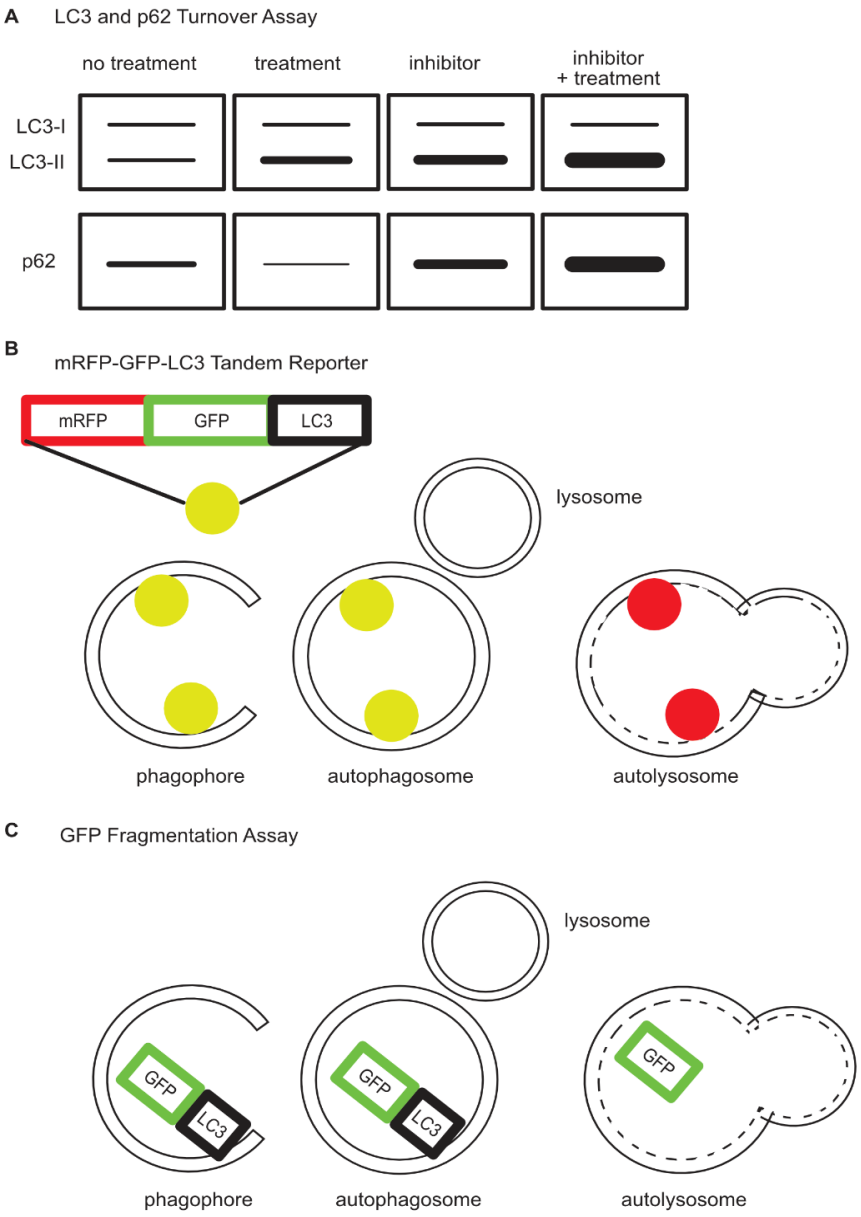
A
LC3 and p62 Turnover Assay
no treatment
treatment
inhibitor
inhibitor
+ treatment
LC3-I
LC3-II
p62
B
mRFP-GFP-LC3 Tandem Reporter
mRFP
GFP
LC3
lysosome
phagophore
autophagosome
autolysosome
C
GFP Fragmentation Assay
lysosome
GFP
LC3
phagophore
autophagosome
autolysosome

Another method used to monitor autophagic flux requires the mRFP-GFP-LC3 tandem reporter. This assay exploits the fact that GFP fluorescence is quenched in a lysosome while RFP or mCh fluorescence is not quenched (Kabeya, 2000; Katayama, Yamamoto, Mizushima, Yoshimori, & Miyawaki, 2008). When the construct is in the cytosol or autophagosome it emits both GFP and mRFP fluorescence which manifests as yellow puncta; if the construct enters the lysosome or autolysosome, only RFP puncta will be detected (Kimura, Noda, & Yoshimori, 2007) (Figure 1.5B). Increases in autophagic flux cause increases in both yellow and red puncta, but if autophagosome maturation is blocked there will be increases in only yellow puncta. Similar to the LC3-GFP construct, aggregates of the tandem reporter can form, leading to increases in yellow puncta that are not autophagosome-associated (Kimura et al., 2007; Kuma et al., 2007).

Lastly, a GFP-cleavage assay also capitalizes on lysosome-mediated changes in GFP to monitor autophagic flux. This assay utilizes a LC3-GFP reporter which upon entering a autolysosome is partially degraded causing the release of a free GFP fragment (Mizushima et al., 2010) (Figure 1.5C). Immunoblotting for GFP will detect the intact LC3-GFP construct as well as the free GFP portion (Mizushima et al., 2010). An increase in free GFP indicates increased autophagic flux. This assay has been used extensively in yeast but is not robust in mammalian cells due to differences in the activity and aciditiy of lysosomes (Klionsky et al., 2012; Mizushima et al., 2010). None of the autophagic flux assays allow monitoring of selective autophagy cargo as they depend on monitoring proteins like LC3- and p62 that are present within the autophagosome and respond robustly to changes in autophagic flux. These methods do not provide data as to what

specific cargoes are present in the autophagosomes and therefore do not give information about selective autophagy.

1.7.3 Methods to Investigate Selective Autophagy Flux

To date, there are very few methods developed to investigate selective autophagy flux and most methods that do exist are specific for mitophagy - the best characterized form of selective autophagy. The first steps towards investigating selective autophagy often rely on knocking down or knocking out selective autophagy receptors and looking for altered cargo turnover via immunofluorescence and immunoblotting. These assays provide important, indirect information suggesting a role for selective autophagy in cargo turnover but provide no information about the relative rates of selective autophagic flux compared to bulk autophagy or other cytosolic cargo. Furthermore, because selective autophagy receptors have multiple roles in cells, cautious interpretation of these results is required.

In the mitophagy field, there are a few fluorescence-based assays developed to monitor mitophagic flux. One such assay involves labelling mitochondria and lysosomes using MitoTracker® and Lysotracker® dyes. Following dye application, microscopy is used to identify and quantify the frequency of dye colocalization which indicates mitophagic events (Dolman, Chambers, Mandavilli, Batchelor, & Janes, 2013). Using this system, it is possible to detect increases or decreases in the incidences of lysosome and mitochondria co-localization in relation to a control (Dolman et al., 2013). This assay provides insight into rates of mitophagic flux and perhaps could be adapted using other dyes or fluorescent proteins to monitor different types of selective autophagy. One of the most promising assays to monitor mitophagic or selective autophagy flux involves the

pH-dependent fluorophore mKeima which will be discussed in Chapter 3. Overall there are insufficient tools available to monitor selective autophagic flux, particularly of cargos other than the mitochondria.

1.8 Rationale and Objectives

1.8.1 KapB Upregulates Autophagic Flux

Recent evidence suggests that MK2-RhoA signaling pathway members can upregulate autophagy (Wei et al., 2015). MK2 phosphorylates serine 90 of autophagy related protein, Beclin-1, promoting autophagy induction (Wei et al., 2015). The MK2 downstream effector, HSP27, was also implicated in stimulating autophagy (Shen et al., 2016). The RhoA effector kinase, ROCK1, also upregulated autophagy by phosphorylating Beclin-1 at a different residue, threonine 119 (Gurkar et al., 2013). Given these data, the Corcoran lab has recently investigated whether KapB upregulates autophagy; numerous unpublished experiments support this hypothesis. KapB-expressing cells displayed increased levels of LC3-II and decreased steady-state levels of p62, indicating autophagic flux is increased compared to vector-transduced control cells. Furthermore, cells expressing KapB have increased number of LC3-II puncta that colocalize with the lysosomal marker LAMP2A, indicating an increase in autophagosome delivery to lysosomes, thus indicating increased autophagy. These results confirm that KapB upregulates autophagic flux (Robinson and Corcoran, unpublished).

1.8.2 KapB Mediated PB Dispersal Requires Autophagy

Several lines of evidence indicate that PB disassembly is regulated by autophagy and perhaps, selective autophagy. Utilizing the PB resident protein Edc3-mCh as a marker for PB assembly in yeast, Buchan and Parker (2013) determined that disruption to

Atg15 resulted in an accumulation of Edc3-mCh in intra-vacuolar compartments targeted by autophagy. This PB marker accumulation implies PB clearance may be facilitated by bulk autophagy (Buchan, Kolaitis, Taylor, & Parker, 2013). Moreover, activation of bulk autophagy with rapamycin enhanced PB clearance and this clearance was prevented using an ULK1 complex inhibitor (Hardy, Shinde, Wang, Wendt, & Geahlen, 2017). These results suggest PB disassembly can be mediated by bulk autophagy. There is also evidence indicating selective autophagy may participate in PB clearance. GFP-DCP1A co-localizes with fluorescently-tagged selective autophagy receptors p62 and NDP52 (Buchan et al., 2013; H. Guo et al., 2014). Moreover, PB protein sequence analysis identifies putative LIR sequences in DCP1A, DDX6, and XRN1 suggesting a role for selective autophagic regulation of PB disassembly (Corcoran, unpublished).

Given evidence that bulk and selective autophagy regulate PB disassembly and that KapB causes PB disassembly and upregulates autophagic flux, the Corcoran lab investigated if autophagy was a requisite intermediate in PB clearance. Several experiments support this hypothesis. Treatment of cells with autophagy inducer Torin decreased the number of PBs detected per cell. RNA interference to decrease the levels of essential autophagy genes (Atg5) and pharmacological inhibition of late-stage autophagy (bafilomycin, chloroquine) in KapB expressing cells reversed PB dispersal. Moreover, preliminary results indicate certain PB proteins such as DCP1A or XRN1 decrease in level with Torin treatment and accumulate with bafilomycin and chloroquine treatment. In conclusion, our data thus far suggest that KapB upregulates autophagy to facilitate PB disassembly.

1.8.3 Objectives

We know that KapB induces autophagic flux and that autophagy is a requirement for KapB-mediated PB disassembly. However, we do not know if KapB induces selective targeting of PBs to phagophores, or whether this effect stems from upregulated bulk autophagic flux. Likewise, the relationship between autophagic degradation of PBs and implications for ARE-mRNA remains unknown. Given these questions, the objective of my M.Sc. research was to determine (1) whether KapB engages selective autophagy to promote degradation of PBs and (2) how manipulating autophagic flux impacts ARE-mRNA levels in response to KapB expression.

1.8.4 Overview

To investigate whether KapB engaged selective autophagy to cause PB disassembly, I used two parallel approaches. First, since there were no tools available for directly assaying selective autophagy of PBs, I developed of fluorescence-based assay to monitor turnover of two different PB-resident proteins. I reasoned that if the PB-tagged constructs were subject to autophagic turnover independent of other cytosolic cargo, these data would strongly support KapB-induced selective PB autophagy. I showed that two PB resident reporter proteins were degraded by autophagy, but my data were inconclusive as to whether KapB expression increased the catabolism of PB components more or less than other cytosolic cargo. Second, I created recombinant lentivirus expressing shRNAs that targeted known selective autophagy receptors and determined that the knockdown of only one of these, NDP52, reversed KapB-mediated PB disassembly. I also determined that NDP52 was required for KapB-mediated ARE-

mRNA stabilization in a luciferase reporter assay. Using qPCR, I characterized several endogenous ARE-mRNAs and showed that many upregulated in response to KapB expression; however, preliminary data showed that the knockdown of NDP52 only decreased steady-state levels of one ARE-mRNA, GM-CSF, in KapB-expressing cells.

In summary, my research elucidates a novel mechanism of PB regulation by the viral protein KapB, in which NDP52 mediates selective PB protein catabolism leading to PB disassembly. Furthermore, disassembly of PBs inversely correlates with increases in inflammatory ARE-mRNA levels, providing new insight into the mechanism by which selective autophagy promotes inflammatory mRNA expression. This work enhances our understanding of how KapB establishes an inflammatory immunological niche that is required for KSHV latent infection and tumourigenesis.

Chapter 2 Materials and Methods

2.1 Cell Culture

All cells were grown at 37 °C in a humidified chamber with 5% CO_2 and 20% O_2. Human embryonic kidney 293T cells (HEK293T) (ATCC) and human cervical epithelial carcinoma cells, (HeLa cells) expressing a tetracycline regulated trans-activator (HeLa Tet-Off) (Clontech) were cultured in Dulbecco's Minimal Essential Medium (DMEM) (Thermo Fisher) supplemented with 100 U/mL penicillin, 100 µg/mL streptomycin, 2 mM L-glutamine (1% PSQ) (Thermo Fisher) and 10% heat-inactivated fetal bovine serum (HI-FBS) (Thermo Fisher). Cells were sub-cultured at 90% confluency using 0.05% trypsin-ethylenediaminetetraacetic acid (EDTA) (0.2 mg/mL) (Thermo Fisher) and media was refreshed every 48h or as needed.

Primary human umbilical vein endothelial cells (HUVECs) (Lonza) were cultured in endothelial cell growth medium (EGM-2) (Lonza). EGM-2 consisted of endothelial basal medium (EBM-2) (Lonza) supplemented with 2% FBS, 0.04% hydrocortisone, 0.4% human fibroblast growth factor-B, 0.1 % vascular endothelial growth factor (VEGF), 0.1% long arginine-3 insulin-like growth factor, 0.1% ascorbic acid, 0.1% human epidermal growth factor, gentamicin sulfate (30 µg/mL), amphotericin (15 ng/mL) and 0.1% heparin. HUVECs were seeded onto tissue culture plates pre-coated with 0.1% (wt/vol) porcine gelatin (Sigma-Aldrich) in phospho-buffered saline pH 7.4 (PBS [137 mM NaCl, 2.7 mM KCl, 10 mM Na_2HPO_4, 1.8 mM KH_2PO_4, 1 mM $CaCl_2 \cdot 2H_2O$, 0.5 mM $MgCl_2 \cdot 6H_2O$]). EGM-2 was refreshed every 48h or as needed. HUVECs were sub-cultured using 0.05% trypsin-EDTA at ratios of 1:3 or 1:4 into 6-well

plates and 1:6 or 1:8 into 12-well plates. All experiments were completed using HUVECs between passage 5 and 8.

The renal carcinoma cell line, iSLK.219 was a kind gift from Don Ganem (University of California San Francisco) (Myoung & Ganem, 2011; Stürzl, Gaus, Dirks, Ganem, & Jochmann, 2013). iSLK.219s were cultured in DMEM supplemented with 1% PSQ, HI-FBS and puromycin (puro) (1 μg/mL). Cells were sub-cultured at 90% confluency using 0.05% trypsin-EDTA and media was refreshed every 72h or as needed. Briefly, iSLK.219s were constructed as follows. Cells contain a doxycycline (DOX)-inducible replication and transcription activator (RTA) and harbour recombinant KSHV.219 virus which contains a RFP/GFP/puro cassette (Myoung & Ganem, 2011; Vieira & O'Hearn, 2004). iSLK.219 cells constitutively express puromycin N-acetyl-transferase and GFP, which permit selection of infected cells with puromycin (1 μg/mL) and the visual identification of cells that harbour the virus cassette (Myoung & Ganem, 2011; Vieira & O'Hearn, 2004). RFP expression is under the control of a PAN promotor that is activated in response to RTA expression (Myoung & Ganem, 2011; Vieira & O'Hearn, 2004).

2.2 Drug and Conditioned Media Treatments

2.2.1 Drug Treatments

Cells were treated with the appropriate DMSO vehicle control and one or more of the following drugs at the concentrations and durations described in Table 1. Torin1 (Torin) is an autophagy inducer which inhibits mTORC1/2; autophagy inhibitor bafilomycin A1 (bafilomycin) inhibits vacuolar H^+-ATPase activity resulting in a inhibition of autophagosome and lysosome fusion and lysosomal acidification (Galluzzi,

Bravo-San Pedro, Levine, Green, & Kroemer, 2017; Thoreen et al., 2009; Yamamoto et al., 1998). Chloroquine also inhibits autophagy by preventing the fusion of lysosomes and autophagosomes (Mauthe et al., 2018). Carbonyl cyanide 3-chlorophenylhydrazone (CCCP) is a protonophore and oligomycin is an inhibitor of membrane bound mitochondrial F_1F_0-ATP synthase; both compounds uncouple oxidative phosphorylation and stimulate mitophagy (Georgakopoulos, Wells, & Campanella, 2017; Kwon, Viollet, & Yoo, 2011; J. W. Park et al., 1997; Penefsky, 1985; Phospholipids & Energy, 1973). NH_4Cl is a H+ ionophore which inhibits lysosomal acidification (Klionsky et al., 2012; Mizushima et al., 2010). MG-132 is a peptide aldehyde that inhibits the proteolytic activity of the 26S proteasome complex (Rock et al., 1994; Tsubuki, Saito, Tomioka, Ito, & Kawashima, 1996). Lipopolysaccharide (LPS) is a bacterial endotoxin that activates toll-like receptors (TLRs) 4 which stimulate the transcription of inflammatory molecules, including many transcripts that contain AREs (Akira & Takeda, 2004; B. S. Park & Lee, 2013). Following treatment with one or more drugs, cells were prepared accordingly for immunoblotting, total RNA lysis, live-cell imaging or flow cytometry.

2.2.2 Conditioned Media Treatment

2 x 10^6 iSLK.219 cells (latently infected with KSHV.219 virus) were sub-cultured into a 10 mL cell culture dish and grown without puromycin for 72h. At 72h, conditioned media was reserved and cleared of cellular debris by centrifugation at 500G for 5 min. Supernatant was collected and filtered through a 0.22 µM polyethersulfone (PES) membrane filter (VWR) and stored in aliquots at -80. Prior to the experiment, conditioned media was thawed at 37°C and combined 1:1 with fresh HUVEC EGM-2

media and used to treat vector or KapB-expressing HUVECs for 0 or 6h prior to total RNA harvest.

Table 1: Duration, source and concentration of drug treatments used in this study

Drug	Company	Catalogue	Cell type	Concentration	Duration (h)
Torin1	Sigma-Aldrich	475991	HUVEC	250 nM	4
			HEK293T	250 nM	6 or 24
Bafilomycin-A1	Sigma-Aldrich	B1793	HUVEC	10 nM	4
			HEK293T	100 nM	6 or 24
Chloroquine	Sigma-Aldrich	C6628	HUVEC	25 μM	4
CCCP	Sigma-Aldrich	C2759	HEK293T	10 μM	6 or 24
Oligomycin	Sigma-Aldrich	75351	HEK293T	1 μg/mL	6
MG-132	Selleckchem	S2619	HUVEC		4
LPS	Sigma-Aldrich	L3129	HUVEC	1 μg/mL	0, 6, 12
NH_4Cl	Sigma-Aldrich	254134	HEK293T	50mM	1

2.3 Plasmids and Cloning

The plasmids used and/or generated in this study are listed in Table 2. All constructs generated in this study were confirmed using Sanger DNA sequencing (GENEWIZ).

Table 2: Plasmids used in this study

Plasmid	Source
mKeima-red-Mito-7 (Mito-mKeima)	Addgene #56018
mKeima-C1	Addgene #54546
mKeima-DCP1A	This study
mKeima-DDX6	This study
mKeima-LC3	This study
mKeima-N1	Addgene #54597
pBMN mCh NDP52 C443K	Addgene #119685
pBMN mCh NDP52 C443K V136S	Addgene #119686
pcDNA 3.1 (+)	Invitrogen
pcDNA KapB BCBL1	Craig McCormick (Dalhousie University)
pcDNA FLAG-MK2EE	Craig McCormick (Dalhousie University)
pLJM1 bsd	Craig McCormick (Dalhousie University)
pLJM1 bsd EGFP	Addgene #19319
pLJM1 bsd EGFP LC3	Craig McCormick (Dalhousie University)
pLJM1 bsd KapB (pulmonary KS)	Craig McCormick (Dalhousie University)
pLJM1 bsd mCh	Craig McCormick (Dalhousie University)
pLJM1 puro	Addgene #91980
pLJM1 puro MK2EE	Craig McCormick (Dalhousie University)
pLJM1 puro RFP-NDP52	This study
pLJM1 puro RFP-NDP52 V248A	This study
pLJM1 puro/bsd mCh-NDP52 C443K	This study
pLJM1 puro/bsd mCh-NDP52 C443K V136S	This study
pLKO.1 bsd shNDP52-3	This study
pLKO.1 bsd shNDP52-4	This study
pLKO.1 TRC bsd	Addgene #10878
pLKO.1 TRC puro	Addgene #26655
pLKO.1 TRC puro shNDP52-1	This study
pLKO.1 TRC puro shNDP52T-2	This study
pLKO.1 TRC puro shOPTN-1	This study
pLKO.1 TRC puro shOPTN-2	This study
pLKO.1 TRC puro shp62	This study
pMD2.G	Addgene #12259
psPAX2	Addgene #12260
pT7-EGFP-DCP1A-C1	Addgene #25030
pT7-EGFP-DDX6-C2	Addgene #25033
pTRE2 Firefly Luciferase-ARE	Craig McCormick (Dalhousie University)
pTRE2 Renilla Luciferase	Craig McCormick (Dalhousie University)
RFP-NDP52 V248A	Dr. Andreas Till (University Hospital of Bonn)
RFP-NDP52	Dr. Andreas Till (University Hospital of Bonn)

2.3.1 Short Hairpin RNAs Selection and Cloning

shRNA sequences were designed to target either the coding sequence or 3'-untranslated region (3'-UTR) of NDP52, OPTN and p62. Target sequences were identified using the Genetic Perturbation Portal of the Broad Institute. In brief, shRNA sequences were selected based on the % GC content, 3' stability and the absence of repeating bases, restriction sites, internal stem-loop structures and off-target effects. Forward and reverse oligomers were ordered from Thermo Fisher with homology to the desired expression plasmid pLKO.1 with the following sequences:

Forward oligomer: 5' CCGG - sense target sequence - CTCGAG- antisense target sequence –TTTTG.

Reverse oligomer: 5'AATTCAAAAA- sense target sequence - antisense target sequence - 3'.

Oligonucleotide sequences are listed in Table 3. Annealed forward and reverse oligomers were ligated into AgeI and EcoRI digested pLKO.1 TRC puro or pLKO.1 bsd. All restriction enzymes were purchased from New England Biolabs.

Table 3: shRNA sequences

shRNA target	shRNA sequence	Target Seq
Non-targeting – Forward	5’ CCGGAGCACAAGCTGGAGTACAACTACTCGA GATCAACATGAGGTCGAACACGATTTG 3’	
Non-targeting – Reverse	5’ AATTCAAAAAGCACAAGCTGGAGTACAACTA ATCAACATGAGGTCGAACACGATTTG 3’	
NDP52(1)-Forward	5’ CCGGGAGCTGCTTCAACTGAAAGAACTCGA GTTCTTTCAGTTGAAGCAGCTCTTTTTG 3’	CDS
NDP52(1)-Reverse	5’ AATTCAAAAAGAGCTGCTTCAACTGAAAGAA CTCGAGTTCTTTCAGTTGAAGCAGCTC 3’	CDS
NDP52(2)-Forward	5’ CCGGGACTTGCCTATGGAAACCCATCTCGAG ATGGGTTTCCATAGGCAAGTCTTTTTG 3’	CDS
NDP52(2)-Reverse	5’ AATTCAAAAAGACTTGCCTATGGAAACCCAT CTCGAGATGGGTTTCCATAGGCAAGTC 3’	CDS
NDP52(3)-Forward	5’ CCGGCCCTTTGTGAACTAAGTTCAACTCGAGT TGAACTTAGTTCACAAAGGGTTTTTG 3’	3’-UTR
NDP52(3)-Reverse	5’ AATTCAAAAACCCTTTGTGAACTAAGTTCAA CTCGAGTTGAACTTAGTTCACAAAGGG 3’	3’-UTR
NDP52(4)-Forward	5’ AATTCAAAAACCTGACTTGATACTAAGTGAT CTCGAGATCACTTAGTATCAAGTCAGG 3’	3’-UTR
NDP52(4)-Reverse	5’ CCGGCCTGACTTGATACTAAGTGATCTCGAG ATCACTTAGTATCAAGTCAGGTTTTTG 3’	3’-UTR
Optineurin (1)-Forward	5’ CCGGGCACGGCATTGTCTAAATATACTCGAG TATATTTAGACAATGCCGTGCTTTTTG 3’	CDS
Optineurin (1)-Reverse	5’ AATTCAAAAAGCACGGCATTGTCTAAATAT ACTCGAGTATATTTAGACAATGCCGTGC 3’	CDS
Optineurin (2)-Forward	5’ CCGGGCCATGAAGCTAAATAATCAACTCGAG TTGATTATTTAGCTTCATGGCTTTTTG 3’	CDS
Optineurin (2)-Reverse	5’ AATTCAAAAAGCCATGAAGCTAAATAATCA ACTCGAGTTGATTATTTAGCTTCATGGC 3’	CDS
p62-Forward	5’ CCGGCCGAATCTACATTAAAGAGAACTCGAG TTCTCTTTAATGTAGATTCGGTTTTTG 3’	CDS
p62-Reverse	5’ AATTCAAAAACCGAATCTACATTAAAGAGAA CTCGAGTTCTCTTTAATGTAGATTCGG 3’	CDS

2.3.2 NDP52 Plasmid Constructs

Several NDP52 constructs were subcloned into pLJM1 to allow for virus production and expression of the constructs in HUVECs. Red fluorescent protein (RFP) NDP52 and RFP-NDP52 V248A were digested with NheI and BamHI and ligated into

NheI- and BamHI-digested pLJM1 puro and pLJM1 bsd. mCherry (mCh) NDP52 constructs were amplified using polymerase chain reaction (PCR) and the following primers from pBMN mCh-NDP52 C443K V136S and pBMN mCh-NDP52 C443K (NDP52 C443K & C443K/V136S BamHI-Forward; NDP52 C443K & C443K/V136S EcoRI-Reverse; see Table 4 for primer sequence).The forward primer incorporated a BamHI restriction site and a reverse primer incorporated a EcoRI restriction site. PCR amplifications were performed using Phusion high-fidelity DNA polymerase (New England Biolabs) according to manufacturer's protocol. The amplification process was as follows: denaturation (98°C for 2 min), 35 amplification cycles (95°C for 30s, 54°C for 30s, 72°C for 30s) and a final extension (72°C for 10 min). This PCR protocol was used for all amplifications unless otherwise stated (minor adjustments in the annealing temperature were used for different primer pairs). The BamHI- and EcoRI-digested PCR products were ligated into BamHI- and EcoRI-digested pLJM1 puro and pLJM1 bsd. All primers used for cloning were ordered from Thermo Fisher.

Table 4: Cloning primers used in this study

Primer	Primer Sequence
NDP52 C443K & C443K/V136S BamHI-Forward	5' TAAGCAGGATCCGCCACCATGGTGAGCAAG 3'
NDP52 C443K & C443K/V136S EcoRI-Reverse	5' TAAGCAGAATTCCAGAGAGAGTGTTTGAACACGT 3'
LC3 BspEI-Forward	5' TAAGCATCCGGAGGAGGAGGAATGCCGTCGGAGAA GACCT 3'
LC3 BglII-Reverse	5' TAAGCAAGATCTATTACACTGACAATTTCATCCCG 3'
DDX6 BspEI-Forward	5' TAAGCATCCGGAGGAGGAGGAATGGGTCTGTCCAG TCAAA 3'
DDX6 BglII-Reverse	5' TAAGCAAGATCTTTAAGGTTTCTCATCTTCTACAGG 3'

2.3.3 mKeima Plasmid Constructs

LC3 and resident PB proteins, DCP1A and DDX6 were cloned into a mKeima-containing vector to create mKeima fusion proteins. BspEI- and SalI-digested pT7 enhanced green fluorescent protein (EGFP) DCP1A was ligated into BspEI- and SalI-digested mKeima-C1. LC3 was PCR amplified from pLJM1 bsd LC3 GFP using a forward primer with a BspEI restriction site and a reverse primer with a BglII restriction site (LC3 BspEI-Forward, LC3 BglII-Reverse, see Table 4 for primer sequences). The BspEI- and BglII- digested LC3 PCR product was ligated into BspEI- and BglIII-digested mKeima-C1. DDX6 was PCR amplified from pT7 EGFP DDX6 using a forward primer with a BspEI restriction site and a reverse primer with a BglII restriction site (DDX6 BspEI-Forward, DDX6 BglII-Reverse, see Table 5 for primer sequence). The BspEI- and BglII-digested DDX6 PCR product was ligated into BspEI- and BglIII- digested mKeima-C1.

2.4 Transfection

HEK293T cells were seeded at 60% confluency into 6-well plates. Cells were washed twice with PBS and 900 µL of serum-free, antibiotic-free DMEM was added to each well. A reaction mixture consisting of 3 µg of the plasmid(s) of interest and 9 µL of polyethylenimine (PEI) (Sigma-Aldrich) was diluted in 100 µL of Opti-MEM (Thermo Fisher). The reaction mixture was added to cells dropwise. 6h following transfection, the medium was replaced with 2 mL antibiotic-free DMEM with 10% HI-FBS and 1% L-glutamine. The plasmid constructs were expressed in cells for 48h prior to fixation for immunofluorescence or lysis for immunoblotting.

2.5 Recombinant Lentivirus Production

A second-generation recombinant lentivirus system was used in this study, comprised of the following: an expression plasmid for the cell attachment and fusion protein derived from Vesicular stomatitis virus (VSV-G; pMD2.G), a expression plasmid for the HIV structural and transactivator genes Gag, Pol, Rev and Tat (psPAX2) which are required for successful packaging, and a transfer plasmid containing the construct of interest and a resistance cassette flanked by lentiviral long terminal repeats (LTRs) and a packaging signal (pLJM1 or pLKO.1 plasmid vectors). These three plasmids were co-transfected into a 10 cm-dish of 80% confluent HEK293Ts as follows. Cells were washed twice with PBS and 4 mL of serum-free, antibiotic-free DMEM was added to the dish. A reaction mixture consisting of 1 µg of pMD2.G, 2 µg of psPAX2, 3.3 µg of the lentiviral transfer vector and 18 µL of PEI diluted in 1 mL of Opti-MEM was added to cells, dropwise. 6h following transfection, the cell medium was replaced with 10 mL antibiotic-free DMEM containing 10% HI-FBS and 1% L-glutamine. 48h later, virus-containing supernatant was collected and filtered through a 0.45 µm PES membrane filter, aliquoted into sterile 1ml Eppendorf tubes, and stored at -80°C until use.

2.6 Lentiviral Transduction

Prior to transduction, HUVECs or HeLa Tet-Off cells were washed with PBS and complete cell culture media (see section 2.1) supplemented with 5 µg/mL hexadimethrine bromide (polybrene) (Sigma-Aldrich) was added to the dish. Lentiviral-containing supernatants were thawed at 37°C in a water bath. Lentiviral-containing supernatants at a dilution of 1:10 to 1:50 (relative to the total volume of media in the cell culture dish) were added to cells dropwise. 24h later virus-containing media was replaced with complete cell culture media supplemented with puro (1µg/mL) or blasticydin (bsd) (5

μg/mL) and transduced cells were selected for 48h or 96h, respectively. Cells recovered for 24h in complete media without selection antibiotics prior to further manipulation.

2.7 Immunofluorescence, Fluorescent Imaging & Microscopy

2.7.1 Immunofluorescence Staining for Confocal Microscopy

Cells were seeded onto #1.5 coverslips and after experimental manipulation were fixed for 10 mins at 37 °C in 4% (v/v) paraformaldehyde (Electron Microscopy Sciences) diluted in PBS. Following fixation, cells were washed 3 times in PBS and were stored at 4°C until further use. Cells were permeabilized with 0.1% (v/v) Triton X-100 (Sigma-Aldrich) diluted in PBS for 10 min at room temperature (RT) and were washed 3 times with PBS before being blocked in 1% human AB serum (Sigma-Aldrich) diluted in PBS for 1 hour at RT. Primary antibodies were diluted in 1% human AB serum in PBS and used at the concentrations and duration dictated in Table 5. Following primary antibody incubation, cells were washed 4 times with PBS before incubation for 1h at RT with one or more secondary antibodies (diluted in 1% human AB in PBS) (Table 5). Subsequently, cells were washed 4 times with PBS. If cells were stained for F-actin, coverslips were incubated in Alexa Fluor 647 phalloidin (Thermo Fisher A22287) diluted 1:200 in PBS for 75 min at RT. Cells were washed twice with PBS and mounted onto a microscope slide with Prolong Gold AntiFade mounting media (Thermo Fisher). Coverslips were cured overnight (O/N) and were visualized at the Cellular and Molecular Digital Imaging Facility at Dalhousie University using the Zeiss LSM 510 Meta Laser-Scanning Confocal microscope 40X, 60X or 100X oil immersion objectives and the Argon (458/477/488/514 nm), HeNe (548 nm), or HeNe (633 nm) lasers. Neutral mKeima fluorescence was detected using the Argon 458 nm laser and a 580/20 nm

emission filter; acidic mKeima fluorescence was detected using a HeNe 543 nm laser and a 670/20 nm emission filter. Images within an experiment were obtained with the same laser power, exposure time, and gain and were processed using Zen Lite Blue software.

Table 5: Primary and secondary antibodies used for immunofluorescence

Antibody	Species	Company	Catalogue	Dilution	Time & Temp
DDX6	Rabbit	Bethyl	A300-461A	1:1000	4°C O/N
Hedls	Mouse	Santacruz	Sc-8418	1:1000	4°C O/N
KapB	Rabbit	Generous gift from Craig McCormick & Don Ganem		1:1000	RT 1h
FLAG	Rabbit	Sigma-Aldrich	F7425	1:400	4°C O/N
LAMP2	Mouse	AbCam	Ab25631	1:500	4°C O/N
NDP52	Rabbit	AbCam	Ab68588	1:500	4°C O/N
TOM20	Rabbit	Santacruz	Sc-11415	1:500	4°C O/N
Alexa Fluor 555-conjugated donkey anti-mouse IgG H+L	Donkey	Thermo Fisher	A31570	1:1000	RT, 1h
Alexa Fluor 555-conjugated donkey anti-rabbit IgG H+L	Donkey	Thermo Fisher	A31572	1:1000	RT, 1h
Alexa Fluor 488-conjugated chicken anti-mouse IgG H+L	Chicken	Thermo Fisher	A21200	1:1000	RT, 1h
Alexa Fluor 488-conjugated chicken anti-rabbit IgG H+L	Chicken	Thermo Fisher	A21441	1:1000	RT, 1h
Alexa Fluor 647-conjugated chicken anti-rabbit IgG H+L	Chicken	Thermo Fisher	A21443	1:1000	RT, 1h

2.7.2 Immunofluorescence Staining for Fluorescence Imaging and Cell Profiler Analysis

Cells were seeded onto coverslips and fixed as above. Prior to permeabilization, cells were stained with wheat germ agglutinin (WGA) Alexa 647 conjugate (Thermo Fisher; W32466) diluted 1:400 in PBS for 10 min at RT. WGA is a lectin that has high affinity for glycans; sialic acid and N-acetylglucosamine. WGA is often used to stain the plasma membrane; we used WGA staining to identify the outer boundaries of the cell although some of the lectin is internalized and binds intracellular carbohydrates (Figure 2.1). Cells were washed, blocked and incubated in primary antibody (Hedls, KapB or FLAG) and secondary antibody as in section 2.7.1 (Table 5). Following secondary antibody, cells were washed 4 times with PBS and stained with 4',6-diamidino-2-phenylindole (DAPI) (Thermo Fisher; D1306) (1 μg/mL) diluted 1:10 000 in PBS. Coverslips were mounted and cured as previously described. Imaging was performed on the Zeiss AxioImager Z2 40X oil immersion objective using the HXP 120V light source. 4 channels with different excitation (ex.) and emission (em.) filters were used to image cells as follows: DAPI (ex. 335-383 nm, em. 420-495 nm), GFP (ex. 450-490 nm, em. 500-550 nm), dsRed (ex. 533-558 nm, em. 570-640 nm) and Cy5 (ex. 625-655 nm em. 665-715 nm). At least 5 fields of view were obtained per treatment, imaging 60+ cells per condition per experiment (for each independent biological replicate). For each experiment, channel exposures and intensities were unchanged throughout imaging. Images were exported (separate channels) as TIF files and inputted into CellProfiler.

2.7.3 Cell Profiler and Processing Body Quantification

2.7.3.1 Cell Profiler Pipeline

Image analysis was performed using CellProfiler (cellprofiler.org), an open source software for image analysis (Carpenter et al., 2006). The pipeline used was designed by E.L. Castle. In brief, nuclei were detected as primary objects using automatic thresholding of the DAPI image (see Figure 2.1 for representative images in the cell profiler pipeline). Cell boundaries were identified by detecting the outer edge of cells in WGA-stained channel images. Individual cells were identified as secondary objects by using the propagate function from the identified nuclei and from the WGA-determined cell outer edge. Following a series of enhancement and masking steps, Hedls puncta were measured in the cytoplasm of cells using a global thresholding with robust background adjustments. The number of Hedls puncta per cell were measured and exported as .csv files.

2.7.3.2 R Analysis of Cell Profiler Output

A R script developed by E. L. Castle on Rstudio was used to analyze CellProfiler output. CSV files exported by cell profiler contain information on PB presence and absence for each cell analyzed; the R-script was designed to assign treatment conditions to each cell and determine the mean number of Hedls puncta per cell per condition was determined. The error and significance of puncta counts within a given experiment was determined using a negative binomial model, commonly used for count data with unequal variance.

2.7.4 Live-Cell Imaging

HEK293T cells were plated onto a 33-mm glass-bottomed dish (#1.5, glass diameter, Grenier Bio-One). Before imaging, cell media was replaced with phenol-red free DMEM (Thermo Fisher) containing L-glutamine (2 mM), D-glucose (4.5 g/L) and

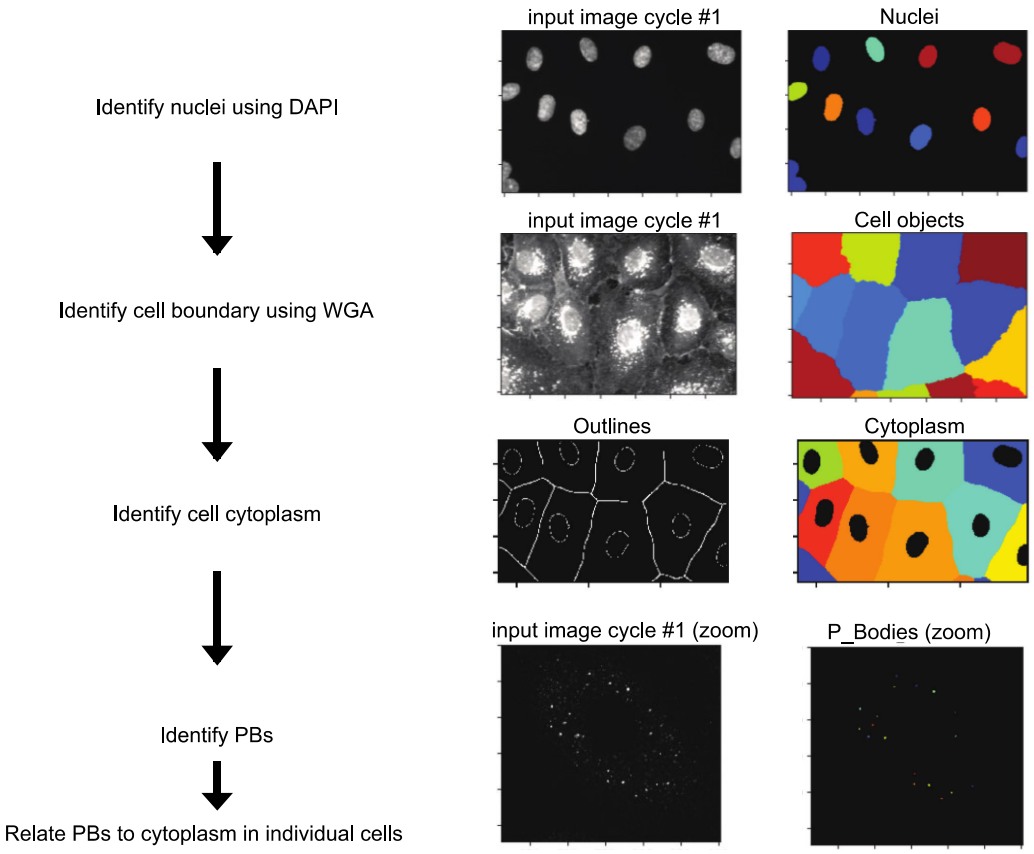

Figure 2.1: Cell Profiler pipeline for identifying the number of PBs in cells. Cells were stained for immunofluorescence with primary antibody for Hedls (PBs) and dyes for DAPI (nuclei) and WGA (cell boundary). Images were imported into the cell profiler pipeline. Automatic thresholding of images identified the nuclei and outer boundaries of cells using DAPI and WGA staining respectively. Individual cells and the cytoplasm were identified by subtracting the outline of the nuclei from the cell boundary. Hedls puncta (P_bodies, PBs) were identified in the cytoplasm and the number of Hedls puncta per cell was measured and exported as .csv files.

4-2-hydroxyethyl-1-piperazineethanesulfonic acid (HEPES) (25 mM). Cells were imaged using the Zeiss LSM 510 Meta Laser Scanning Confocal Microscope as described in section 2.1. Cells were imaged within 10 mins of removal from a cell culture incubator to reduce impacts of having no temperature, humidity and CO_2 control on cell viability and mKeima fluorescence. Images within the same experiment and condition were obtained using the same laser power, exposure and gain and were processed using Zen Lite Blue software.

2.8 Protein Electrophoresis and Immunoblotting

Cells were washed with PBS, lysed in an appropriate volume of 2X Laemmli buffer (120 mM Tris-HCl, pH 6.8, 4% sodium dodecyl sulfate [SDS], 20% glycerol) and stored at -20°C until use. Upon thawing, cell lysates were mechanically sheared by passing the lysate through a 21-gauge needle. The DC Protein Assay (Bio-Rad) was used to quantify protein concentration as per the manufacturer's instructions. 10µL of 300mM dithiothreitol (DTT) (Sigma-Aldrich) and 5µL of 0.1% bromophenol blue diluted in dH_2O (Sigma-Aldrich) was added to lysates prior to boiling lysates for 5 min at 95°C. 10-15 µg of protein was separated by TGX Stain-Free FastCast Acrylamide gel Kits, (12% or 7.5%; Bio-Rad) and SDS-polyacrylamide gel electrophoresis (SDS-PAGE). TGX Stain-Free gels were activated using the ChemiDoc Touch Imaging system (Bio-Rad) and protein was transferred to polyvinylidene membranes (PVDF) (Bio-Rad) using the Trans-Blot Turbo transfer system (Bio-Rad). Total protein on PVDF membranes was visualized using the ChemiDoc Touch Imaging system. Membranes were blocked in either 2.5% bovine serum albumin (BSA) (Bioshop) or 2.5% skim milk diluted in Tris-buffered saline (TBS) (50 mM Tris-HCL pH 7.5, 150 mM NaCl) with 0.01% Tween 20 (TBST) (Sigma-

Aldrich) or for 45 min at RT. Primary antibodies were diluted (as in Table 6) in 2.5% BSA or skim milk in TBST and were incubated O/N rocking at 4°C. Membranes were washed 2 times for 10 mins with TBST and then incubated with a secondary IgG antibodies conjugated to horseradish peroxidase diluted in 2.5% BSA or skim milk in TBST (Table 6). Membranes were washed 4 times for 5 mins with TBST and were incubated in Clarity Western ECL substrate (Bio-Rad). The ChemiDoc Touch Imaging system was used to visualize chemiluminescence signal. Where appropriate, protein band intensity was normalized to total lane protein using Bio-Rad Image Lab software.

The following amendments apply to samples immunoblotted for mKeima. 40-100 µg of protein was separated by SDS-PAGE; a large amount of protein lysate was required due to small amounts of processed mKeima. Following transfer, PVDF membranes were blocked in 5% skim milk diluted in PBS for 45 min at RT. Membranes were incubated O/N in mKeima antibody diluted in PBS with 0.01% Tween (PBST) and PBST was used for all membrane washes. Secondary antibody was diluted in 2.5% skim milk in PBST.

Table 6: Primary and secondary antibodies used for immunoblotting

Antibody	Species	Company	Catalogue	Dilution	Time & Temp
p62	Rabbit	CST	7695	1:1000	4°C O/N
NDP52	Rabbit	CST	60732	1:1000	4°C O/N
KapB	Rabbit	Generous gift from Craig McCormick (Dalhousie University) & Don Ganem (UCSF)		1:1000	4°C O/N
mKeima	Mouse	MBL	M182-3M	1:1000	4°C O/N
OPTN	Rabbit	AbCam	Ab23666	1:1000	4°C O/N
Anti-mouse IgG HRP-linked antibody		CST	7076	1:1000-1:4000	1h RT
Anti-rabbit IgG HRP-linked antibody		CST	7074	1:2000-1:4000	1h RT

2.9 Luciferase Reporter Assay for AU-Rich Element mRNA-Mediated Decay

A luciferase assay developed by Corcoran, Khaperskyy, & McCormick (2011) was used to determine impact of selective autophagy receptors on KapB- or MK2EE-induced ARE-mRNA stabilization. HeLa Tet-Off cells were transduced with recombinant lentivirus expressing a NS shRNA or an shRNA targeting NDP52, OPTN or p62. Following selection, 10^5 HeLa Tet-Off cells were seeded into a 12-well plate. 24h later, cells were co-transfected with a reaction mix as follows: 90 ng pTRE2 Firefly Luciferase ARE, 10 ng pTRE2 Renilla Luciferase, 900 ng of pcDNA (+) 3.1, pcDNA KapB BCBL or pcDNA FLAG-MK2EE diluted in 50 µL Opti-MEM supplemented with 3 µL of Fugene HD Transfection Reagent (Promega). 36h post transfection, DOX (1 µg/mL)

(Sigma-Aldrich) was added to cells to inhibit *de novo* transcription of the Firefly Luciferase ARE and Renilla Luciferase. 12h later cells were lysed in 200µL of 1X passive lysis buffer (Dual Luciferase Assay Kit, Promega) and were rocked for 15 min at RT before freezing at -20°C until further use. Lysates were processed according to the manufacturer's instructions (Dual Luciferase Assay Kit, Promega) and a GloMax 20/20 luminometer (Promega) was used to determine the Firefly and Renilla luciferase luminescence (expressed as relative light units [RLUs]) of each sample. The Firefly RLUs was normalized to the Renilla RLUs to account for differences in transfection efficiency and results are expressed as relative luciferase activity. The mean fold change in the relative luciferase activity of samples relative to controls was calculated to express changes between samples in ARE-mRNA stabilization.

2.10 Quantitative PCR

Cells were lysed for total RNA according to the manufacturer's instructions (RNeasy Mini Kit, Qiagen) and stored at -80°C until further use. The QIAshredder (Qiagen) and the RNeasy Mini Kit (Qiagen) were used to extract total RNA from samples; extracted RNA was stored at -80°C until further use. RNA concentration was determined and depending on total RNA harvest, between 100 ng and 1 µg of total RNA was reverse transcribed using Maxima H Minus First Strand cDNA Synthesis Kit (Thermo Fisher) using a combination of random and oligo (dT) primers according to the manufacturer's instructions. cDNA was diluted 1:5 for all qPCR reactions. qPCR reaction mixes were assembled in duplicate as follows: 5uL qPCR GoTaq qPCR Master Mix (Promega), 0.2 µM forward primer, 0.2 µM reverse primer, 4 µL of diluted cDNA, up to 10µL nuclease free water. Reaction mixes were subjected to the following qPCR cycling

conditions: initial denaturation (95ºC for 3 min), 40 cycles of denaturation (95ºC for 10s), annealing and extension (58ºC for 30s), 1 cycle of final extension (65ºC for 5s followed by 95ºC for 5s).

The ΔΔquantitation cycle (Cq) method was used to determine the fold change in expression of target transcripts in one sample, relative to the expression of the target transcript in a chosen control sample as is shown below:

Fold change = $2^{-[\Delta C_{q(target\ sample)} - \Delta C_{q(control\ sample)}]}$.

The ΔCq value was determined by subtracting the mean Cq of the target gene from the mean Cq of the chosen reference gene (HPRT-1, B2M, 18S). The stable expression and efficiency of the reference genes HPRT-1, B2M and 18S was previously confirmed. qPCR primer sequences are in Table 7 and were ordered from Thermo Fisher.

Table 7: qPCR and ddPCR primer sequences

Primer	Primer Sequence
HPRT-1- Forward	5' CTTTCCTTGGTCAGGCAGTATAA 3'
HPRT-2 - Reverse	5' AGTCTGGCTTATATCCAACACTTC 3'
18S - Forward	5' TTCGAACGTCTGCCCTATCAA 3'
18S - Reverse	5' GATGTGGTAGCCGTTTCTCAGG 3'
B2M - Forward	5' TTTCCATTCTCTGCTGGATGA C 3'
B2M - Reverse	5' TGCTGTCTCCATGTTTGATGTA 3'
IL-6 - Forward	5' GAAGCTCTATCTCGCCTCCA 3'
IL-6 - Reverse	5' TTTTCTGCCAGTGCCTCTTT 3'
CXCL8 - Forward	5' AAATCTGGCAACCCTAGTCTG 3'
CXCL8 - Reverse	5' GTGAGGTAAGATGGTGGCTAAT 3'
IL-1β - Forward	5' CTCTCACCTCTCCTACTCACTT 3'
IL-1β - Reverse	5' TCAGAATGTGGGAGCGAATG 3'
TNF - Forward	5' TCGAACCCCGAGTGACAA 3'
TNF - Reverse	5' AGCTGCCCCTCAGCTTG 3'
GM-CSF - Forward	5' AAATGTTTGACCTCCAGGAGC C 3'
GM-CSF - Reverse	5' ATCTGGGTTGCACAGGAAGTT 3'
COX-2 - Forward	5' CCCTTGGGTGTCAAAGGTAA 3'
COX-2 - Reverse	5' GCCCTCGCTTATGATCTGTC 3'
VEGF - Forward	5' CGAGACCTTGGTGGACATC 3'
VEGF – Reverse	5' CTGCATGGTGACGTTGAAC 3'

2.11 Droplet Digital PCR

RNA extraction and cDNA synthesis were performed as in section 2.10. cDNAs were diluted 1:4 for reaction mixes with IL-6, CXCL8, HPRT-1 & COX-2 primers and 1:200 for reaction mixes with B2M (see Table 7 for primer sequences). A ddPCR reaction mix was produced as follows: 4 µL cDNA, 0.2 µM forward primer, 0.2 reverse primer µM, 10µL QX200 EvaGreen ddPCR Supermix (Biorad), up to 20 µL nuclease free water. 20µL of the ddPCR reaction mix was added to the sample wells of the DGE Cartridge for QX100/QX200 Droplet Generator (Bio-Rad) and 65 µL Droplet Generation Oil for EvaGreen (Bio-Rad) was added to the appropriate oil wells of the cartridge. The cartridge was loaded into the QX200 Droplet Generator to partition the cDNA into oil emulsion droplets. The oil droplets were transferred to a 96-well plate (Eppendorf) and the plate was sealed with a Pierceable Foil Heat Seal (Bio-Rad) using the PX1 PCR Plate Sealer (180°C for 6s). PCR amplification on the droplets was completed using the C1000 Touch instrument (Bio-Rad) as follows: initial denaturation and Taq activation (95ºC for 5 min), 50 cycles of denaturation (95ºC for 30s), annealing (58°C for 1 min) and extension (72ºC for 1 min), a signal stabilization step (4°C for 5 min followed by 90°C for 5 min) and a final hold at 4°C. The ramp rate was 2°C/s. After PCR, plates were loaded into QX200 Droplet Reader (Bio-Rad) for detection.

The absolute concentration of each target transcript present in the sample (copies/µL) is calculated by modelling the data as a Poisson distribution where:

$$\text{Copies of transcript per sample/µL} = -\ln(1-P)$$

$$P = \frac{\text{number of positive droplets}}{\text{total number of droplets}}$$

To achieve data normalisation the following method was used:

$$\text{Normalized sample amount (NSA)} = \frac{\text{copies of transcript of interest in sample}}{\text{copies of reference transcript in sample}}$$

$$\text{Fold change in expression} = \frac{\text{NSA of sample of interest}}{\text{NSA of control sample}}$$

This method allows the determination of the fold change in expression of a target transcript of one sample relative to a chosen control sample.

2.12 Flow Cytometry

Treated cells were washed twice with PBS, and isolated by centrifugation for 5 min at 500G. Cells were resuspended in either neutral flow cytometry buffer (1× PBS, 1 mM EDTA, 1% HI-FBS, 25 mM HEPES, final pH 7.3–7.5) or acidic flow cytometry buffer (1× PBS, 1 mM EDTA, 1% HI-FBS, 25 mM HEPES, final pH 5). DAPI (200 ng/mL) was added to each sample as a viability marker. Cells resuspended in the acidic flow cytometry buffer were incubated for ~20 min prior to flow cytometry analysis.

Cells were analyzed by flow cytometry using the LSR Fortessa (BD Biosciences), at least 100,000 events were counted for each condition using the laser excitations and emission optical filter sets described in Table 8. Flow cytometry and compensation was performed by Derek Rowter or Renee Raudonis (Flow Cytometry Facility, Dalhousie University). Cell doublets were excluded from further analysis using the forward (FSC) and side scatter (SSC) measurements. Each condition was subsequently gated for double positive neutral and acidic mKeima-expressing cells that were DAPI-negative. In brief, as seen in Lazarou et al., (2015) & Nezich, Wang, Fogel, & Youle (2015), a gate was set to determine the percent of cells displaying high acidic mKeima expression relative to that seen in the vehicle control for each mKeima construct (see section 2.12.1 and Figure 2.2

for more detail). Gating analysis was completed using FCS express 6 Plus Research Edition (De Novo Software).

Table 8: Optical filter excitations and emissions for detecting mKeima-constructs

	Filter Number	Peak Excitation (nm)	Peak Emission (nm)
Neutral mKeima-detecting filters	1	405	605
	2	405	650
	3	405	610
Acidic mKeima-detecting filters	4	532	610
	5	532	660
	6	628	670
DAPI-detecting filter	**7**	405	460

2.12.1 Optimization of Optical Filters to Detect Neutral and Acidic mKeima fluorescence

HEK293T cells were transfected with mKeima-LC3 to determine which optical excitation and emission filters to use for the optimal detection of neutral vs. acidic mKeima-LC3. 48h post transfection, cells were collected in either a pH 7 flow cytometry buffer or in a pH 5 flow cytometry buffer. mKeima-LC3 cells collected at pH 7 were expected to emit mainly neutral mKeima signal while cells collected at pH 5 were expected to emit an increase in acidic signal. Subsequently, three optical filters meant to detect neutral mKeima fluorescence and three intended to detect acidic fluorescence were tested using the mKeima-LC3 cells (see specifications in Figure 2.2).

Cells were plotted in a density plot such that the fluorescence intensity for filters detecting neutral and acidic mKeima were on the x- and y-axis respectively (such as in Figure 2.1B). Doublets were removed from the cell populations and a gate for mKeima-expressing cells was applied to each cell population. For each filter set tested, an arbitrary

gate was set to define the percent of cells expressing a high acidic to neutral mKeima signal ratio using cells collected in the pH 7 buffer (example gate shown in Figure 2.2B; filter set combinations shown in Figure 2.2D). Most cells in this population should have low acidic and higher neutral mKeima signal thus, most of these cells were excluded when creating the gate to identify cells with a high acidic to neutral mKeima fluorescence ratio (hereafter referred to as the high acidic mKeima signal gate) (Figure 2.2B-C). The same gate created for mKeima-LC3 cells collected in the pH 7 buffer was applied to cells collected in the pH 5 buffer. A cell population shift towards and up the Y-axis (intended to detect acidic mKeima fluorescence) indicates an increase in the number of cells with a high acidic to neutral mKeima expression ratio.

For each filter set combination tested, the percent of cells in the high acidic mKeima gate (pH 5) was normalized to the percent of cells in the high acidic mKeima gate (pH 7) (Figure 2.2C). Of the filter combinations tested, three displayed > 20-fold change in the percent of cells detected in the high acidic mKeima signal gate between cells collected in neutral buffer and cells collected in acidic buffer (red boxes, Figure 2.2D). The combination of filters 3 and 5 displayed the largest fold increase in the percent of cells with high acidic mKeima signal (23-fold) and was used in all future experiments to detect changes in neutral and acidic mKeima signal.

2.13 Statistical Analysis

N refers to the number of biologically independent experiments conducted and is noted in the figure legends where appropriate. Experimental data was analyzed using GraphPad Prism 8.0 software. A two-tailed one-sample Student's t-test was used to determine statistical significance for data analyzed by comparing the mean fold change in

expression of one sample to another sample. A two-way analysis of variance (ANOVA) with a post hoc Tukey multiple comparison's test was used to determine the statistical significance of data analyzed by comparing sample means. Statistical significance was determined as $p < 0.05$.

Figure 2.2: Flow cytometer optical filter optimization for detecting neutral and acidic mKeima. (A) Schematic of the mKeima excitation and emission spectrum. Arrowheads denote where on the spectrum the parameters of the optical filters intended to detect neutral mKeima (1-3) and acidic mKeima (filter 4-6) are located. (B-C) HEK293T cells were transfected with mKeima-LC3. 48h post transfection, mKeima-LC3 cells were suspended in a pH 7 or pH 5 flow cytometry buffer. Cells were subjected to live-cell flow cytometry (LSR Fortessa) using combinations of optical filters intended to detect the neutral and acidic mKeima fluorescence intensity of cells. (B) Example of cell gating to detect cells expressing high acidic mKeima signal. Cells were plotted in a density plot such that the fluorescence intensity for filters detecting neutral mKeima and acidic mKeima were on the x-axis (Filter 3) and y-axis respectively (Filter 5). A gate was set to determine percent of cells expressing a high acidic mKeima signal for the mKeima-LC3-expressing cells collected in pH 7 flow cytometry buffer and the same gate was applied to cells collected in the pH 5 flow cytometry buffer. This gate is indicated by the blue line. (C-D) The percent of cells expressing high acidic mKeima was determined for all the filter set combinations indicated for cell populations collected in both the pH 7 and the pH 5 buffer. Comparing the same filter sets combination (e.g. filter 3 and 5), the percent of cells present within the high acidic mKeima detection gate for cells collected in the pH 5 buffer was normalized to the percent of cells in the high acidic mKeima detection gate for cells collected in pH 7 buffer. (D) The three filter combinations with the highest fold change in the percent of cells detected in the high acidic mKeima signal gate between cells collected in a pH 7 buffer and cells collected in a pH 5 buffer are indicated in red boxes.

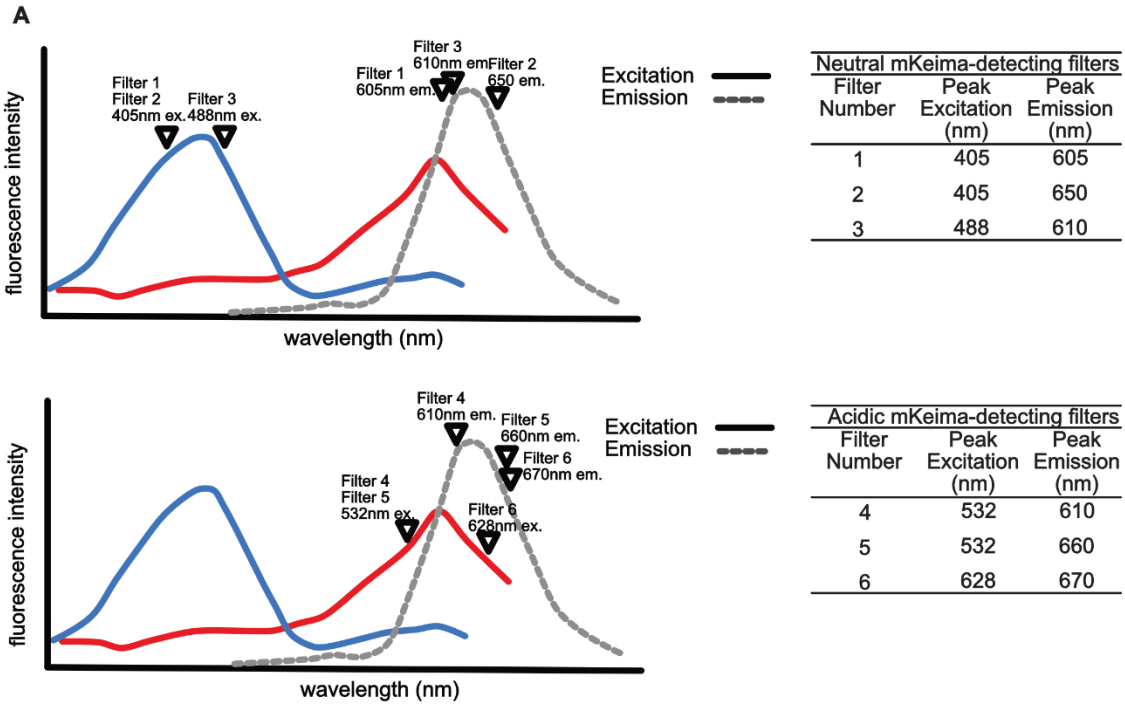

Neutral mKeima-detecting filters

Filter Number	Peak Excitation (nm)	Peak Emission (nm)
1	405	605
2	405	650
3	488	610

Acidic mKeima-detecting filters

Filter Number	Peak Excitation (nm)	Peak Emission (nm)
4	532	610
5	532	660
6	628	670

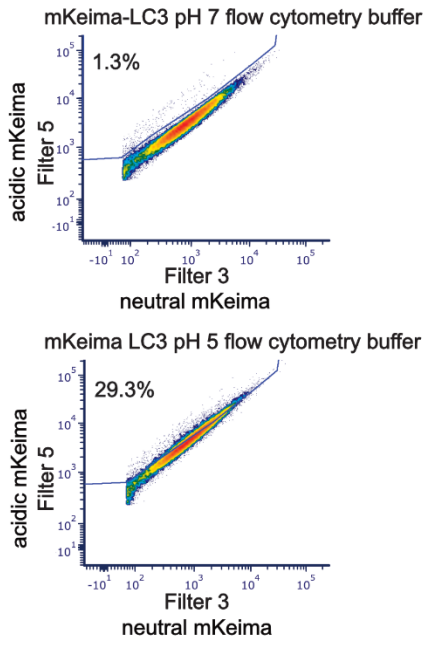

C e.g. detection of neutral and acidic mKeima with Filters 3 & 5

pH 7 flow cytometry buffer - 1.3% cells expressing high acidic mKeima signal

↓

set to 1 = 1.3% / 1.3%

pH 5 flow cytometry buffer- 29.3% of cells expressing high acidic mKeima signal

↓

Normalize to % of cells in high acidic mKeima gate in pH 7 collection condition

↓

22.5 fold increase in % cells with high acidic mKeima signal = 29.3% / 1.3%

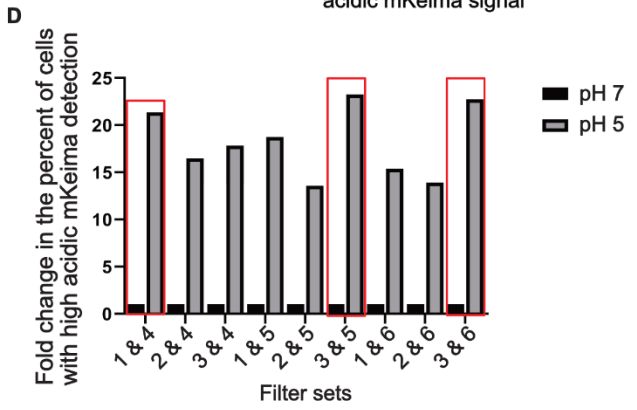

Chapter 3 Development of a Fluorescence-Based Method to Monitor Selective Autophagy

3.1 PB Proteins DCP1A, Pat1B and XRN1 are Not Degraded by the Proteasome

Recent evidence from our lab showed that KapB upregulates autophagy and that autophagy is required for PB disassembly. Among this evidence included the observation that steady-state levels of some PB-resident proteins responded to changes in autophagic flux. To confirm and extend these observations, I investigated whether PB protein levels were regulated by the proteasome. An alternative to autophagy, the proteasome is a major quality control pathway responsible for targeted protein turnover (Ji & Kwon, 2017). To investigate whether PB proteins were degraded by the proteasome or by autophagy, I treated HUVECs with the autophagy inducer Torin, the late-stage autophagy inhibitors, bafilomycin and chloroquine, a combination of an autophagy inducer and late-stage inhibitor (Torin and bafilomycin) and a proteasome inhibitor (MG-132) for 4h prior to lysis for immunoblotting of PB proteins and p62.

p62 steady-state levels inversely correlate with autophagic flux; therefore, I used p62 immunoblotting to monitor autophagic flux and confirm the efficacy of autophagy modulating drugs in this experiment (Mizushima, Yoshimori & Levine, 2010). As expected, Torin treatment slightly decreased p62 indicating increased autophagy induction, whereas treatment with either bafilomycin or chloroquine resulted in p62 accumulation indicating that the final degradative step of autophagy was blocked (Figure 3.1A). The combination treatment of Torin and bafilomycin caused the largest

accumulation of p62 (approximately 8-fold). This result is interpreted as follows: the Torin treatment increased autophagic flux and increased the accumulation of p62 in autophagosomes; however, bafilomycin treatment inhibited the fusion of autophagosomes with the autolysosomes thereby preventing the degradation of accumulated p62 (Figure 3.1A). MG-132 treatment was not predicted to impact p62 levels, but a 2-fold accumulation of p62 was detected indicating that this length or concentration of MG-132 treatment may induce autophagy (Figure 3.1A).

Since I predicted that PB proteins were degraded through autophagic flux, I expected their steady state levels to decrease after Torin treatment and increase with bafilomycin, chloroquine or a combination of Torin and bafilomycin treatment, in a manner similar to p62. The steady-state levels of Pat1B remained unchanged with all drug treatments indicating that the steady-state levels are not subject to rapid degradation via either autophagy or the proteasome (Figure 3.1B). By contrast, the combined Torin/bafilomycin treatment caused a 2.5-fold increase in the steady-state levels of XRN1, suggesting that XRN1 may be degraded by autophagic machinery. Bafilomycin, chloroquine and the combination Torin/bafilomycin treatment caused a substantial accumulation of DCP1A (Figure 3.1B). Of note, none of the PB proteins displayed increased steady-state levels when the proteasome was inhibited by with MG-132 treatment, indicating that Pat1B, XRN1 and DCP1A are unlikely to be subject to proteasomal turnover. Together, these data support the hypothesis that select (but not all) PB proteins are subject to turnover via the autophagy machinery.

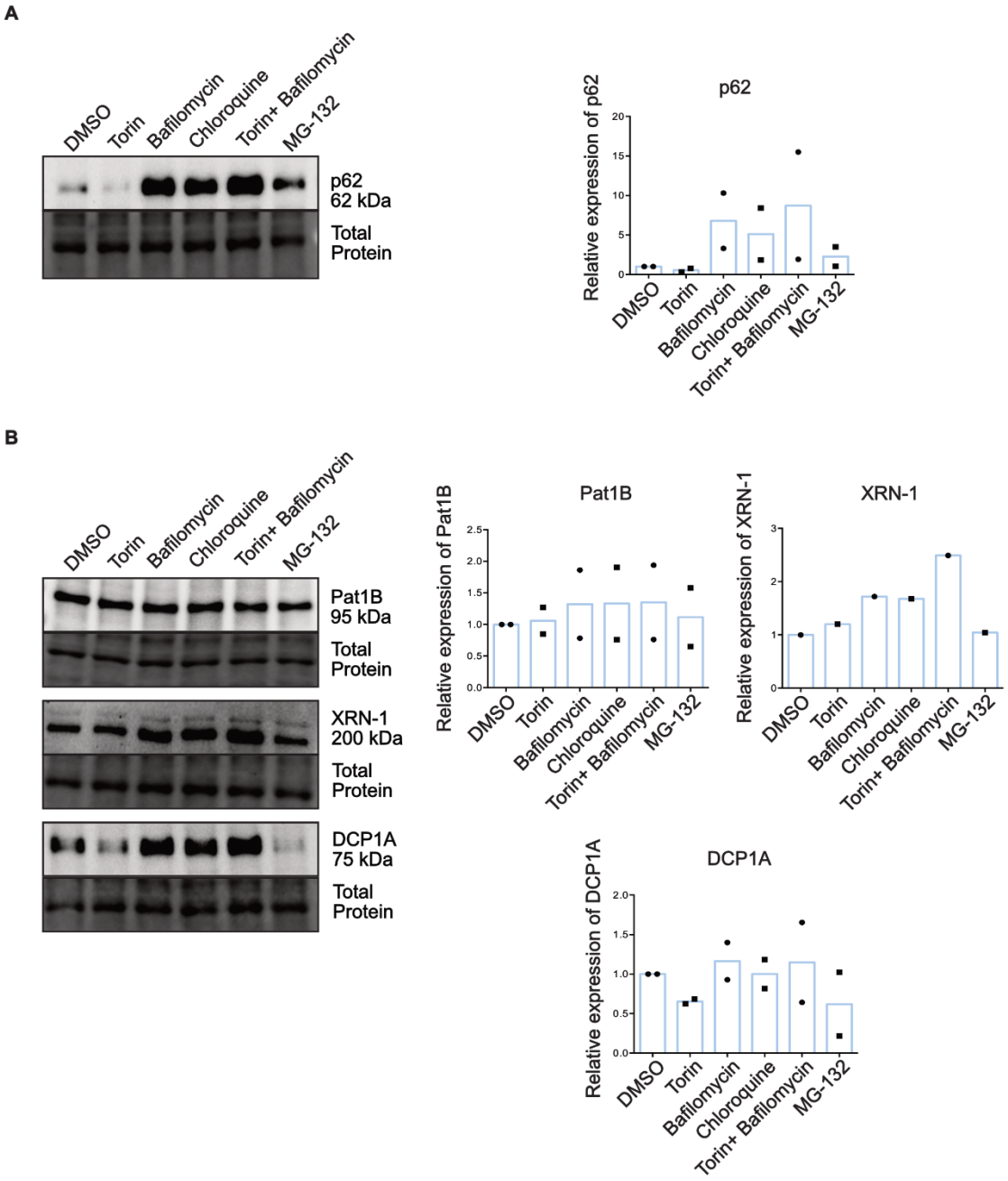

Figure 3.1: Proteasome inhibition does not cause increases in PB protein steady-state levels. (A-B) HUVECs were treated with a DMSO vehicle or one or more of the following drugs for 4h: Torin (250 nM), bafilomycin (10 nM), chloroquine (25 μM), or MG-132 (5 μM). Following treatment, cells were lysed and immunoblotted using primary antibodies against p62 (A) or Pat1B, XRN1 and DCP1A (B). Protein band intensity was normalized to total lane protein using Bio-Rad Image Lab software and is expressed as the mean fold change in expression relative to DMSO (p62, PAT1B and DCP1A; n=2) (XRN1; n=1).

3.2 Autophagy Induction Increases Steady-state levels of CXCL8 and COX-2

We know that steady-state levels of some PB proteins are regulated by autophagy, and that PBs are important for the constitutive decay of cellular ARE-containing mRNAs. Therefore, one of the first experiments I performed was to determine if the steady-state levels of mRNA encoding selected endogenous ARE-containing genes were altered in response to changes in bulk autophagic flux. To manipulate macroautophagy, HUVECs were treated with Torin and bafilomycin for 4h prior to lysis for total RNA (Carolyn Robinson performed the experiment while I performed that RNA analysis). The low yield of RNA from this lot of HUVECs made ddPCR the ideal technique for this experiment. Following RNA extraction and cDNA synthesis, ddPCR was used to determine the relative expression of COX-2 and CXCL8 as these transcripts contain AREs and are upregulated during KS. Torin treatment increased the expression of COX-2 and CXCL8 by 8- and 9- fold, respectively (Figure 3.2). Bafilomycin treatment had no significant effect on COX-2 or CXCL8 expression (Figure 3.2). Because Torin-induced macroautophagy increased the expression of endogenous inflammatory ARE-mRNAs, COX-2 and CXCL8, this supports our hypothesis that autophagic flux contributes to regulating levels of ARE-containing inflammatory transcripts. With the preliminary data to suggest that KapB increases autophagy to facilitate PB disassembly and elevate levels of ARE-mRNAs, I expanded my investigation to determine if KapB-induced PB loss, and concomitant ARE-mRNA stabilization, was selective.

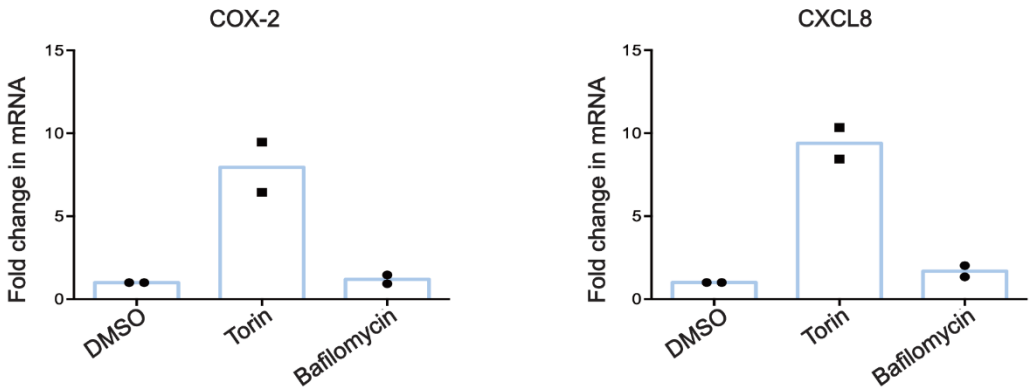

Figure 3.2: Autophagy induction increases expression of endogenous ARE-mRNAs. HUVECs were treated with DMSO vehicle control, Torin (250nM) or bafilomycin (10nM) for 4h prior to lysis for total RNA. 200 ng of total RNA was reverse-transcribed and amplified by ddPCR. The copies/µL of CXCL8 and COX-2 were normalized to the reference gene, B2M. Data is represented as the fold change in target transcript expression relative to DMSO; n=2.

3.3 mKeima: A Fluorescence-Based Method to Monitor Autophagic Flux

Methods including the LC3-turnover assays and the mRFP-GFP-LC3 tandem reporter fail to consider rates of selective autophagic flux as they focus entirely on the modification of bulk autophagic component, LC3 (Klionsky et al., 2012). Moreover, the addition of mRFP and GFP to LC3 causes probe aggregation outside of autophagosomes and may impact the function of the protein (Hu et al., 2015; Katayama, Kogure, Mizushima, Yoshimori, & Miyawaki, 2011). Although GFP-fragmentation assays can be adapted to monitor the lysosomal delivery of many substrates, the assay is not robust in mammalian cells (Klionsky et al., 2012). Consequently, there are few-existing assays that can compare the autophagic activity of different selective autophagy cargoes at a single time point or over time and no assays developed to investigate PB protein autophagic degradation.

We know that autophagy is required for KapB-mediated PB disassembly because inhibition of bulk autophagy (using drug treatments or knockdown of canonical autophagy genes) reverses the KapB-mediated PB loss. However, these assays do not differentiate between two possibilities: 1) KapB induces a non-selective increase of autophagic flux functionally equivalent to macroautophagy or 2) KapB selectively recruits PBs or PB components to the autophagosome to cause their selective catabolism independent of other cytosolic cargo. I sought to differentiate between these possibilities by developing a fluorescence-based method to determine whether PB proteins are selectively degraded under KapB expression. To do this I used the coral-derived fluorophore mKeima (Kogure et al., 2006).

mKeima is an acid stable, pH-sensitive fluorophore that exhibits a bimodal excitation spectrum (Katayama et al., 2011; Kogure et al., 2006). Under neutral pH, the fluorophore has a peak excitation at 440 nm (em. 620 nm) while under an acidic pH (pH 5) the excitation peak shifts to 586 nm (em. 620 nm), due to the ionization of a phenolic hydroxyl moiety present in mKeima (Katayama et al., 2011; Violot, Carpentier, Blanchoin, & Bourgeois, 2009) (Figure 3.3A). This pH-dependent shift in mKeima excitation can be an advantage, as mKeima excitation can differentiate between different autophagy stages and track mKeima fluorophore movement from the neutral cytosol/ autophagosome to the acidic autolysosome (Katayama et al., 2011) (Figure 3.3B).

Under homeostatic conditions, mKeima is subject to autophagic degradation. This is detected by an increase in the fluorophore excitation fluorescence at 586 nm (hereafter referred to as acidic mKeima signal) relative to the fluorophore excitation fluorescence at 440 nm (hereafter referred to as neutral mKeima signal), and this ratio of acidic/neutral mKeima signal represents basal autophagic flux. Autophagy induction (starvation, Torin) increases the delivery of mKeima to autolysosomes and therefore increases ratio of the acidic/neutral mKeima compared to homeostatic conditions (Katayama et al., 2011) (Figure 3.3B). The simultaneous autophagy induction and late-stage autophagy inhibition (Torin and bafilomycin treatment) increases autophagy induction, but also prevents delivery of cargo to acidic autolysosomes. Therefore, cells with this treatment did have decreased acidic mKeima signal detection relative to that detected with autophagy induction alone (Katayama et al., 2011).

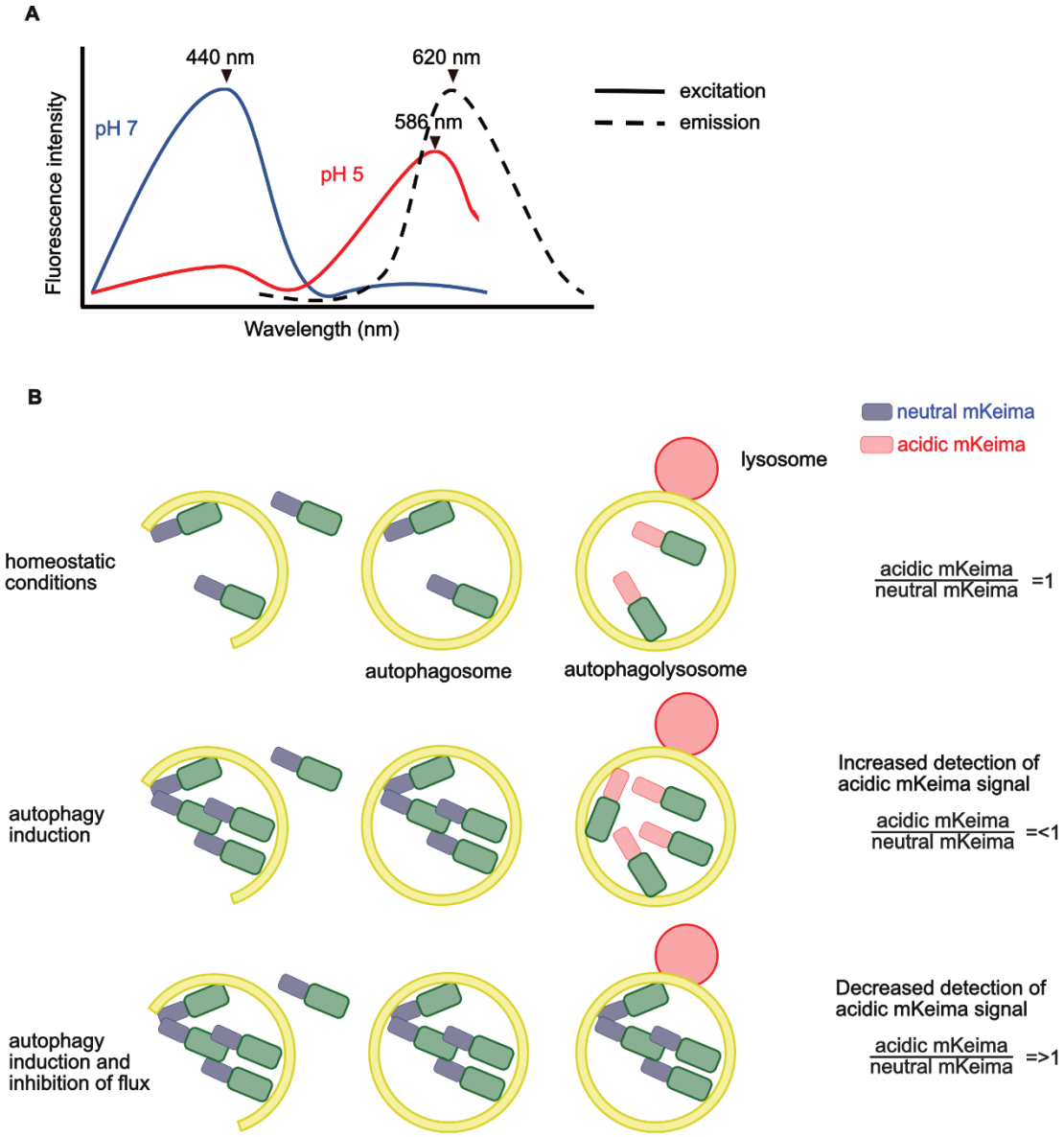

Figure 3.3: Fluorescence-based detection autophagic flux changes using mKeima. (A) Adapted from Katayama et al., (2011). mKeima is a pH-sensitive fluorophore that exhibits a bimodal excitation. At neutral pH, the fluorophore has a peak excitation at 440 nm (em. 620 nm). At an acidic pH, the excitation peak shifts to 586 nm (em. 620 nm). (B) The pH-dependent shift in excitations allows the monitoring of autophagic flux with mKeima by comparing the detection of neutral vs. acidic mKeima fluorescence. Autophagosomes and cytosolic cargo are in a neutral environment, whereas cargo in an autolysosome is in an acidic environment. Under homeostatic conditions, detection of both neutral and acidic mKeima represents normal turnover of the mKeima-containing construct. Autophagy inducer addition (Torin) is expected to increase the detection of acidic mKeima signal. Autophagy inducer and late-stage autophagy inhibitor (Torin/ bafilomycin) is expected to decrease acidic mKeima signal detection relative to the signal present with autophagy induction.

In addition to using the mKeima protein alone to monitor bulk autophagy, the fusion of mKeima to other target proteins allows the acidic exposure of those proteins to be monitored and compared to that of a macroautophagy reporter such as mKeima-LC3 (H. An & Harper, 2017; Katayama et al., 2011). Several groups have monitored mitophagy using a mitochondria-targeted mKeima (mito-mKeima) construct; in this case, mKeima has been fused to a COX VIII pre-sequence that targets the mKeima to the mitochondrial inner membrane (Lazarou et al., 2015; Nezich et al., 2015; N. Sun et al., 2017; Villa et al., 2017). To capitalize on this method to understand PB turnover, I created two mKeima PB reporters by tagging the resident PB proteins DCP1A or DDX6 with mKeima (mKeima-DCP1A, mKeima-DDX6). To fully understand how PB catabolism may or may not differ from the regulation of macroautophagy or mitophagy, I generated a macroautophagy reporter, LC3-mKeima and obtained a mitophagy reporter, mito-mKeima. Together, these four mKeima fusion proteins allowed me to investigate if KapB expression increases non-selective macroautophagy or if it increases the selective autophagy of PB proteins.

3.4 mKeima Fusion Proteins Show Appropriate Sub-Cellular Localization by Confocal Microscopy

As a first step towards building this new assay, I validated the subcellular localization of my four mKeima reporter constructs using confocal microscopy of fixed cells. Cells were transfected with mKeima-DCP1A, mKeima-DDX6, mKeima-LC3 and mito-mKeima. 48h post transfection, cells were fixed and stained for the endogenous PB marker Hedls, lysosomal marker LAMP2, or mitochondrial marker TOM20. mKeima has a large stoke shift which permits the simultaneous detection of Alexa-Fluor-488 or GFP-

labelled structures (Katayama et al., 2011). mKeima-DCP1A and mKeima-DDX6 displayed punctate cytoplasmic fluorescence consistent with staining for PB granules previously observed and constructs co-localized with endogenously labelled Hedls (Figure 3.4). mKeima-LC3 colocalized with the endogenous lysosomal marker LAMP2, suggesting that LC3-mKeima was being trafficked to the lysosome. Mito-mKeima co-localized with endogenous TOM20, validating the appropriate mitochondrial localization (Figure 3.4).

Several methods including microscopy, flow cytometry and immunoblotting have been employed to quantify changes in acidic mKeima excitation however, all of these assays must be conducted on live cells because fixation alters cell pH and causes loss of pH gradients across lysosomal membranes (Katayama et al., 2011). Therefore, I used live-cell confocal microscopy to determine whether I could detect both a neutral and acidic mKeima-signal for each fusion protein construct and if this signal was visually responsive to altered autophagic flux. HEK293T cells were transfected with mKeima-DCP1A, mKeima-DDX6, mKeima-LC3 or mito-mKeima. 24h later, cells were treated with DMSO vehicle control or one or more of the following: Torin (250 nM), bafilomycin (10 nM), the electron transport chain uncoupler, CCCP (10 μM) for 24h or NH_4Cl, to neutralize acidic compartments (50 mM), for 1h prior to imaging. The LSM 510-laser scanning confocal microscope was configured to detect neutral and acidic mKeima signal (section 2.7.1). mKeima-LC3 construct expression was relatively robust (Figure 3.5). Control mKeima-LC3 cells expressed low baseline mKeima fluorescence that was detectable on the acidic channel while Torin treatment substantially increased

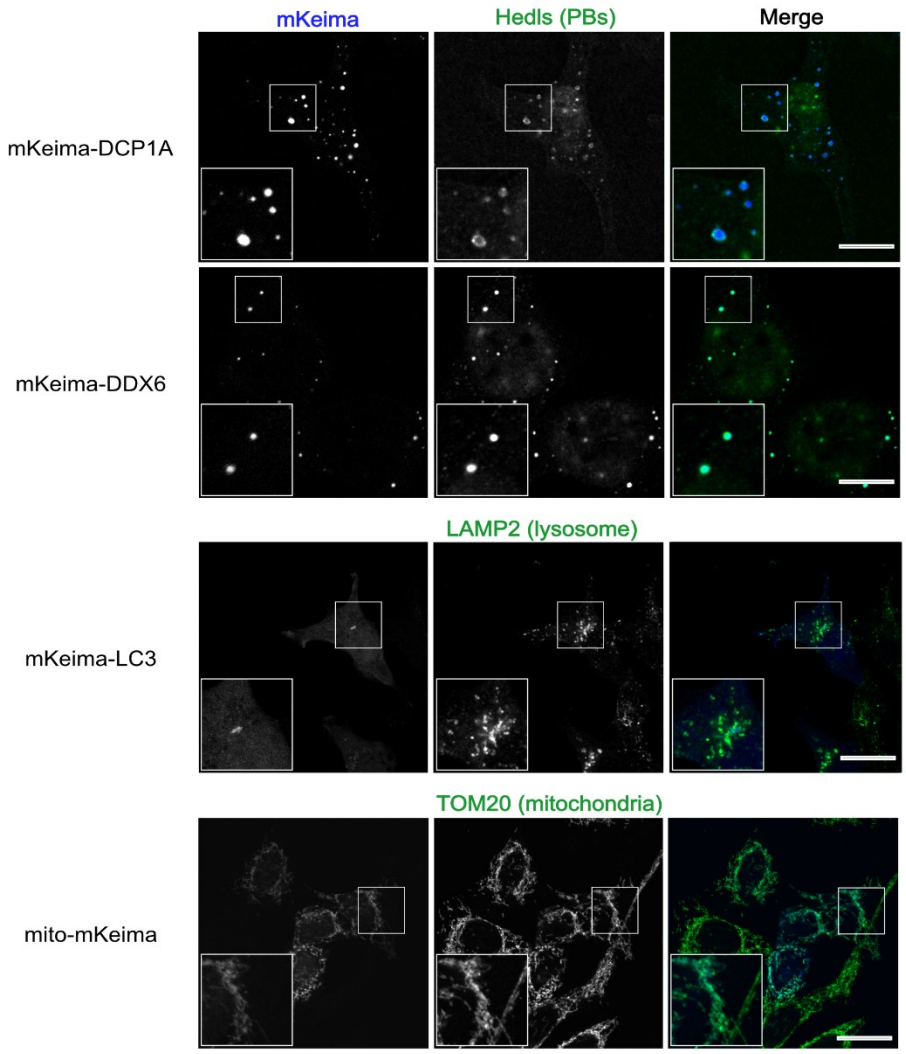

Figure 3.4: mKeima fusion proteins demonstrate appropriate sub-cellular localization. HEK293T cells were transfected with mKeima-DCP1A, mKeima-DDX6, or mKeima-LC3 and HeLa Tet-Off cells were transfected with mito-mKeima. 48h post transfection cells were fixed for immunofluorescence. Cells were stained with primary antibodies for endogenous Hedls (PBs), LAMP2 (lysosomes) or TOM20 (mitochondria). Images for each condition were taken using the Zeiss LSM 510 Meta configured to detect mKeima and Alexa Fluor 488-labelled Hedls, LAMP2 or TOM20. Scale bar = 10 µM.

the mKeima detection on the acidic channel (Figure 3.5). Conversely, cells treated with Torin and bafilomycin reduced the amount of acidic channel mKeima detected relative to cells treated with Torin alone (Figure 3.5). These results indicate that the mKeima-LC3 construct responds as expected to autophagy modulating drugs.

Control mito-mKeima-transfected cells expressed a high baseline of acidic mKeima fluorescence (Figure 3.6). Treatment with CCCP, which uncouples the electron transport chain and stimulates mitophagy, did not increase mKeima signal detected in the acidic channel in my experiments (Georgakopoulos et al., 2017; J. W. Park et al., 1997; Penefsky, 1985). However, treatment with CCCP followed by NH_4Cl reduced mKeima fluorescence detected in both the neutral and acidic channels (Figure 3.6). Upon close examination, these cells were rounded, and mitochondria were fragmented, suggesting cells were not healthy (Figure 3.6). These data confirm that mitophagy can be visualized using mito-mKeima and suggest that HEK293T cells have a high baseline of mitophagy. Furthermore, a combination of mitophagy stimulating drugs or different drug doses may be necessary to detect differences in mitophagy in mito-mKeima-expressing cells.

mKeima-DCP1A-transfected cells formed punctate cytoplasmic mKeima-DCP1A granules as previously seen in Figure 3.4, but granules were not detected on the acidic mKeima channel in DMSO vehicle control cells (Figure 3.7). After Torin treatment, mKeima puncta were detected on the acidic channel but the overall signal was very low and difficult to detect (Figure 3.7). This result did not change in mKeima-DCP1A cells treated with Torin and bafilomycin, although there appeared to be more mKeima-DCP1A granules detected with the neutral mKeima channel in cells treated with Torin and bafilomycin (Figure 3.7).

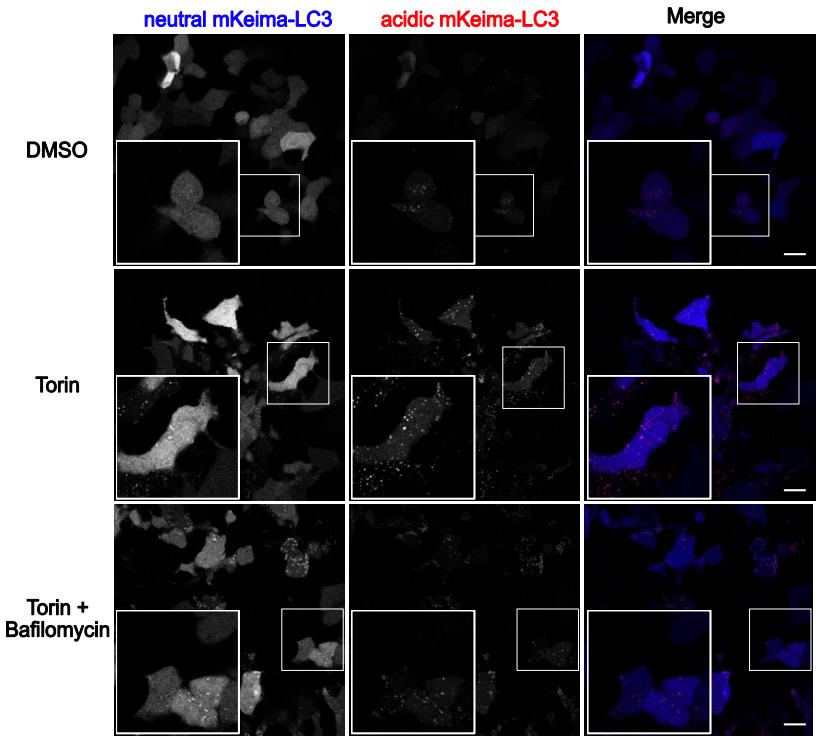

Figure 3.5: mKeima-LC3 reporter responds to changes in autophagic flux. HEK293T cells were transfected with mKeima-LC3 and the construct was expressed for 24h before treatment with DMSO vehicle control and one or more of the following: Torin (250 nM), bafilomycin (10 nM) for 24h prior to imaging. Cells were imaged within 10 mins of removal from a cell culture incubator and representative images for each condition were taken using the Zeiss LSM 510 Meta configured to detect neutral and acidic mKeima. Images are representative from two independent experiments. Scale bar = 20 μM.

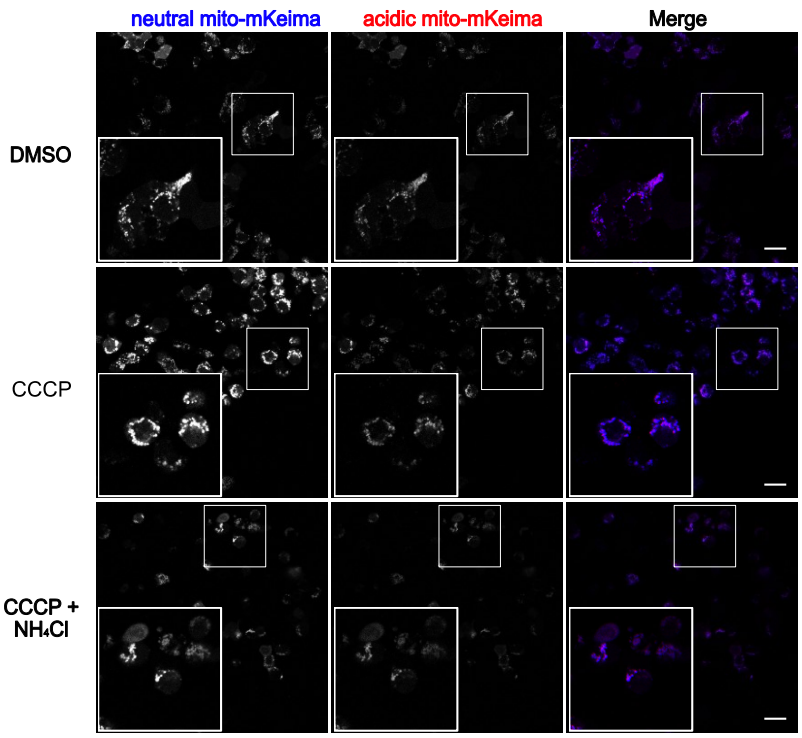

Figure 3.6: Mitophagy detection using a mito-mKeima reporter. HEK293T cells were transfected with mito-mKeima and the construct was expressed for 24h before treatment with a DMSO vehicle control or one or more of CCCP (10µM for 24h) or NH_4Cl (50m M for 1h). Cells were imaged as in Figure 3.5. Images are representative of two independent experiments. Scale bar = 20 µM.

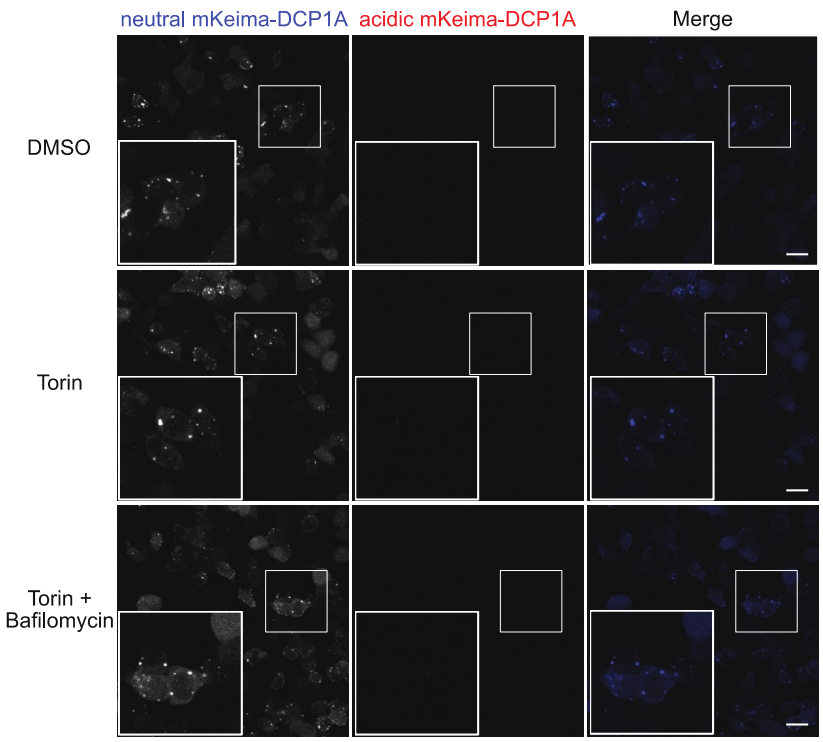

Figure 3.7: mKeima signal detection in cells expressing mKeima-DCP1A. HEK293T cells were transfected with mKeima-DCP1A and the construct was expressed for 24h before treatment and imaging as in Figure 3.5. Images are representative from two independent experiments. Scale bar = 20 μM.

mKeima-DDX6-transfected cells formed fewer puncta than that seen in mKeima-DCP1A cells but similarly, very little mKeima-DDX6 signal was detected in the acidic channel in control cells (Figure 3.8). With Torin treatment, many cells displayed mKeima-DDX6 puncta detectable in the acidic channel and the number of cells with these puncta decreased in frequency during Torin and bafilomycin treatment (Figure 3.8). These preliminary results suggest the mKeima-DDX6 reporter responds to Torin treatment by re-localizing to acidic compartments and may be undergoing autophagic degradation.

mKeima signal was detected for all reporter constructs on the neutral channel and mKeima signal on the acidic channel could be detected for mKeima-LC3, mito-mKeima and mKeima-DDX6. Katayama et al., (2009) used live-cell microscopy images to quantify the ratio of acidic and neutral mKeima expression to total cellular area for individual cells. However, due to difficulties controlling the cell environment and the limited number of cells that can be imaged, I decided to use flow cytometry to quantify changes in the number of cells expressing high acidic mKeima signal and confirm the responsiveness of the constructs to changes in autophagy.

3.5 Validating Responsiveness of mKeima-Constructs to Autophagy-Modulating Drugs via Flow Cytometry

Using flow cytometry to monitor mKeima has several advantages, including its amenability to high throughput applications and the large number of cells that can be analyzed. Furthermore, several groups have successfully used flow cytometry to demonstrate the responsiveness of the mito-mKeima acidic-channel fluorescence to changes in mitophagy (Lazarou et al., 2015; Nezich et al., 2015)

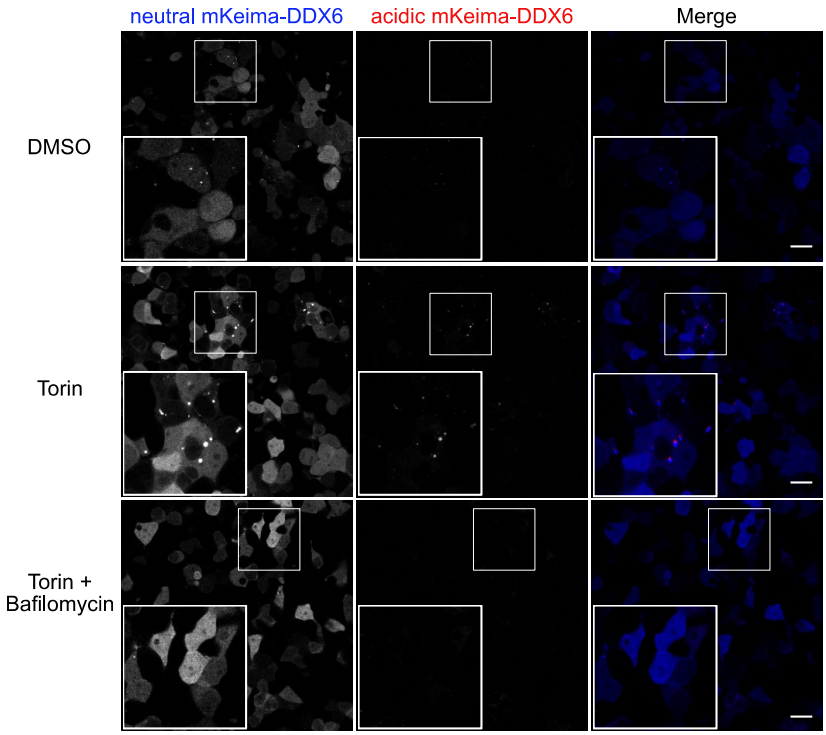

Figure 3.8: Acidic mKeima signal detected in DDX6-mKeima reporter cells. HEK293T cells were transfected with mKeima-DDX6 and the construct was expressed for 24h before treatment and imaging as in Figure 3.5. Images are representative from two independent experiments. Scale bar = 20 µM.

Having determined the appropriate optical filter settings to best detect changes in mKeima acidification, I validated the responsiveness of the mKeima reporter constructs to autophagic modulators and quantified these changes using flow cytometry (see section 2.12 for optical filter optimization experiment). HEK293T cells were transfected with mKeima-LC3, mito-mKeima, mKeima-DCP1A or mKeima-DDX6. Constructs were expressed for 36h prior to treatment with DMSO vehicle or one or more of the following: Torin, bafilomycin, CCCP, oligomycin for 6h prior to cell collection for flow cytometry. Control cells for all constructs were expected to have low acidic mKeima signal; therefore, most of these cells were excluded when assigning the arbitrary gate to detect cells with high acidic mKeima signal for each construct (Figure 3.9 and 3.10).

Based on my microscopy results and previous publications using mito-mKeima, I expected mKeima-LC3 and mito-mKeima to show increased acidification with Torin and CCCP & oligomycin treatment, respectively, and for this acidification to be inhibited by bafilomycin treatment. In mKeima-LC3 control cells, 2% of cells were within the high acidic mKeima gate; after Torin treatment, this value significantly increased to 7.4% (Figure 3.9A-B). mKeima-LC3 cells treated with Torin and bafilomycin had only 0.67% of cells in the high acidic mKeima gate; a significant decrease relative to Torin treatment alone (Figure 3.9A-B). 3.2% of mito-mKeima control cells were detected in the high acidic mKeima gate (Figure 3.9A-B). This was the highest value of any construct in the control condition but, this result is consistent with mito-mKeima microscopy data (see Figure 3.6). For mito-mKeima flow cytometry experiments, both CCCP & oligomycin treatment were used to stimulate mitophagy and overall increased the number

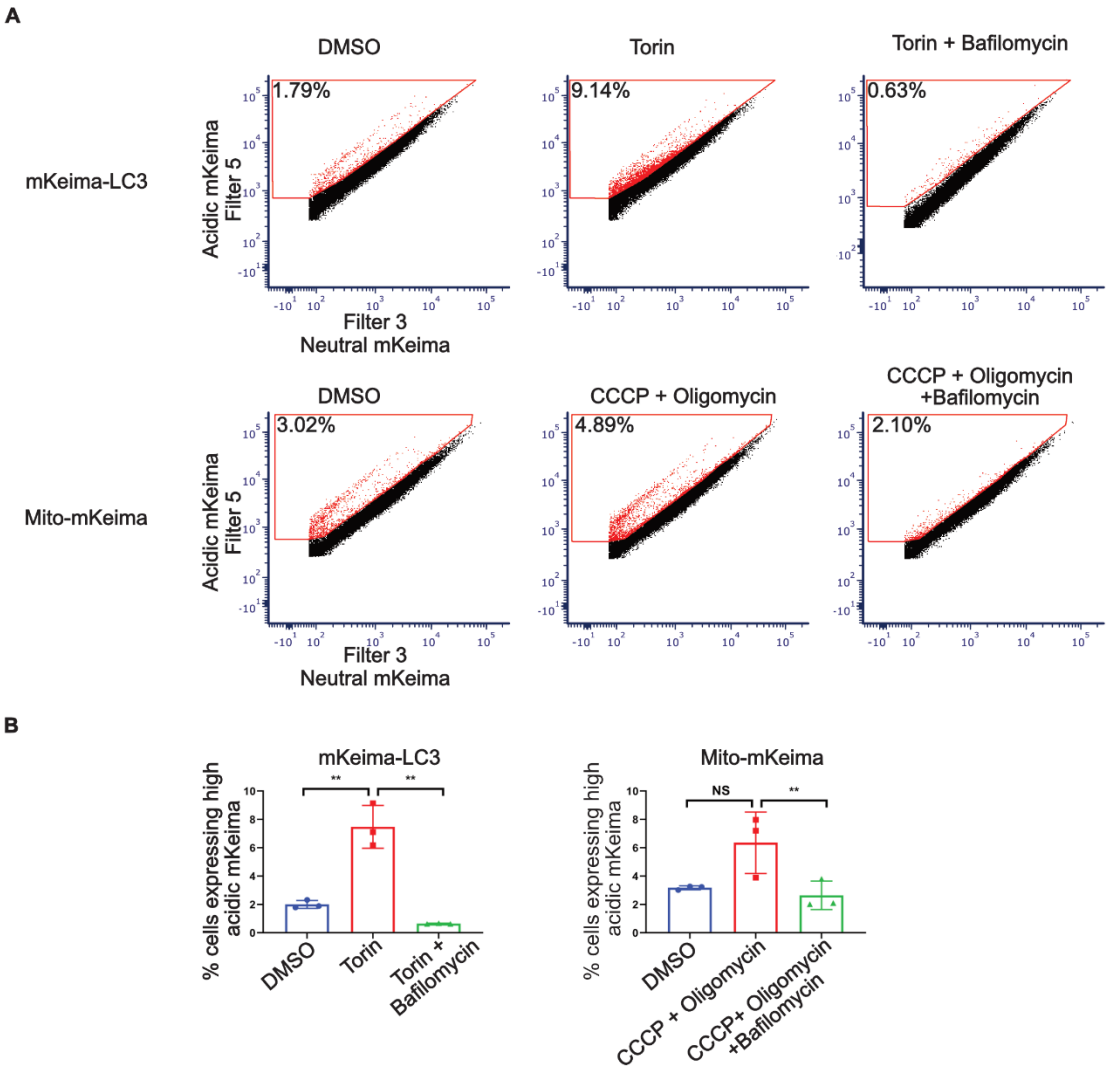

Figure 3.9: mKeima reporter constructs respond to altered autophagic and mitophagic flux. HEK293T cells were transfected with mKeima-LC3 or mito-mKeima. 42h post transfection, cells were treated with DMSO or one or more of the following: Torin (250 nM), bafilomycin (100 nM), CCCP (10 µM), oligomycin (1 µg/mL) for 6 h prior to suspension in pH 7 flow cytometry buffer. Live-cell flow cytometry was used to detect the neutral and acidic mKeima fluorescence intensity of cells (LSR Fortessa). (A) Cells from each condition were plotted in a dot plot such that the fluorescence intensity for filters detecting neutral mKeima and acidic mKeima were on the x-axis (Filter 3) and y-axis respectively (Filter 5). An arbitrary gate for the percent of cells expressing high acidic mKeima was set using the vehicle control condition for each construct and subsequently applied to all other conditions for that construct. The cells that fall within this gate are labelled in red. Representative dot plots are shown from one of three independent experiments (B) The mean percent of cells expressing high acidic mKeima signal are quantified for each condition of each construct ± SEM. Statistical significance of was data determined by two-way repeated measures ANOVA with Tukey's multiple comparison test; * = $P<0.05$ **= $P<0.01$.

of cells detected in the high acidic mKeima gate to 6.4% of the cell population (Figure 3.9). Relative to CCCP & oligomycin treatment, treatment with CCCP & oligomycin & bafilomycin significantly decreased the percent of cells in the high acidic mKeima gate to a mean of 2.6% (Figure 3.9). Notably, for both mKeima-LC3 and mito-mKeima expressing populations, there is a small group of cells with high acidic mKeima fluorescence separated from the main population in the DMSO control and Torin conditions, however in both cases, treatment with bafilomycin expunges this population (Figure 3.9A). Overall, autophagic-modulating treatments of cells expressing the mKeima-LC3 or mito-mKeima constructs showed dynamic and mainly significant changes in the percent of cells detected in the acidic mKeima gate set for each construct.

DMSO control mKeima-DCP1A and mKeima-DDX6 cells both exhibited a mean of 1.3% of cells detected in the high acidic mKeima gate (Figure 3.10). Torin treatment slightly, but significantly, increased the percent of mKeima-DCP1A and mKeima-DDX6 cells detected within this gate to 2.8% and 3.5% respectively and treatment of mKeima-DCP1A and mKeima-DDX6 cells with Torin and bafilomycin significantly decreased the percent of cells detected in the high acidic mKeima gate to 0.8% and 1.0% respectively (relative to Torin treatment alone; Figure 3.10). The magnitude of change in the percent of cells entering the high acidic mKeima gate in response to Torin was greater for cells expressing mKeima-LC3 and mito-mKeima than for those expressing the PB-mKeima reporters. Nonetheless, these results indicate both mKeima-DCP1A and -DDX6 do undergo a small but significant increase in the percent of cells detected in the high acidic mKeima gate in response to Torin and this increase is inhibited with bafilomycin. Thus, supporting the hypothesis that autophagic flux promotes PB disassembly.

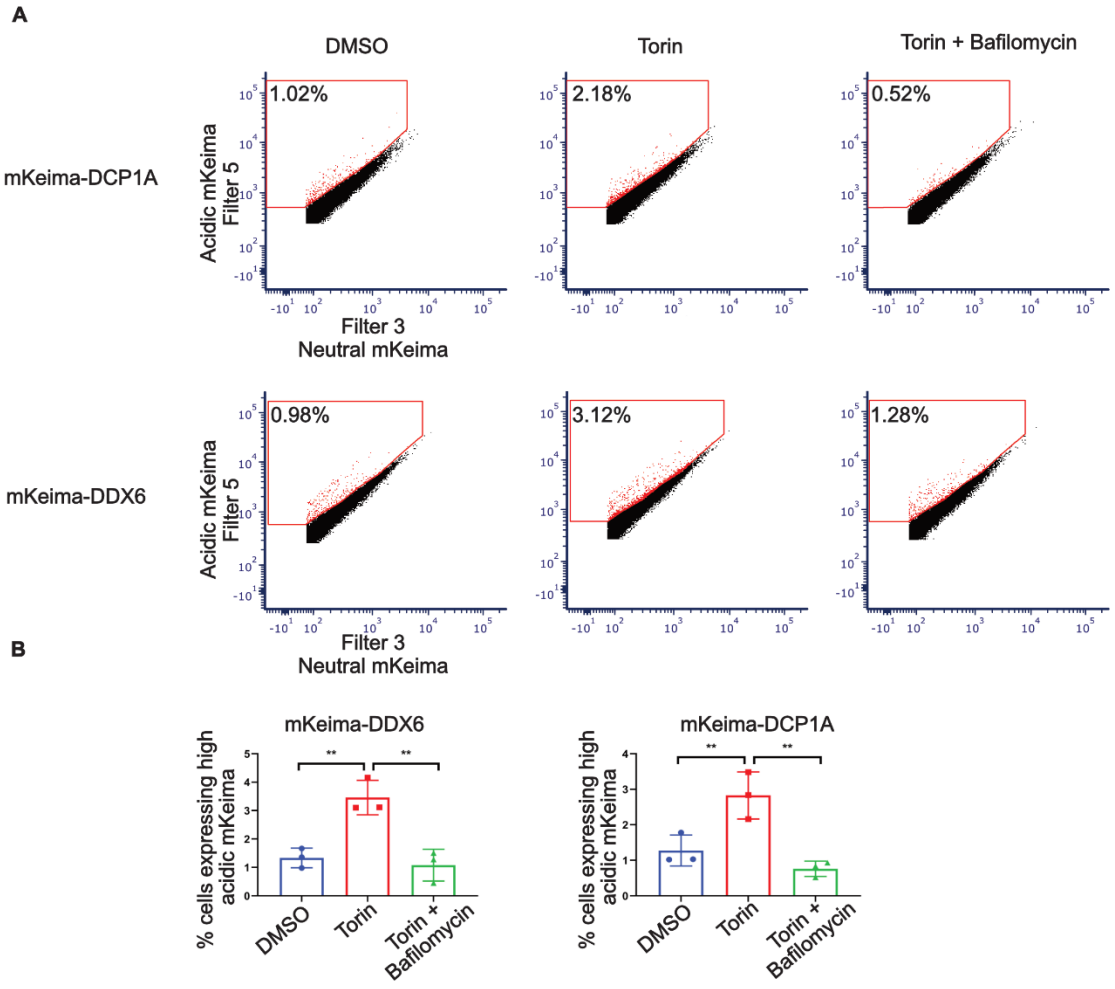

Figure 3.10: mKeima-DDX6 and mKeima-DCP1A reporters respond to changes in autophagic flux. HEK293T cells were transfected with mKeima-DCP1A or mKeima-DDX6. 42h post transfection, cells were treated and suspended as in Figure 3.9. Live-cell flow cytometry was used to detect the neutral and acidic mKeima fluorescence intensity of cells (LSR Fortessa). (A) Cells from each condition were plotted and gated as in Figure 3.9. Representative dot plots are shown from one of three experiments (B) The mean percent of cells expressing high acidic mKeima signal are quantified for each condition of each construct ± SEM. Statistical significance of data was determined by two-way repeated measures ANOVA with Tukey's multiple comparison test ; * = $P<0.05$ **= $P<0.01$.

3.6 KapB Expression Does Not Cause Detectable Changes in mKeima Construct Acidification

Having confirmed that all mKeima constructs show varying degrees of responsiveness to changes in autophagic flux, I next examined whether KapB impacted the turnover of the mKeima reporters. I hypothesized that if KapB was causing an increase in the selective degradation of PBs or PB proteins, KapB expression would cause an increase in the percent of cells with high acidic mKeima expression for PB reporter constructs and mKeima-LC3 but not mito-mKeima. This result would indicate a selective response for PB degradation independent of other cytosolic cargo. To investigate this hypothesis, I co-transfected HEK293T cells with vector or KapB and one of the following: mKeima-LC3, mito-mKeima, mKeima-DDX6, mKeima-DCP1A. 36h post transfection, cells were treated with Torin for 6h to enhance any small changes in mKeima acidification that could be induced by KapB expression. Cells were harvested and subjected to flow cytometry as previously described. Arbitrary gates detecting cells with high acidic mKeima signal were set as previously described in vector control cells and then applied to KapB-expressing cells for each construct.

Co-transfection of KapB or vector controls into the HEK293T cells greatly reduced the number of cells expressing mKeima constructs (Figure 3.12). For all constructs tested, there was no substantial difference in mKeima expression between vector and KapB cells (Figure 3.12). Given our previous results showing KapB increases autophagic flux, these preliminary results suggest that this method may not be sensitive enough to detect KapB-mediated changes in mKeima acidification or that KapB

transfection efficiency was too low to produce a discernable population change in autophagic flux.

Due to the difficulty detecting changes in the population of mKeima after KapB transfection, I attempted another method to assay mKeima turnover after KapB expression. mKeima immunoblotting has been previously used to study ribophagy (H. An & Harper, 2017). mKeima is acid-stable; consequently, mKeima-fusion proteins are only partially degraded in the lysosome and a 25kDa degradation resistant mKeima polypeptide called 'processed mKeima' appears. Immunoblotting can detect this processed mKeima form and the processed mKeima reflects how much of a given mKeima construct was delivered to autolysosomes (H. An & Harper, 2017; Katayama et al., 2011; Yoshii & Mizushima, 2017). Normalizing the processed mKeima amount to the intact mKeima construct amount produces a ratio that reflects construct turnover. An exception to this is processed mKeima from cells expressing mKeima-LC3 which, because LC3 is autophagic machinery, not cargo, should be normalized to total protein (H. An & Harper, 2017).

HEK293T cells were co-transfected with empty vector or KapB and one of the following: mKeima-LC3, mito-mKeima, mKeima-DDX6, mKeima-DCP1A. 36h post transfection, cells were treated with Torin for 6h to induce autophagy. KapB mKeima-LC3 cells contained a 4-fold greater processed mKeima levels than vector cells, confirming our previous observations that KapB expression increases autophagic flux (Figure 3.12A). Separation between intact mito-mKeima and processed mKeima is very small because the COX VIII targeting pre-sequence of mito-mKeima is only 7kDa.

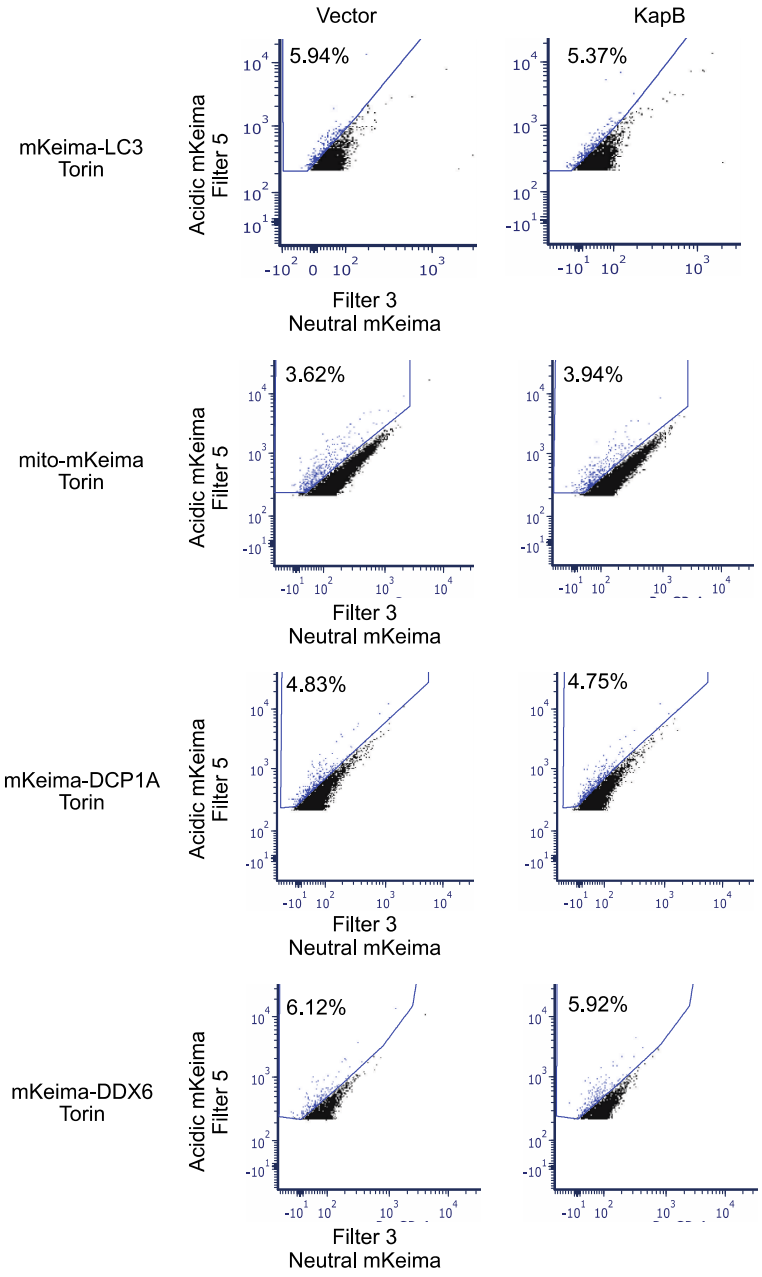

Figure 3.11: KapB expression does not cause changes in mKeima construct acidification as detected by flow cytometry. HEK293T cells were co-transfected with vector or KapB and one of following: mKeima-LC3, mito-mKeima, mKeima-DCP1A or mKeima-DDX6. 42h post transfection, cells were treated with Torin (250 nM) for 6h prior to suspension in a pH 7 flow cytometry buffer. Live-cell flow cytometry and gating was performed as in Figure 3.9; n=1.

mito-mKeima cells also had large amounts of processed mKeima relative to intact mKeima (Figure 3.12B). Cells expressing both KapB and mito-mKeima displayed less processed mKeima relative to vector cells, indicating that KapB expression does not increase mitophagy (Figure 3.12B).

The same experiments were performed with the two mKeima-tagged PB reporter proteins; however, the construct expression level was very low. Despite loading 80-100 μg of total protein, immunoblotting of DCP1A-mKeima expressing cells failed to detect any processed mKeima (Figure 3.12C). Both intact and processed mKeima-DCP1A and mKeima-DDX6 appear as doublets - it is unknown if both bands of the doublet or just one are intact or processed-mKeima (Figure 3.12C). mKeima-DDX6 expression exceeded that of mKeima-DCP1A, yet I detected only faint bands at 25kDa that may be processed mKeima. To confirm whether these faint bands were processed mKeima, I cut, re-probed and re-exposed only the lower portion of the blot expressing the putative mKeima signal; this confirmed that 25kDa bands were observed in DDX6-mKeima-expressing cells but not in DCP1A-mKeima cells. However, due to blot alteration, I was unable to quantify the relative levels of processed mKeima to intact mKeima-DDX6. Taken together, these preliminary results confirmed previous experiments to show that KapB increases autophagic flux, but has no impact on mitophagy. Finally, experiments with mKeima-tagged PB reporter constructs in the presence of KapB expression were inconclusive.

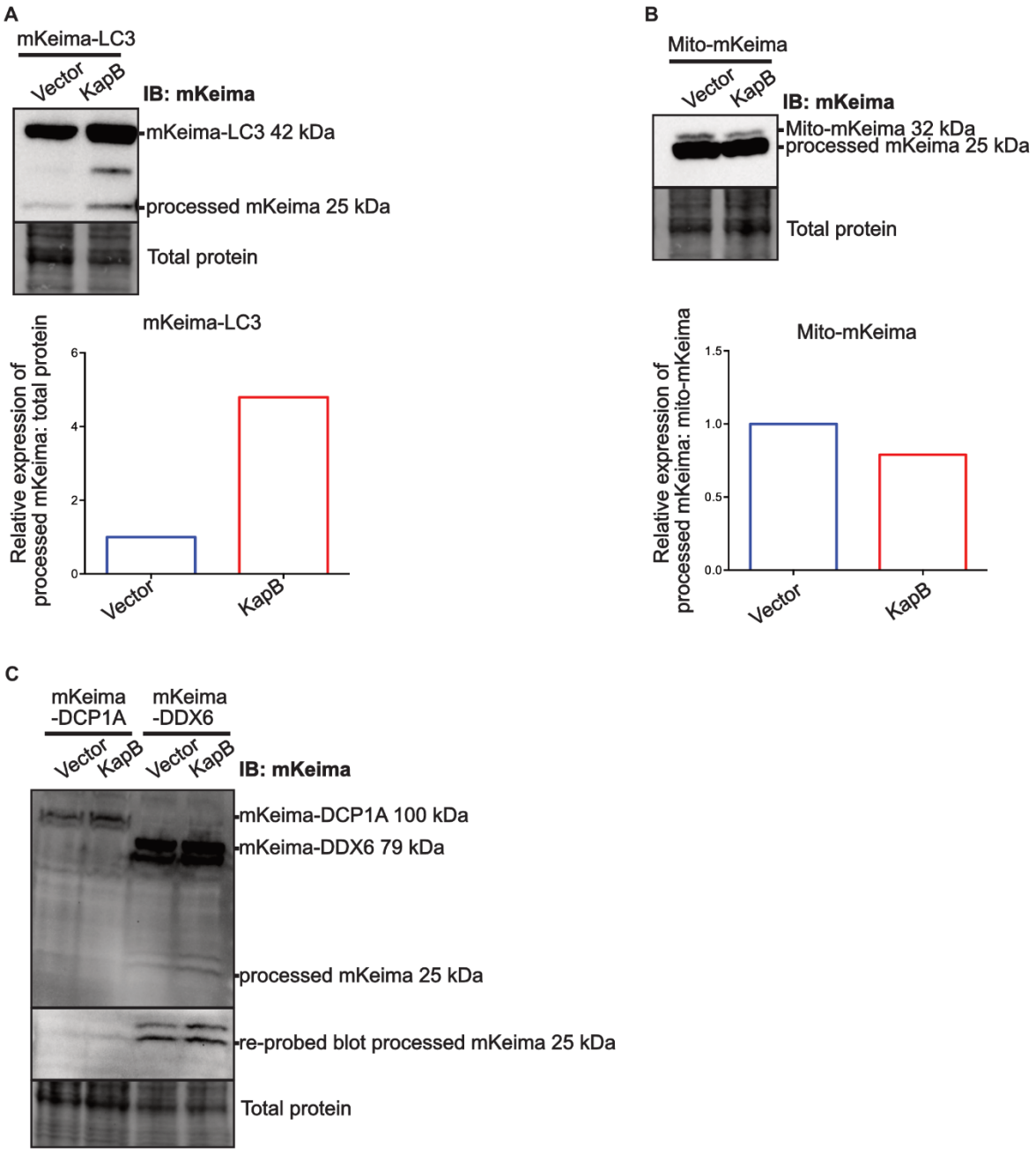

Figure 3.12: KapB increases mKeima-LC3 turnover. (A-C) HEK293T cells were co-transfected with vector or KapB and one of following: mKeima-LC3, mito-mKeima, mKeima-DCP1A or mKeima-DDX6. 42h post transfection, cells were treated with Torin (250 nM) for 6 h prior to lysis for immunoblotting. Cells were immunoblotted using primary antibody against mKeima. The intensity of the processed mKeima was normalized to the intact mKeima construct except for mKeima-LC3 cells where processed mKeima was normalized to total protein. This ratio was set to 1 for vector-transfected cells and the ratio for KapB-transfected cells was normalized to that of vector; n=1. Total protein was used as a loading control.

Chapter 4 KapB-Mediated PB Disassembly Requires NDP52

4.1 KapB-Mediated PB Disassembly Requires Selective Autophagy Receptor NDP52

To determine if known selective autophagy receptors were required for KapB-mediated PB disassembly, I designed shRNAs to reduce the steady-state expression of known selective autophagy receptors; NDP52, OPTN and p62. Subsequently, I produced recombinant lentivirus expressing the shRNAs and determined the knockdown efficiency for NDP52, OPTN and p62 in HUVECs using immunoblotting (Figure 4.1A). Analysis of knockdown efficiency was performed in parallel with phenotypic characterization (Figures 4.2 and 4.3) in all cases; therefore, I was able to determine if any result variability was due to knockdown efficiency. All shRNAs (shNDP52-1, shNDP52-2, shOPTN-1, shOPTN-2 and shp62) reduced the steady-state expression of the respective targeted protein by over 70% relative to the shNS control in vector and KapB-expressing HUVECs (Figure 4.1A-B).

For each experiment, HUVECs were sequentially transduced; first with a lentivirus expressing KapB (or vector control), and next with lentiviruses expressing selective autophagy receptor targeted shRNAs. Changes in PBs were monitored both qualitatively and quantitatively using two microscopy-based techniques: confocal microscopy for PB visualization and fluorescence microscopy for PB quantification using a PB-specific pipeline on the automated image analysis platform, CellProfiler. PBs were

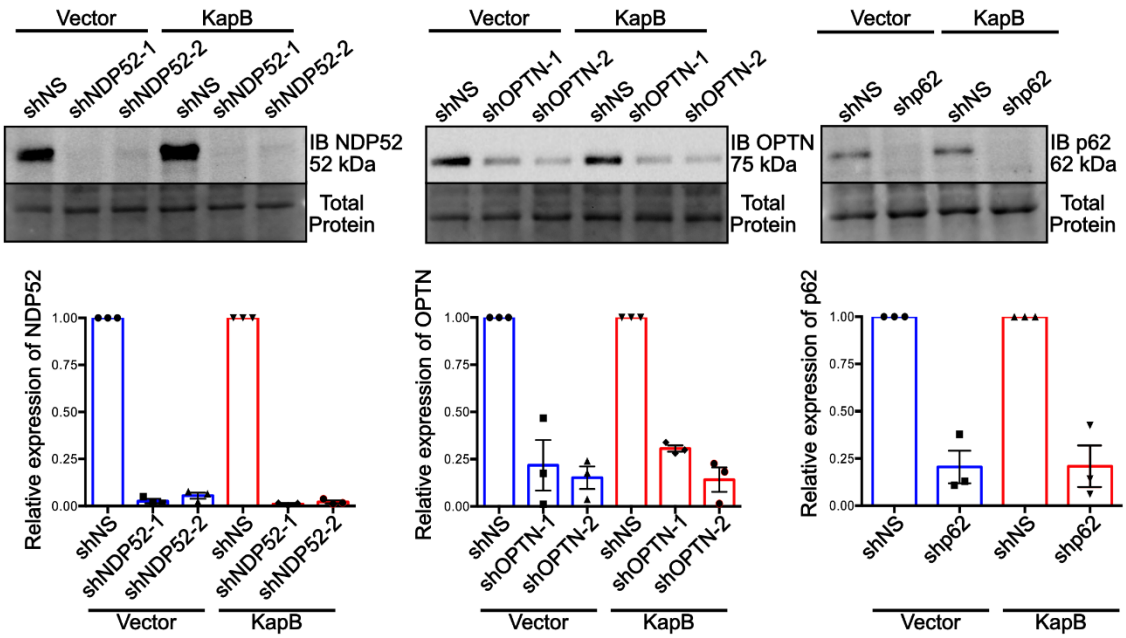

Figure 4.1: RNA interference reduces steady-state levels of selective autophagy receptors in control and KapB-expressing cells HUVECs were transduced with recombinant lentivirus expressing KapB or a vector control and were selected with bsd. After recovery, cells were re-seeded, transduced with recombinant lentivirus expressing shRNAs targeting NDP52, OPTN, p62 or a non-specific shRNA (shNS) control and selected with puro prior to lysis for immunoblotting. Lysates were immunoblotted using primary antibodies against NDP52, OPTN or p62 to confirm knockdown of the target proteins. Representative immunoblots are shown. Protein band intensity was normalized to total lane protein using Bio-Rad Image Lab software and is expressed as the mean fold change in expression relative to the respective vector or KapB shNS control ± SEM; n=3.

identified by staining for the PB resident protein Hedls, a decapping cofactor; this PB protein co-stains cytoplasmic puncta along with other PB marker proteins(S. Jain & Parker, 2013; Parker & Sheth, 2007b). My prediction was that if a selective autophagy receptor was important for PB disassembly (in either control or KapB cells), the receptor knockdown would increase the mean PB number per cell in that condition relative to the respective shNS control.

PB visualization via confocal microscopy confirmed PB presence in most vector cells (Figure 4.2A). CellProfiler quantification revealed vector cells contained 2.9 PBs per cell. Reducing vector cell NDP52 expression caused an increase in the number PB granules per cell to 9.5 (shNDP52-1) and 5.5 (shNDP52-2) and appeared to cause cellular actin rearrangement (Figure 4.2A-B).Reducing vector OPTN and p62 expression did not result in a discernable visual change in the number or size of PBs relative to vector shNS control. CellProfiler quantification supported this observation. Vector cells-expressing shOPTN-1, shOPTN-2 and shp62 contained a mean of 1.7, 2.9 and 2.6 PBs per cell respectively (Figure 4.2). Only the knockdown of NDP52 substantially increased the mean number of PBs per cell in vector cells.

As expected from previous studies (Corcoran et al., 2015), ectopic expression of KapB in HUVECs caused PB disassembly from 2.9 PBs per vector shNS cell to 1.2 PBs per KapB shNS cell (Figure 4.3). Similar to vector cells, only NDP52 knockdown caused a large increase in the mean number of PBs per cell (shNDP52-1 - 7.8; shNDP52-2 - 8.0 PBs per cell) while OPTN knockdown (shOPTN-1 - 2.1; shOPTN-2 - 2.1 PBs per cell) and p62 knockdown (2.4 PBs per cell) had little effect on the mean number of PBs per cell relative to KapB shNS (Figure 4.3).

Figure 4.2: NDP52 silencing increases the mean number of PB per cell in control cells. (A-B) HUVECs were sequentially transduced with vector control and shRNA-expressing lentiviruses and selected as in Figure 4.1, prior to fixation for immunofluorescence. (A) HUVECs were stained using primary antibodies for Hedls (PBs; red) and KapB (green) and phalloidin (F-actin; blue). Representative images for each condition were taken using the Zeiss LSM 510 Meta. Scale bar = 20 μM (B) HUVECs were stained using primary antibodies for Hedls (PBs) and KapB and WGA (to denote cellular membranes) and DAPI (nuclei). Cells were imaged on the Zeiss AxioImager Z2 (100+ cells, >5 fields of view) and the mean number of PBs per cell were quantified using an automated image analysis pipeline in CellProfiler. Data is represented as the mean number of PBs per cell per condition; n=3.

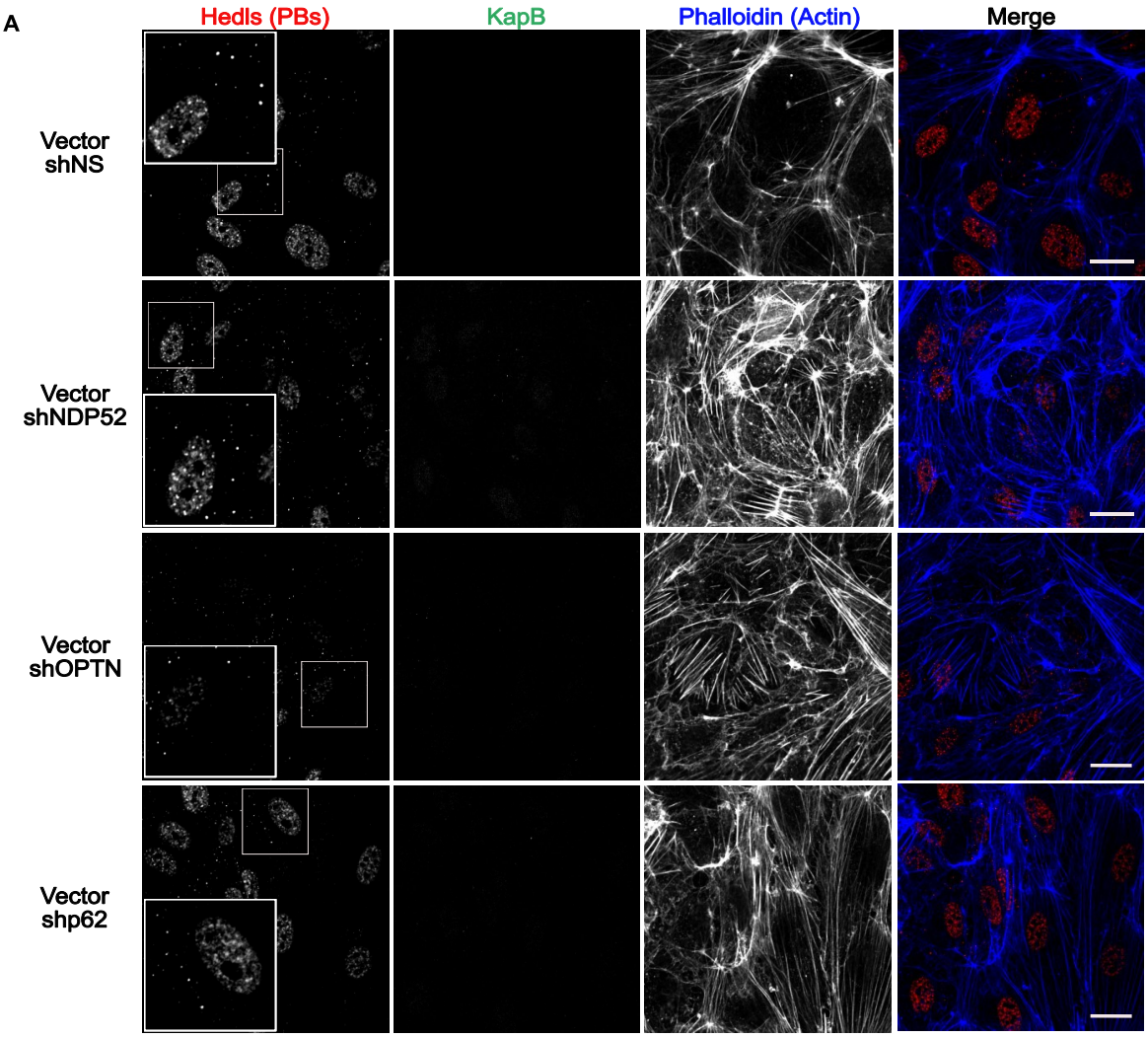
A
Hedls (PBs)
KapB
Phalloidin (Actin)
Merge
Vector shNS
Vector shNDP52
Vector shOPTN
Vector shp62
B
Vector-expressing cells
Mean number of PBs/cell
0
2
4
6
8
10
12
14
shNS
shNDP52-1
shNDP52-2
shOPTN-1
shOPTN-2
shp62

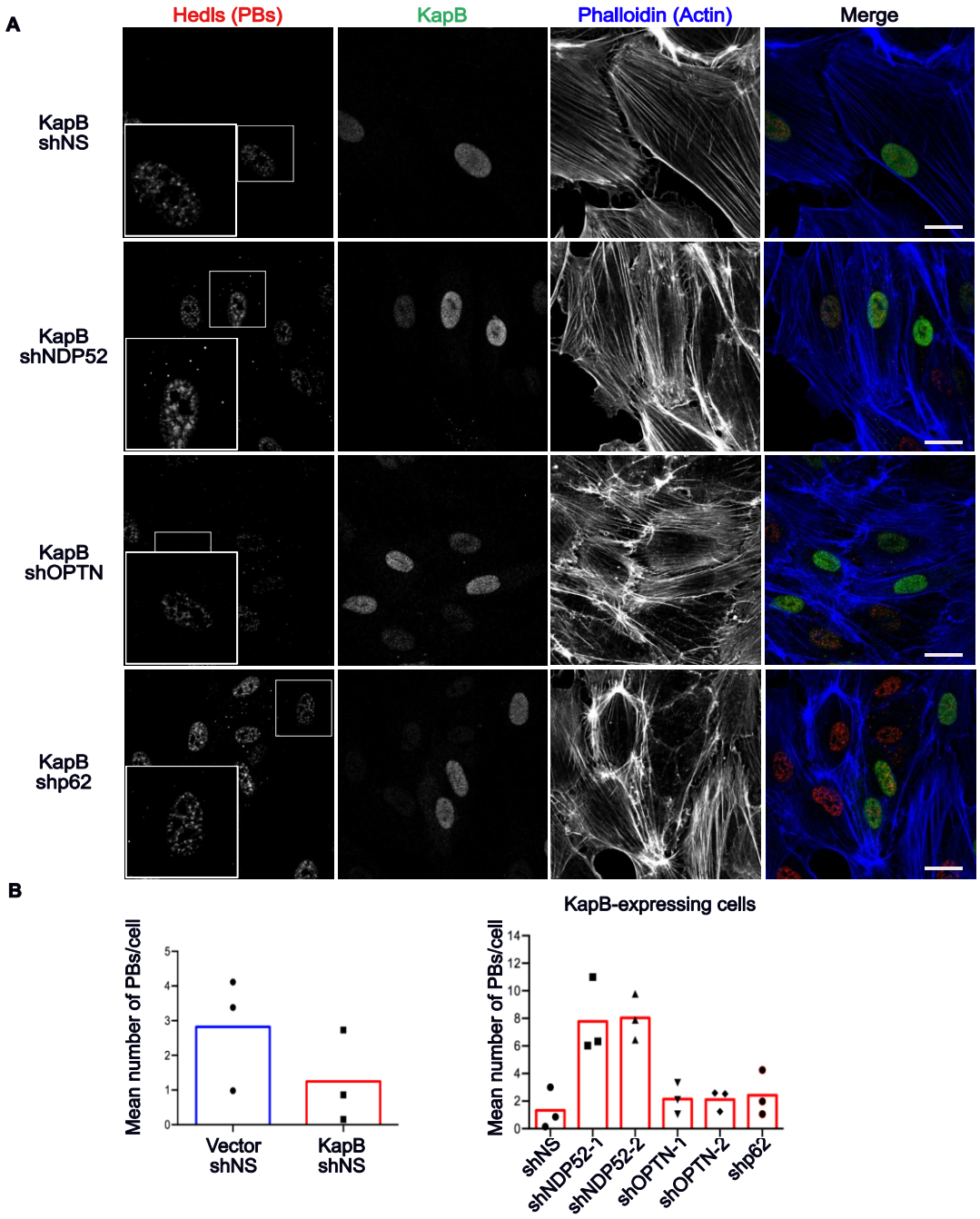

Figure 4.3: NDP52 silencing reverses KapB-mediated PB disassembly.
(A-B) HUVECs were sequentially transduced with KapB and shRNA-expressing lentiviruses and selected in parallel with control vector cells shown in Figure 4.2., prior to fixation for immunofluorescence (A) HUVECs were stained and imaged as in Figure 4.2 (A). Scale bar = 20 μM. (B) HUVECs were stained, imaged and PB numbers were quantified as in Figure 4.2. Data is represented as the mean number of PBs per cell per condition; n=3.

NDP52 silencing increased the mean number of PBs in both vector and KapB-expressing cells, demonstrating that NDP52 is required for PB disassembly and is not KapB-specific. This data identifies NDP52 as being a selective autophagy receptor that is required for PB disassembly.

NDP52 has many functions in selective autophagy, autophagosome maturation and transcription promotion (Ellinghaus et al., 2013; Fu et al., 2018; Lazarou et al., 2015; Morriswood et al., 2007; Verlhac, Gregoire, et al., 2015). To clearly elucidate if NDP52 was required because of its ability to promote selective autophagy, I decided to perform a rescue experiment using wild-type and mutated forms of NDP52. If NDP52 was acting as a selective autophagy receptor for PB proteins in KapB-expressing cells, I expected that the mean number of PBs per cell would decrease when wild-type NDP52 expression was restored, but not when selective autophagy-related NDP52 mutants were expressed.

NDP52 contains structural domains that are important for its function as a selective autophagy receptor (Figure 4.4A). These include a non-canonical LC3-C interacting region (cLIR) that binds LC3 decorating the autophagosome and a ubiquitin binding domain (UBD) that binds ubiquitinated cargo proteins, linking them to the autophagosome for engulfment (Figure 4.4A). For my studies, I obtained a UBD mutant (mCh-NDP52 C443K), a LC3-C LIR and UBD mutant; mCh-NDP52 V136S/C443K (Padman et al., 2019). I also used a NDP52 variant that predisposed individuals to developing Crohn's disease (RFP-NDP52 V248A), which is suggested to alter the activity of the UBD (Ellinghaus et al., 2013; Till et al., 2013)

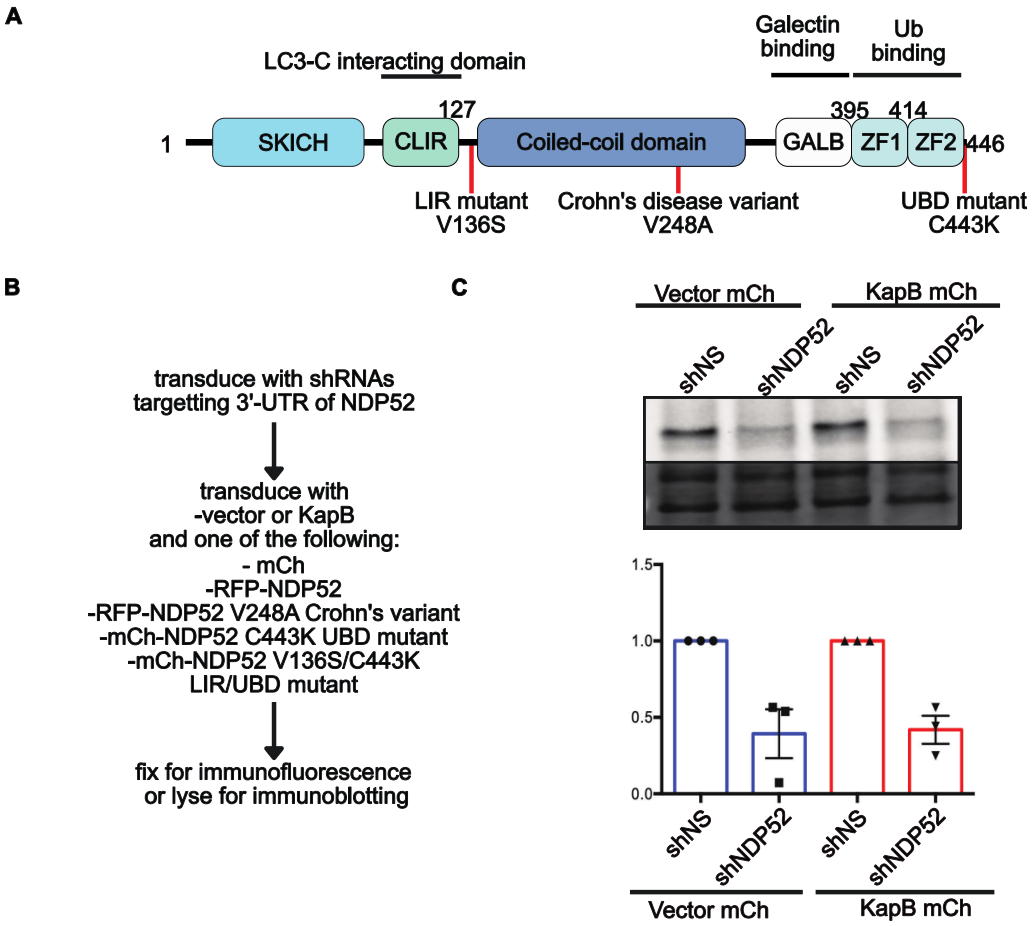

Figure 4.4: Targeting the 3'-UTR of endogenous NDP52 reduces its steady-state level. (A) NDP52 contains the following domains and interacting regions: SKICH domain (SKIP-carboxyl homology domain), CLIR (non-canonical LC3-interaction motif), coiled-coil domain, GALB (galectin binding domain) ZF1 & ZF2 (zinc finger domains). Known mutations that disrupt NDP52 function include: V136S which prevents binding to LC3-C, C443K which prevents binding to ubiquitin, and V248A (Crohn's disease variant. (B-C) HUVECs were first transduced with recombinant lentivirus expressing 2 shRNAs targeting the 3'-UTR of NDP52 (shNDP52-3, shNDP52-4) or a shNS control and were selected with bsd. Cells were seeded and co-transduced with a mixture of lentiviruses: either vector or KapB and one of the following: mCherry control (mCh), RFP-NDP52 wt, RFP-NDP52 V248A, mCh-NDP52 C443K or mCh-NDP52 V136S/C443K. Cells were recovered for 48h in complete media prior to fixation for immunofluorescence or lysis for immuoblotting. (C) Lysates were immunoblotted using NDP52 primary antibody to confirm endogenous NDP52 knockdown. Immunoblots were normalized as in Figure 4.1 and one representative blot is shown. Results are expressed as the mean fold change in expression relative to the respective vector or KapB shNS mCh control ± SEM; n=3.

For this experiment, I also had to use new shRNAs to target the 3'-UTR of NDP52 (shNDP52-3, shNDP52-4) instead of the coding region to permit the overexpression of the fluorescently-tagged NDP52 constructs. For the rescue experiment, HUVECs were transduced with shNDP52-3 and shNDP52-4 recombinant lentivirus or a shNS control, selected, and then re-seeded and transduced with a mixed population of lentiviruses: either vector or KapB *and* mCh or NDP52 constructs (Figure 4.4B). The mean knockdown efficiency of NDP52 in vector and KapB cells transduced with both shNDP52-3 and shNDP52-4 was approximately 60% relative to control shNS mCh cells (Figure 4.4C). Analysis of knockdown efficiency was performed in parallel with phenotypic characterization (Figures 4.5 and 4.6) in all cases.

Having determined the knockdown efficiency of shNDP52-3 and shNDP52-4, I investigated if NDP52 construct over-expression impacted the mean number of PBs per cell in vector and KapB cells. HUVECs were transduced as previously described and fixed for immunofluorescence (Figure 4.3) As observed in earlier experiments, NDP52 silencing increased the mean PB number per cell from 3.3 in vector control shNS mCh cells to 12.8 in vector shNDP52 mCh cells (Figure 4.5). In cells with NDP52 knockdown, the over-expression of RFP-NDP52 and the Crohn's NDP52 variant (RFP-NDP52 V248A) resulted in cells containing a mean of 11.8 and 14.6 PBs per cell respectively. Over-expression of the UBD mutant (mCh-NDP52 C443K) and the LIR/UBD mutant (mCh-NDP52 V136S/C443K) reduced the mean number of PBs per cell to 5.7 and 9.4 (Figure 4.5). In vector cells, knockdown rescue with RFP-NDP52 did not considerably reduce the number of PBs in these cells.

Figure 4.5: NDP52 over-expression does not cause PB disassembly in shNDP52 vector-expressing cells. (A-B) HUVECs were transduced and selected as in Figure 4.4 prior to fixation for immunofluorescence. (A) HUVECs were stained for immunofluorescence using a primary antibody for Hedls (PBs; green). Red cells mark successful transductions expressing an mCh control, wt. NDP52 or other constructs. Representative images for each condition were taken with the Zeiss LSM 510 Meta. Scale bar = 20 μM (B) HUVECs were stained for immunofluorescence using WGA (to denote cellular membranes), DAPI (nuclei) and a primary antibody for Hedls (PBs; green). Cells were imaged on the Zeiss AxioImager Z2 (60+ cells, >7 fields of view) and the mean number of PBs per cell were quantified using an automated image analysis pipeline in CellProfiler. Data is represented as the mean number of PBs per cell per condition; n=3.

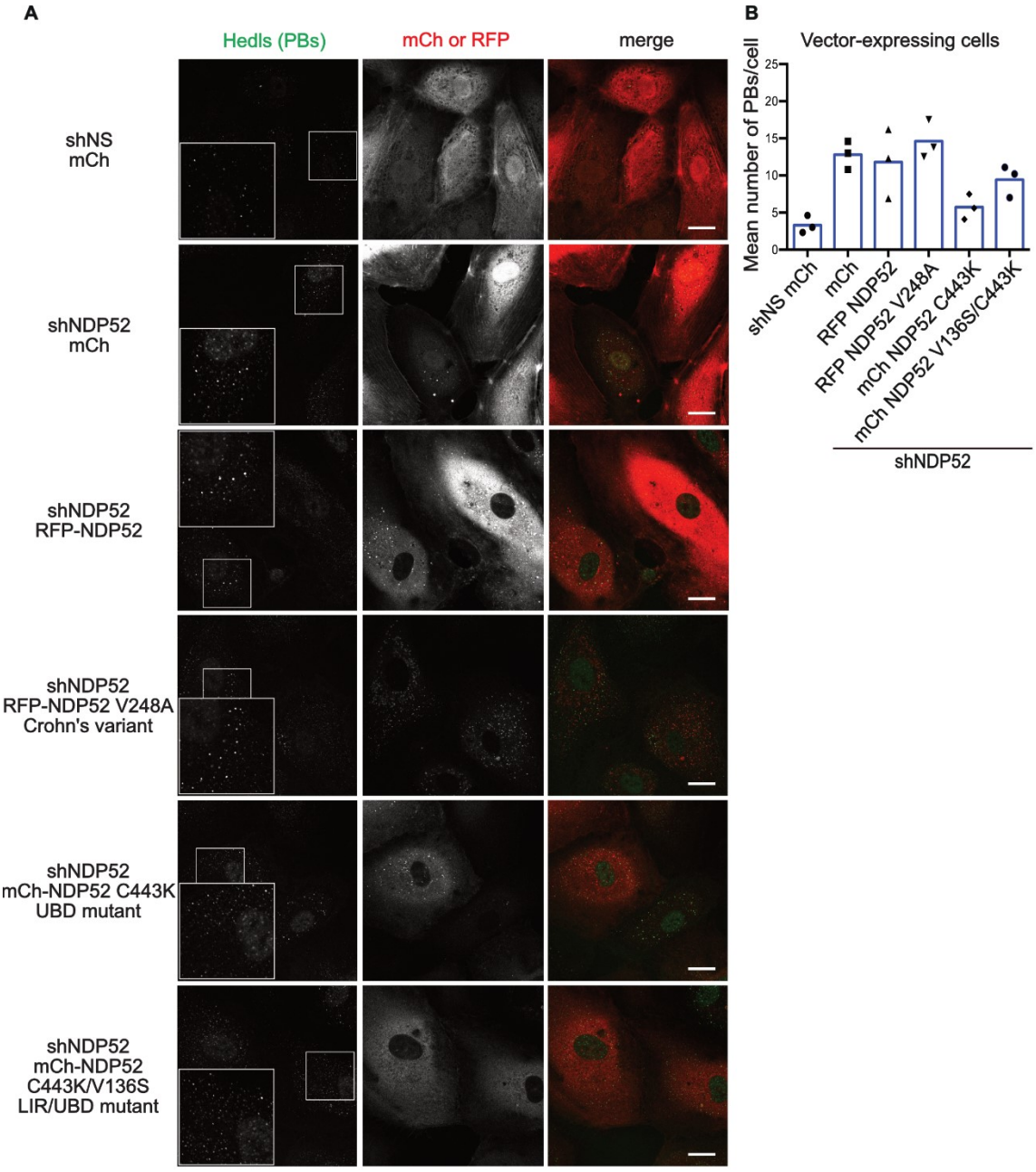
A
Hedls (PBs)
mCh or RFP
merge
shNS mCh
shNDP52 mCh
shNDP52 RFP-NDP52
shNDP52 RFP-NDP52 V248A Crohn's variant
shNDP52 mCh-NDP52 C443K UBD mutant
shNDP52 mCh-NDP52 C443K/V136S LIR/UBD mutant
B
Vector-expressing cells
Mean number of PBs/cell
0
5
10
15
20
25
shNS mCh
mCh
RFP NDP52
RFP NDP52 V248A
mCh NDP52 C443K
mCh NDP52 V136S/C443K
shNDP52

Interestingly, the UBD and UBD/LIR mutant over-expression decreased the mean PB number per cell, however, confocal imaging shows that cells in these conditions appear to have an increased number of small Hedls puncta compared to what is seen in other conditions (Figure 4.5A). Given the size of these puncta and the limit of resolution of the fluorescent and confocal microscopes, these small puncta would not be identified as PBs by CellProfiler thresholds.

KapB shNS mCh cells contained on average 1.2 PBs per cell; with NDP52 silencing the mean number of PBs in KapB mCh cells increased to 14.3 PBs per cell (Figure 4.6). Notably, in KapB cells with NDP52 knockdown, overexpression of RFP-NDP52 decreased the mean number of PBs per cell to 5.2. The over expression of the NDP52 Crohn's variant, UBD mutant and LIR/UBD mutant in KapB cells with NDP52 knockdown resulted in cells containing a mean of 12.4, 9 and 9.3 PBs per cell respectively (Figure 4.6). These data indicate that in KapB cells, NDP52 acts as a selective autophagy receptor for PB disassembly and that this activity is dependent on the UBD and LIR domains of NDP52. Like vector cells, cells expressing RFP-NDP52 V248A and mCh-NDP52 C443K had many smaller Hedls puncta (Figure 4.6A), perhaps suggesting that select PB proteins but not entire PB granules are undergoing degradation. Remarkably, overexpression of RFP-NDP52 rescued KapB-mediated PB disassembly in a KapB-specific manner and the UBD, LIR/UBD and Crohn's variant constructs failed to restore KapB-mediated PB disassembly to the same extent as the over expression of wild-type NDP52. These results are important because they 1) confirm the requirement for NDP52 in the mechanism of KapB-mediated PB disassembly and 2) pinpoint that the LIR and UBD domains of NDP52 are required for this mechanism.

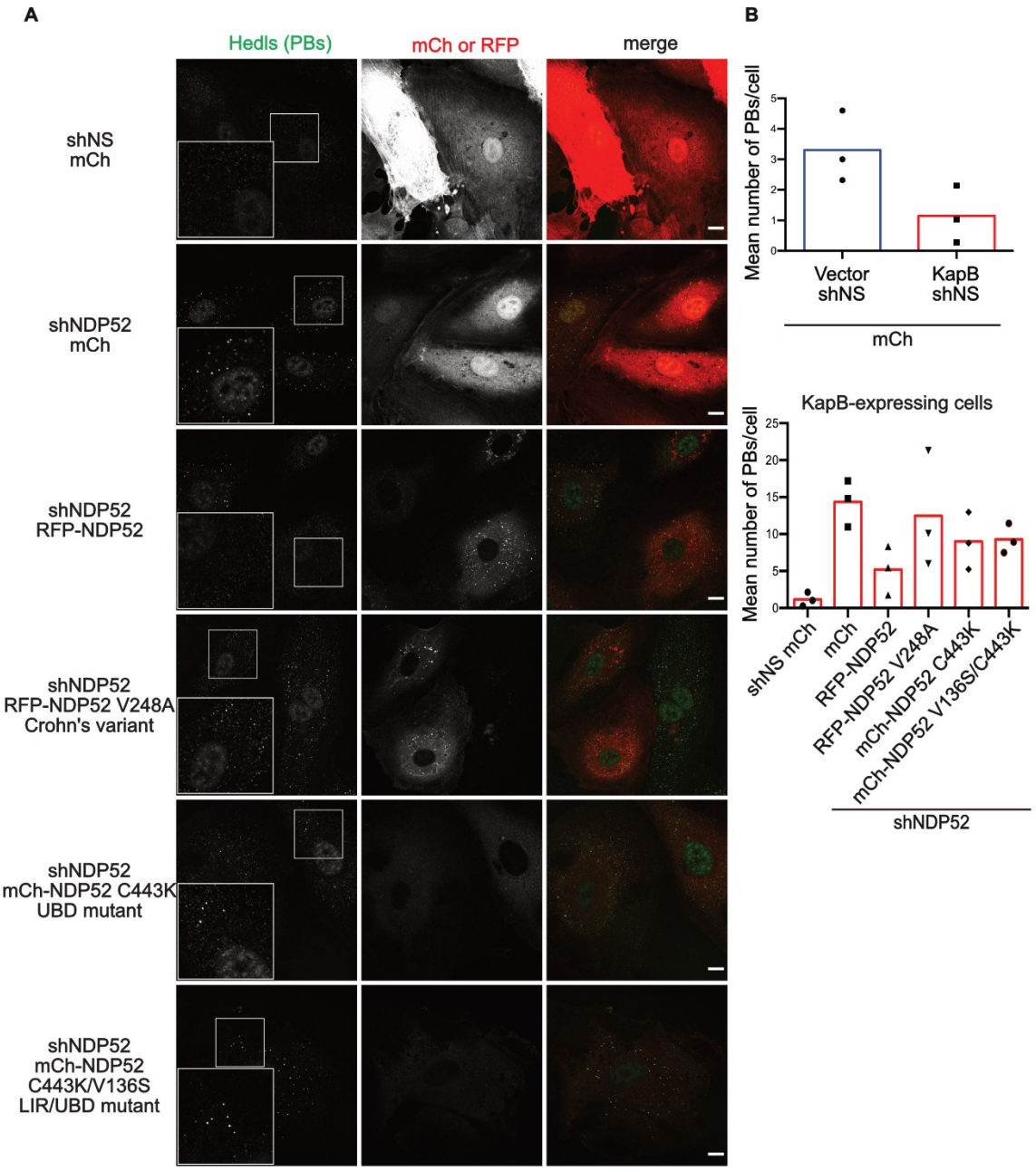

Figure 4.6: NDP52 over-expression rescues PB disassembly in shNDP52 KapB-expressing cells. (A-B) HUVECs were transduced and selected in parallel with control cells in Figure 4.5 prior to fixation for immunofluorescence. (A) HUVECs were stained for immunofluorescence and imaged as in Figure 4.5 (A). Scale bar = 20 μM (B) HUVECs were stained for immunofluorescence, imaged and PB numbers were quantified as in Figure 4.5 (B). Data is represented as the mean number of PBs per cell per condition; n=3.

These results confirm that it is the ability of NDP52 to act as a selective autophagy receptor, and not another function, that is important for KapB-mediated PB disassembly.

Since NDP52 is required for KapB-mediated PB disassembly, and we know from previous work that PB disassembly correlates with increased ARE-mRNA stability, I used shRNA-expressing lentiviruses to knockdown NDP52, OPTN and p62 and examined KapB-mediated ARE-mRNA stabilization (Corcoran et al., 2015, 2011). This approach capitalized on an established reporter assay that measures luciferase activity of a firefly luciferase (Fluc) construct that harbours an AU-rich element derived from GM-CSF in its 3'UTR, making the mRNA subject to constitutive decay (Corcoran et al., 2011). For this assay, HeLa Tet-Off cells were transduced with recombinant lentivirus expressing a control shNS or an shRNA targeting NDP52, OPTN or p62 (Figure 4.7A-B). Following selection and recovery, cells were co-transfected with the Fluc-ARE, a Renilla luciferase construct lacking an ARE (Rluc) as a transfection control, and a KapB expression plasmid or vector control (Figure 4.7A-B). 36h following transfection, DOX was added to cells to inhibit *de novo* transcription of both the Fluc and Rluc genes and 12h later, cell lysates were collected and assayed for Firefly and Renilla luciferin protein levels by luminescence (Figure 4.7A-B). The protein function reflects the level of mRNA remaining for translation 12h following the inhibition of *de novo* transcription, making this a robust assay to detect changes in Fluc mRNA stability or turnover (Figure 4.7A-B).

As expected from previous data, KapB expression results in Fluc ARE-mRNA stabilization compared to vector cells (Corcoran et al., 2011; Corcoran, Johnston & McCormick, 2015). KapB expression increased normalized relative luciferase activity by 21-fold on average compared to vector (Figure 4.7C).

Figure 4.7: NDP52 is required for KapB-mediated ARE-mRNA stabilization.
(A-B) HeLa Tet-Off cells were transduced with recombinant lentivirus expressing shRNAs targeting NDP52, OPTN, p62 or a shNS control. Following puro selection, cells were seeded and co-transfected with an ARE-containing Firefly luciferase (Fluc) reporter plasmid, a Renilla luciferase (Rluc) reporter plasmid lacking an ARE, and either a KapB expression plasmid or vector control. 36h post transfection, cells were treated with DOX to inhibit *de novo* transcription of Fluc and Rluc for 12h before lysis. (C-D) Fluc luminescence recordings were normalized to Rluc luminescence and the relative of the control (vector shNS or KapB shNS) was set to 1. Data is represented as the mean fold change in the relative luciferase activity of each condition compared to vector shNS or KapB shNS; n=3. An un-paired, one sample, two-tailed non-parametric T-Test was performed; * = $P<0.05$ **= $P<0.01$. (E) Protein knockdown was confirmed by immunoblotting using primary antibodies for NDP52, OPTN or p62. Representative immunoblots are shown. Immunoblots were normalized as in Figure 3.1 and are expressed as the mean fold change in expression relative to the respective shNS control ± SEM; n=3.

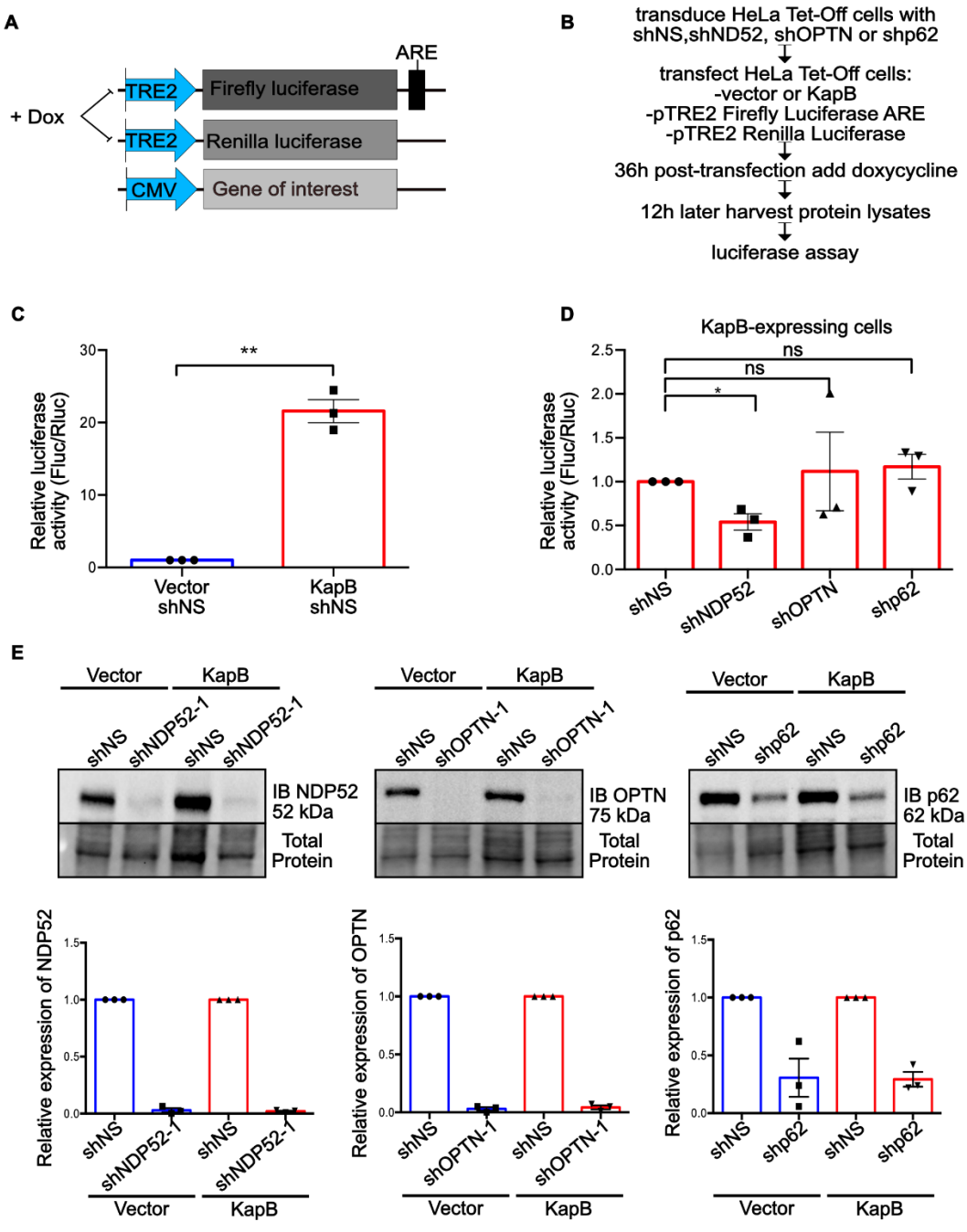
A
ARE
+ Dox
TRE2
Firefly luciferase
TRE2
Renilla luciferase
CMV
Gene of interest
B
transduce HeLa Tet-Off cells with shNS,shND52, shOPTN or shp62
transfect HeLa Tet-Off cells: -vector or KapB -pTRE2 Firefly Luciferase ARE -pTRE2 Renilla Luciferase
36h post-transfection add doxycycline
12h later harvest protein lysates
luciferase assay
C
Relative luciferase activity (Fluc/Riluc)
**
Vector shNS
KapB shNS
D
KapB-expressing cells
Relative luciferase activity (Fluc/Riluc)
ns
ns
*
shNS
shNDP52
shOPTN
shp62
E
Vector
KapB
shNS
shNDP52-1
IB NDP52 52 kDa
Total Protein
shOPTN-1
IB OPTN 75 kDa
shp62
IB p62 62 kDa
Relative expression of NDP52
Relative expression of OPTN
Relative expression of p62

Given the substantial increase in cells with normal PBs, observed in KapB-expressing cells with NDP52 knockdown, I hypothesized that there would be a decrease of ARE-mRNA stability in KapB-expressing cells with NDP52 knockdown as the labile RNAs would be shuttled to the available PBs for degradation. The knockdown of NDP52 in KapB-expressing cells significantly reduced relative luciferase activity compared to KapB shNS by approximately 50% suggesting that NDP52 is required for KapB-mediated ARE-mRNA stabilization (Figure 4.7D). This effect was specific to NDP52, as the knockdown of OPTN and p62 did not significantly alter KapB-mediated ARE-mRNA stabilization (Figure 4.7D). For each independent experiment, paired lysates were immunoblotted to confirm shRNA knockdown efficiency. The mean knockdown efficiency for shNDP52-1, shOPTN-1 and shp62 was over 70% on average for each construct (Figure 4.7E). Therefore, NDP52 but not OPTN and p62 is required for KapB-mediated ARE-mRNA stabilization.

4.2 Characterizing KapB-Induced Increases in Steady-State ARE-mRNA Expression

We know KapB induces autophagy and PB disassembly and these PB changes correlate with increased ARE-mRNA stabilization, as has been determined by our ARE-mRNA luciferase reporter assay (Corcoran, Johnston, & McCormick, 2015; Corcoran et al., 2011, Corcoran (unpublished)). However, we do not know if KapB expression also increases steady-state levels of endogenous ARE-mRNAs that code for many inflammatory cytokines. To determine whether inflammatory ARE-mRNAs were upregulated by KapB expression, I first used LPS to stimulate the transcription of inflammatory mRNAs. This is because under basal conditions, many inflammatory ARE-

mRNAs are expressed at low levels in endothelial cells without stimulation, preventing accurate detection even after mRNA stability changes (Nilsen et al., 1998). Vector and KapB-transduced HUVECs were stimulated with LPS for 6 or 12h prior to lysis for total RNA. Following RNA extraction and reverse transcription, I used qPCR to determine the relative expression of the ARE-mRNAs; IL-6, CXCL8, TNF, GM-CSF and IL-1β. Fold change in transcript expression for each condition was normalized to the untreated vector control.

To our surprise, KapB expression increased the steady-state levels of IL-6 relative to vector control cells by 2.6-fold without any LPS treatment; this was magnified at 6h post LPS, where KapB expression increased IL-6 275.2-fold relative to the untreated vector control (Figure 4.8). The increase in IL-6 transcript detection was KapB specific, as vector cells increased IL-6 4.6-fold at 6h post LPS (Figure 4.8). By 12h post LPS this KapB-mediated increase in IL-6 had decreased substantially (20-fold relative to untreated vector), indicating the transient nature of this response. KapB expressing cells contained an approximately 2-fold increase in levels of CXCL8 without treatment. CXCL8 steady state levels did not significantly differ between vector and KapB after 6h and 12h of LPS treatment (Figure 4.8). COX-2 expression was not significantly changed by KapB expression at steady-state or after LPS treatment (Figure 4.8). KapB-expressing cells display increased steady-state levels of both GM-CSF (3.8-fold increase) and TNF (5.3-fold increase) (Figure 4.8).

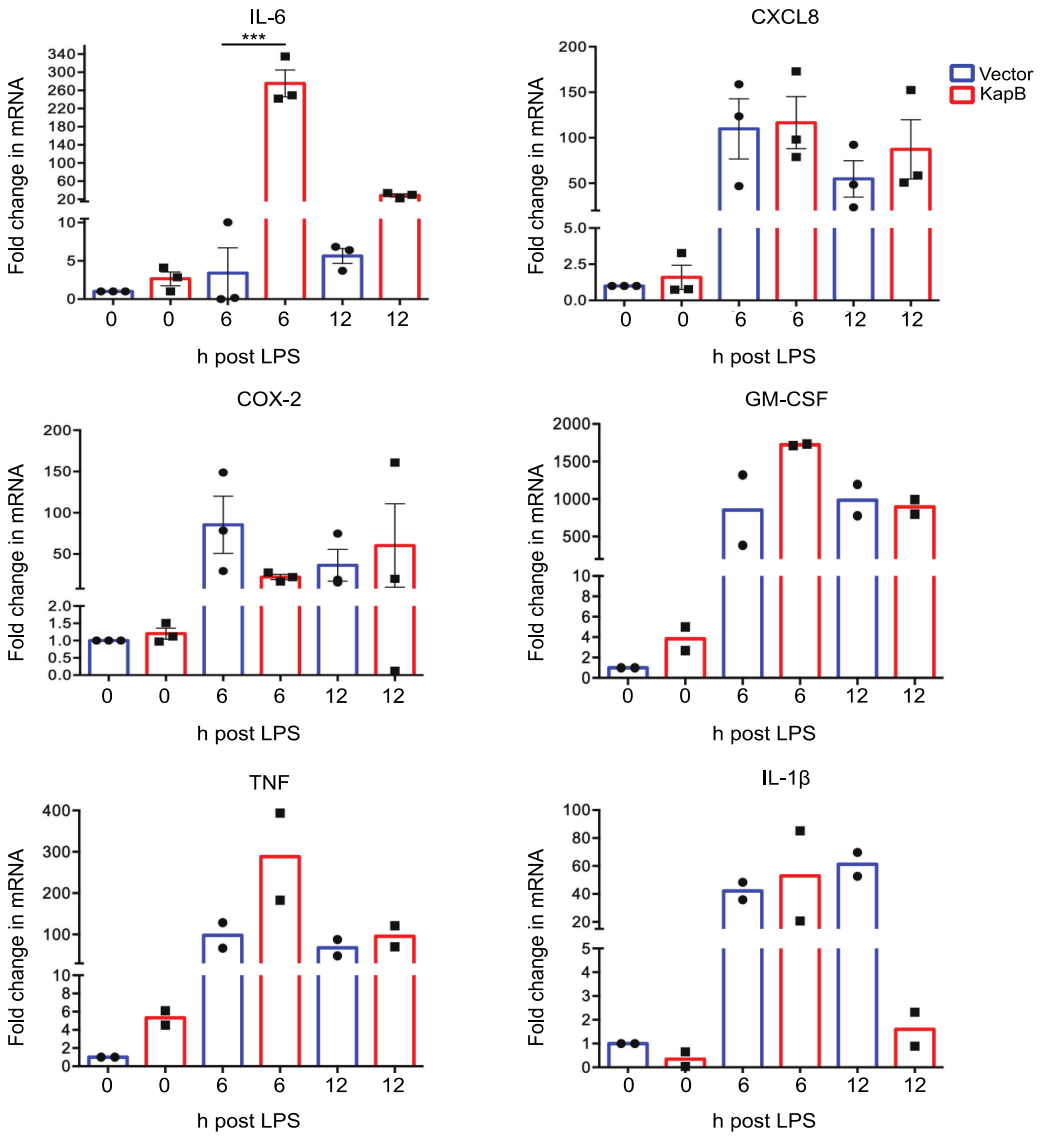

Figure 4.8: KapB increases select endogenous ARE-mRNAs. HUVECs were transduced with recombinant lentivirus expressing KapB or a vector control. Cells were selected with bsd and recovered for 24h prior to treatment with LPS (1 µg/mL) for 6 or 12h. At each time point cells were lysed for total RNA. 750 ng of total RNA was reverse-transcribed and amplified by qPCR. IL-6, CXCL8, COX-2, GM-CSF, TNF and IL-1β Cqs were normalized to the reference gene, 18S. Data is represented as the fold change in target transcript expression relative to the untreated vector control and was quantified using the ΔΔCq method ± SEM where appropriate. Data for IL-6, CXCL8 and COX-2; n=3. Data for GM-CSF, TNF and IL-1β; n=2. Statistical significance of data for IL-6, CXCL8 and COX-2 was determined by two-way repeated measures ANOVA with Tukey's multiple comparison test.

At 6h post LPS, KapB cells displayed a KapB specific increase in levels of GM-CSF and TNF). Interestingly, steady-state levels of IL-1β were decreased in KapB-expressing cells, while at 6h post LPS both vector and KapB cells respond similarly to this length of treatment and display a respective 42- and 52- fold increase in IL-1β (Figure 4.8). Notably at 12h post LPS, vector cells contain a 61- fold increase in IL-1β while transcript expression in KapB-expressing cell drops to a mere 1.6-fold increase relative to vector control (Figure 4.8). These results suggest KapB may be down-regulating the expression of IL-1β in response to LPS stimulation.

In summary, these data demonstrate that without LPS stimulation, KapB expression promotes a small increases in the steady-state levels of certain endogenous ARE-mRNAs; IL-6 (2.6-fold), GM-CSF (3.8-fold) and TNF (5.3-fold) relative to vector control cells (Figure 4.8). Ectopic expression of KapB caused a more substantial increase in the levels of IL-6 ($p<0.001$), GM-CSF and TNF transcripts 6h post LPS relative to vector cells at the same time point (Figure 4.8). Overall, these data highlight the complex role KapB plays in influencing immune-modulatory ARE-mRNA expression and suggest that KapB increases levels of some inflammatory ARE-mRNAs but not others. The precise reasons for this complexity are not understood.

We know that KS lesions are surrounded by a proinflammatory and angiogenic environment that is required for KS progression, and that latently infected endothelial cells can recapitulate this effect *in vitro* by producing cytokines that are secreted into the surrounding media (J. An et al., 2002; Barbara Ensoli et al., 2010; Barbara Ensoli & Stürzl, 1998; Montaner et al., 2003). KapB would normally be expressed in KSHV latent infection in an environment where these cells are bathed in cytokine-containing

surroundings. I speculated that mimicking the KSHV infection environment by exposing cells to these secreted cytokines would cause paracrine and autocrine signaling, which would enhance levels of ARE-mRNAs in KapB cells. To mimic this in the lab, I treated KapB-expressing or control HUVECs with conditioned media from iSLK.219 cells which harbor the latent KSHV.219 virus. The conditioned media was combined 1:1 with fresh HUVEC EGM-2 media and used to treat vector and KapB-expressing HUVECs for 0 or 6h. At 0 and 6h post treatment with conditioned media, total RNA was harvested and the relative expression of IL-6, CXCL8, IL-1β and COX-2 in vector and KapB HUVECs was assessed using qPCR; all conditions were normalized to the vector untreated control.

Without treatment, the steady-state levels of IL-6, CXCL8, IL-1β and COX-2 in KapB cells were increased by 2.6-, 2.0-, 5.4- and 2.0- fold relative to vector control (Figure 4.9). In Figure 4.8, IL-6 and CXCL8 were increased at a similar magnitude to that seen in Figure 4.9; however, in this set of experiments there is an increase in the steady state expression of COX-2 an IL-1β not detected in Figure 4.8. The reason for this inconsistency is not known; however, it may result from improved KapB transduction efficiency in this later experiment. At 6h post media transfer, transcript increases in IL-6 (9.9-fold) and COX-2 (4-fold) were specific to KapB-expressing cells (Figure 4.9). Relative to vector and KapB untreated controls, there were no noteworthy changes in CXCL8 or IL-1β levels in vector or KapB cells at 6h post conditioned media treatment (Figure 4.9). Although there is some variation in the biological replicates obtained for these experiments, these data further support previous work that and suggests that KapB amplifies the mRNA increases that are observed from or conditioned media or LPS-mediated increased transcription alone.

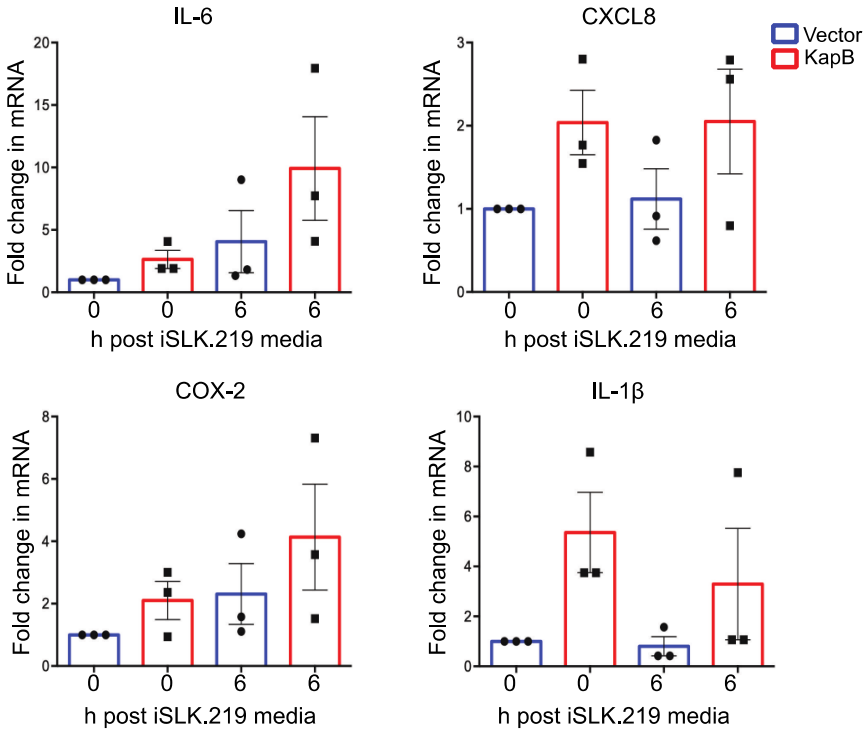

Figure 4.9: KapB-expressing cells treatment with conditioned media from KSHV infection increases IL-6. HUVECs were transduced with recombinant lentivirus expressing KapB or a vector control. Cells were selected with bsd and recovered for 24h prior to treatment with conditioned media derived from 72h cultures of iSLK.219 cells (KSHV latently infected) media for 6h. At each time point cells were lysed for total RNA. 750 ng of total RNA was reverse-transcribed and amplified by qPCR. IL-6, CXCL8, COX-2, and IL-1β Cqs were normalized to the reference gene 18S. Data is represented as the fold change in target transcript expression relative to the untreated vector control and was quantified using the ΔΔCq method ± SEM; n=3.

4.3 NDP52 Knockdown Reduces Levels of Select ARE-mRNAs

Having determined that several endogenous immuno-modulatory ARE-mRNAs are upregulated by KapB, I investigated whether the knockdown of NDP52 impacted steady-state levels of the same endogenous ARE-mRNAs. Vector and KapB-expressing HUVECs were transduced with a recombinant lentivirus expressing an shRNA targeting NDP52 (shNDP52-1) or a shNS control. Cells were recovered and treated with LPS for 6h. Treated and control cells were lysed for total RNA and the relative expression of IL-6, CXCL8, COX-2 and GM-CSF was determined using qPCR. All conditions were normalized to vector shNS untreated control. Given that the knockdown of NDP52 increased PB number in both vector and KapB-expressing cells; I anticipated that NDP52 knockdown would decrease the levels of certain ARE-mRNAs relative to a shNS control.

Although only one biological replicate was completed for this experiment, preliminary results show that in vector cells, NDP52 knockdown reduces the expression of ARE-mRNAs; GM-CSF (Vector: shNS - 367-fold increase shNDP52 -233-fold increase) and CXCL8 slightly (Vector: shNS - 73-fold increase; shNDP52 - 58-fold increase) 6h post LPS stimulation. There was no substantial impact of shNDP52 knockdown on the surveyed transcripts without exogenous stimulation. In KapB-expressing cells, the knockdown of NDP52 had very little impact on mRNA expression without LPS stimulation. With LPS stimulation the relative expression of IL-6 and CXCL8 was not impacted by NDP52 knockdown while the expression of COX-2 was slightly increased and the expression of GM-CSF was decreased substantially (KapB: shNS - 620-fold increase; shNDP52 - 389-fold increase).

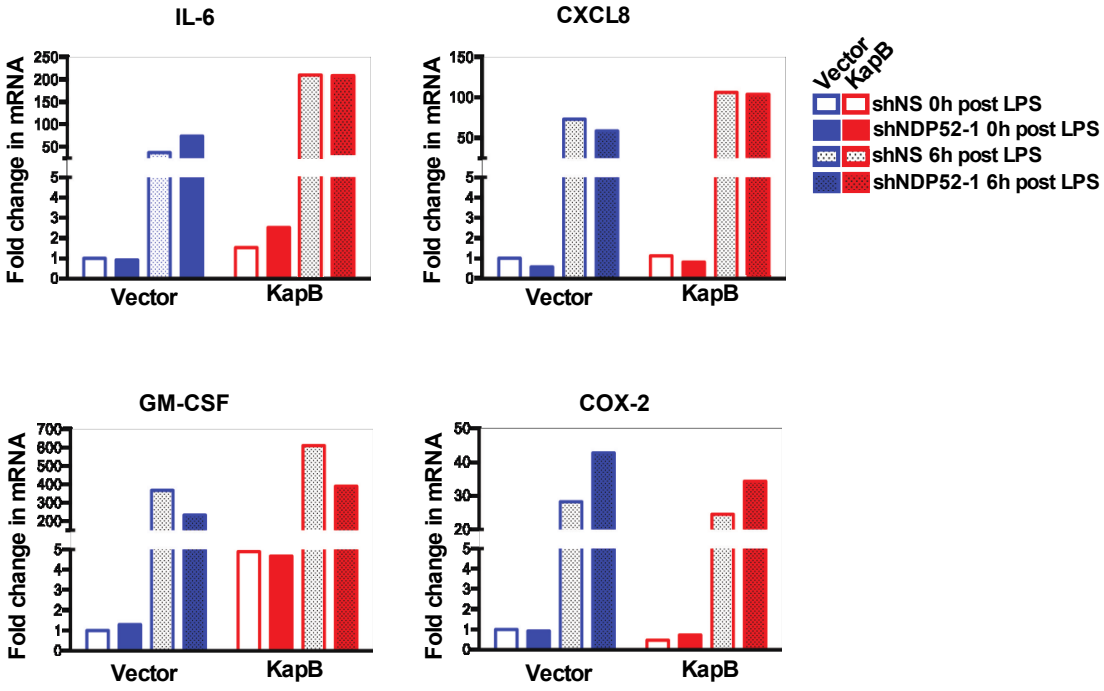

Figure 4.10: NDP52 Knockdown reduces expression of GM-CSF post LPS stimulation. HUVECs were sequentially transduced with recombinant lentivirus expressing KapB or a vector control. Cells were selected with bsd and transduced with recombinant lentivirus expressing shRNAs targeting NDP52 (shNDP52-1) or a shNS control. Cells were selected with puro and treated with LPS (1 µg/mL) for 6h. At each time point cells were lysed for total RNA. 500 ng of total RNA was reverse-transcribed and amplified by qPCR. IL-6, CXCL8, COX-2 and GM-CSF were normalized to the reference gene 18S. Data is represented as the fold change in target transcript expression relative to the untreated vector shNS control and was quantified using the ΔΔCq method; n = 1.

Although preliminary, these results show an interesting role for NDP52 in the regulation of GM-CSF expression, and highlight the complicated role NDP52 plays in inflammatory transcript expression in both vector and KapB-expressing cells.

4.4 NDP52 is Not Required for MK2EE-Mediated PB Disassembly and ARE-mRNA Stabilization

Previous research from our lab demonstrated that KapB binds and activates MK2 and that the downstream MK2 signaling cascade causes PB disassembly (Corcoran et al., 2015; McCormick & Ganem, 2005). Consequently, I sought to establish whether the selective autophagy receptor, NDP52, was responsible for PB disassembly independent of KapB by using a phosphomimicking form of MK2 called MK2EE. In MK2EE, threonines 205 and 317 that are normally phosphorylated by upstream kinase p38 are substituted with glutamate to mimic the negatively charged phosphates, opening MK2 to its active form in a constitutively active manner (Engel et al., 1995).

In order to investigate the role of selective autophagy in MK2-mediated PB disassembly, I utilized the lentiviruses expressing shRNAs targeting NDP52, OPTN and p62 in vector and MK2EE-expressing HUVECs as described in section 4.1. The mean knockdown efficiency of NDP52, OPTN and p62 were greater than 88%, 53% and 76% respectively in vector and MK2EE expressing cells (Figure 4.11). Analysis of knockdown efficiency was performed in parallel with phenotypic characterization (Figure 4.12) in all cases. In parallel experiments, I stained cells for PBs as in section 4.1. shNS vector-expressing cells contained 6.5 PBs per cell; as expected, MK2EE expression reduced the mean number of PBs per cell to 2.2 PBs per cell (Figure 4.12B). In vector cells NDP52 knockdown increased the mean PB number per cell 8.3, while the

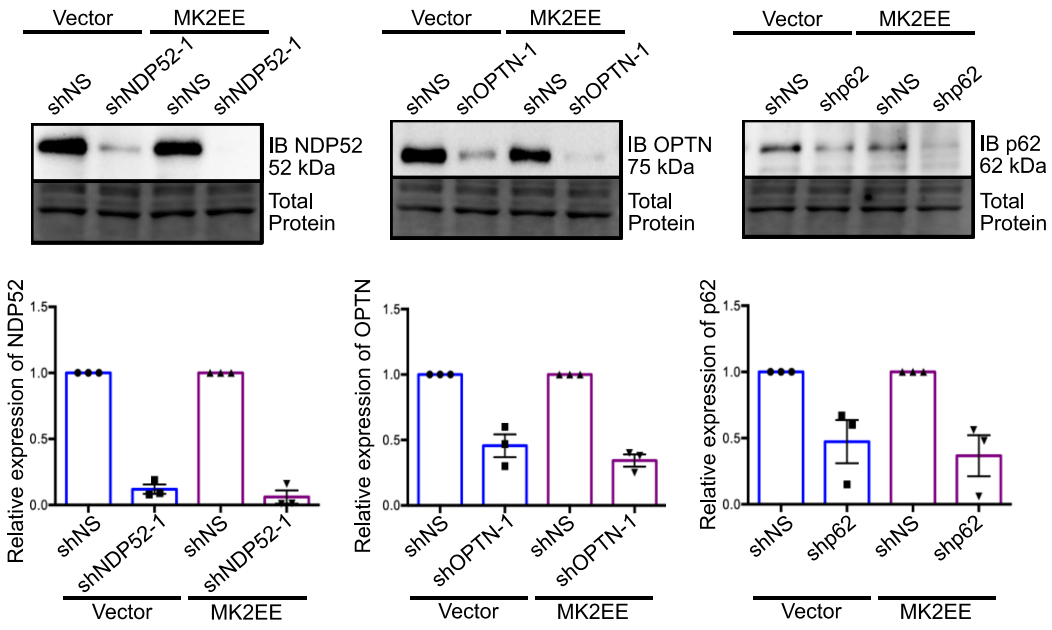

Figure 4.11: RNA interference reduces steady-state levels of selective autophagy receptors in control and MK2EE-expressing cells. HUVECs were transduced with recombinant lentivirus expressing constitutively active FLAG-MK2EE (MK2EE) or a vector control and were selected with bsd. Cells were re-seeded and transduced with recombinant lentivirus expressing shRNAs targeting NDP52, OPTN, p62 or a shNS shRNA control and were selected with puro prior to lysis for immunoblotting. Lysates were immunoblotted and quantified as in Figure 4.1. Representative immunoblots are shown. Data is expressed as the mean fold change in expression relative to the respective vector or MK2EE shNS control ± SEM; n=3.

Figure 4.12: NDP52 knockdown does not reverse MK2EE-mediated PB disassembly. (A-B) HUVECs were transduced and selected as in Fig 4.11 prior to fixation for immunofluorescence. (A) HUVECs were stained using primary antibodies for Hedls (PBs; red) and FLAG (green) and phalloidin (F-actin; blue). Representative images for each condition were taken using the Zeiss LSM 510 Meta. Scale bar = 20 μM (B) HUVECs were stained for immunofluorescence with DAPI (nuclei), WGA (to denote cellular membranes and using primary antibodies for Hedls (PBs) and FLAG (MK2EE). Cells were imaged on the Zeiss AxioImager Z2 (100+ cells, >6 fields of view) and the mean number of PBs per cell were quantified using an automated image analysis pipeline in CellProfiler. Data is represented as the mean number of PBs per cell per condition; n=3.

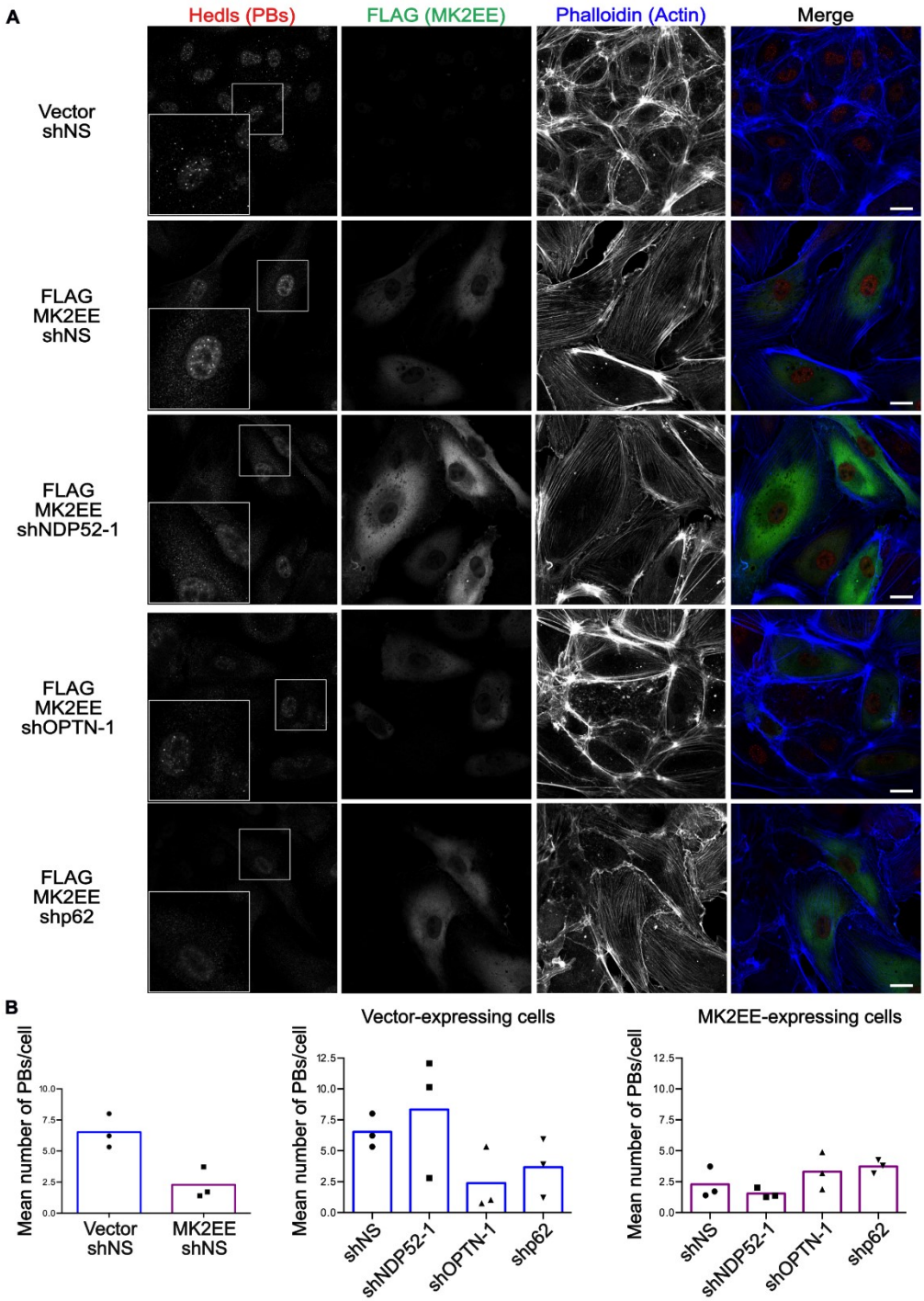
A
Hedls (PBs)
FLAG (MK2EE)
Phalloidin (Actin)
Merge
Vector shNS
FLAG MK2EE shNS
FLAG MK2EE shNDP52-1
FLAG MK2EE shOPTN-1
FLAG MK2EE shp62
B
Mean number of PBs/cell
Vector shNS
MK2EE shNS
Vector-expressing cells
MK2EE-expressing cells
shNS
shNDP52-1
shOPTN-1
shp62

knockdown of OPTN and p62 caused a reduction in the mean number of PBs per cell (OPTN – 2.3 PBs per cell; p62 – 3.6 PBs per cell) (Figure 4.12). Contrary to our expectations, MK2EE-expressing cells with NDP52 knockdown displayed further decreases in the number of PBs per cell (1.5 PBs per cell) while the knockdown of OPTN and p62 caused a slight increase in the mean number of PBs per cell in these conditions (OPTN- 3.3 PBs per cell; p62 – 3.7 PBs per cell) (Figure 4.12). Neither OPTN, NDP52 or p62 knockdown substantially increased the number of PBs within MK2EE-expressing cells. In addition to causing PB disassembly, MK2EE expression also increases ARE-mRNA stabilization, as previously observed (Corcoran et al., 2015).

Given my results indicating that the knockdown of NDP52, OPTN and p62 does not reverse MK2EE-mediated PB disassembly, I examined whether the knockdown of the selective autophagy receptors impacted ARE-mRNA stabilization using the ARE-mRNA stabilization luciferase assay described in section 4.1. I expected that NDP52 OPTN and p62 knockdown would not cause a decrease in ARE-mRNA stabilization as there are few PBs within these cells. HeLa Tet-Off cells were transduced as in Figure 4.7 and transfected with a vector control or MK2EE and Fluc-ARE, Rluc. Cells were treated, harvested and assayed for Firefly and Renilla luciferin protein levels as described in section 4.1. As anticipated, MKEE expression increased the relative luciferase activity by approximately 10-fold (Figure 4.12 A). The knockdown of NDP52 significantly increased MK2EE-mediated increases in relative luciferase activity by 80%; while knockdown of OPTN and p62 increased the relative luciferase activity by 30% and 6% respectively (Figure 4.12 B). The knockdown efficiency from lysates collected in parallel to this experiment were confirmed by immunoblotting. The mean knockdown efficiency

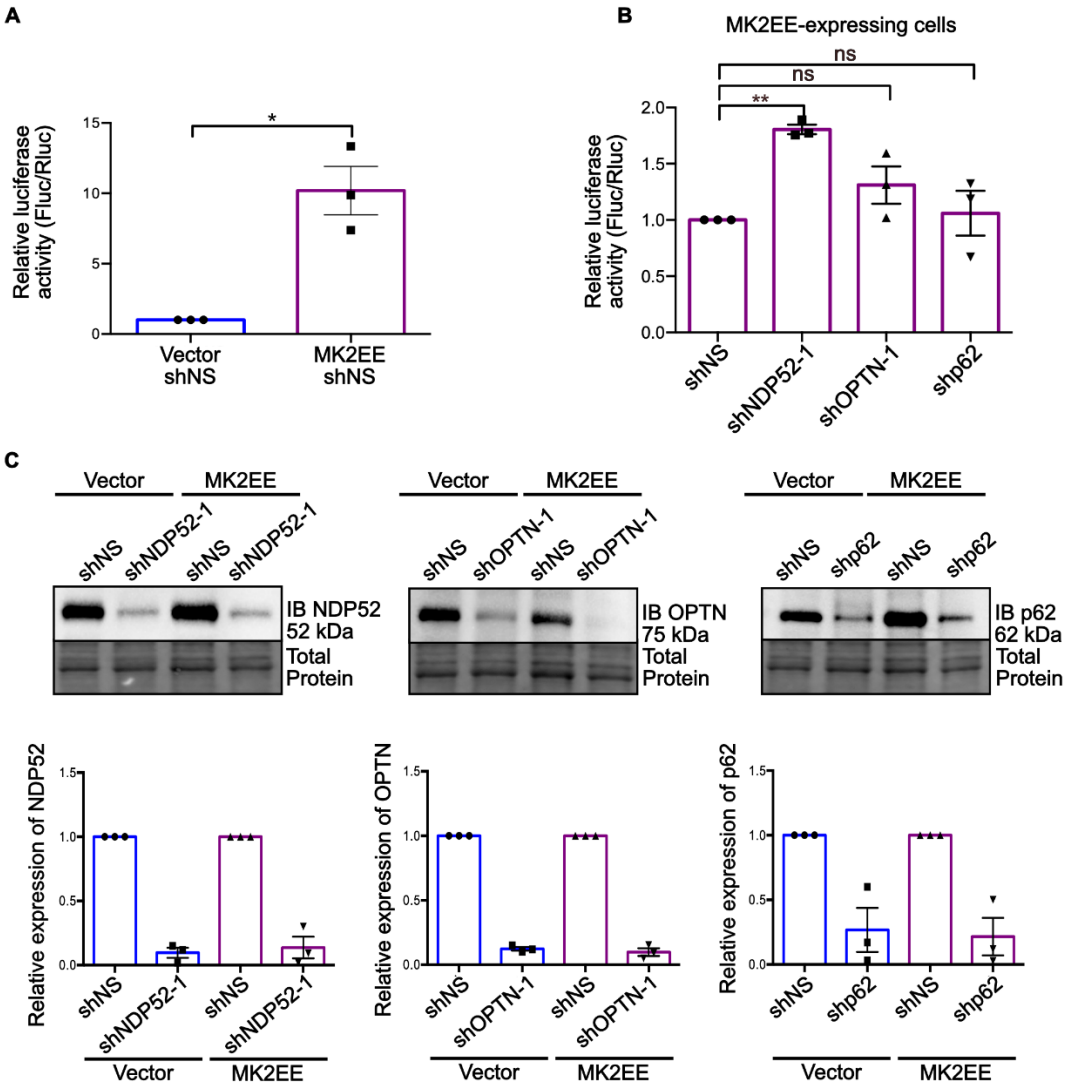

Figure 4.13: NDP52 knockdown increases MK2EE-mediated ARE-mRNA stabilization. (A-C) HeLa Tet-Off cells were transduced with recombinant lentivirus expressing shRNAs targeting NDP52, OPTN, p62 or a shNS control. Following puro selection, cells were re-seeded and co-transfected with an ARE-containing Firefly luciferase (Fluc) reporter plasmid, a Renilla luciferase (Rluc) reporter plasmid lacking an ARE, and either a MK2EE expression plasmid or vector control. 36h post transfection, cells were treated with DOX to inhibit *de novo* transcription of Fluc and Rluc for 12h before lysis. (A-B) Fluc luminescence recordings were normalized to Rluc luminescence and the relative of the control (vector shNS or MK2EE shNS) was set to 1. Data is represented as the mean fold change in the relative luciferase activity of each condition compared to vector shNS or MK2EE shNS; n=3. An un-paired, one sample, two-tailed non-parametric T-Test was performed; * = $P<0.05$ **= $P<0.01$. (C) Protein knockdown was confirmed by immunoblotting using primary antibodies for NDP52, OPTN or p62. Representative immunoblots are shown. Immunoblots were normalized as in Figure 3.1 and are expressed as the mean fold change in expression relative to the respective shNS control ± SEM; n=3.

of NDP52 OPTN and p62 was greater than 70% for all shRNAs (Figure 4.13). Overall these results suggest that neither NDP52, p62 or OPTN are essential for MK2-EE induced PB disassembly or ARE-mRNA stabilization. Moreover, these data suggests that while both KapB and MK2EE can induce PB disassembly, the precise mechanistic details of this process may differ; an important observation that will be the subject of future work in the Corcoran lab.

Chapter 5 Discussion

5.1 Overview

KSHV hijacks normal cellular signaling to create an environment that allows life-long viral infection. This cellular de-regulation in conjunction with immunodeficiency can cause oncogenic transformation of ECs resulting in KS. KS is characterized by prolonged inflammation, angiogenesis and proliferation (Chang & Moore, 1996; Ensoli & Stürzl, 1998; Ensoli et al., 2010). Primary ECs infected with KSHV display a characteristic spindled phenotype and express high levels of proinflammatory cytokines and angiogenic mediators. These phenotypes, in conjunction with PB disassembly, are detected when the viral protein, KapB is ectopically expressed in primary ECs (Corcoran et al., 2015; McCormick & Ganem, 2005). Unpublished data from the Corcoran lab shows that KapB upregulates autophagy and that inhibiting autophagy inhibits KapB-mediated PB disassembly in ECs. However, several questions remain including (1) does KapB induce selective autophagy to induce selective targeting of PBs or PB components for degradation? (2) do changes in selective autophagy alter the expression of ARE-mRNAs during KapB expression?

I used two approaches to determine if KapB induced selective autophagy to facilitate PB disassembly. I developed a fluorescence-based assay to monitor bulk autophagy, mitophagy and selective autophagy of PB components DCP1A and DDX6. I determined that autophagic flux regulates both DCP1A and DDX6, but results were inconclusive as to whether KapB expression induced PB component selective catabolism more than other cytosolic cargos. Next, I used shRNAs to reduce the levels of NDP52, OPTN and p62 and monitored PB dynamics by immunofluorescence. I determined that

NDP52 is required for KapB-mediated PB disassembly. Furthermore, I showed that NDP52 is required for ARE-mRNA stabilization using an established luciferase assay. Using qPCR, I determined that KapB-expression increased levels of certain ARE-mRNAs and preliminary results suggested that the levels of one of these ARE-mRNAs encoding GM-CSF, is affected by NDP52 expression. These results are consistent with a unique model in which a viral protein induces the specific disassembly of PBs via the selective autophagy receptor NDP52. PB disassembly promotes inflammatory ARE-mRNA stabilization, thereby contributing to the proinflammatory environment typical of KSHV latent infection and KS lesions.

5.2 Developing a Fluorescent Tool to Monitor Selective Autophagy

5.2.1 mKeima-Based Assays: Advantages and Limitations

The selective autophagy field suffers from a lack of convenient and established methods designed to monitor the autophagic degradation of specific cargos; therefore, there is value in developing an mKeima-based assay to monitor the PB selective autophagy. Creating mKeima-fusion proteins provides a unique opportunity to measure many different types of selective autophagy including pexophagy, xenophagy and granulophagy. This approach has been used by An & Harper (2017) to compare rates of ribophagy to bulk autophagy (mKeima-LC3) and other cytosolic cargo such as the cytoskeletal reporter (mKeima-actin) or a mitophagy reporter (mKeima-TOM20). An & Harper (2017) demonstrated that arsenite induced the comparatively selective acidification of ribo-mKeima reporters but not LC3-mKeima, mKeima-actin or mKeima-TOM20.

There are several advantages of mKeima-based assays to monitor selective autophagy. Unlike most autophagic flux assays, mKeima probes do not rely on LC3 modification and thus can monitor Atg5-independent autophagic flux (Katayama et al., 2011). This is important because some incidences of mitophagy are Atg5-independent, indicating that other cargos degraded by selective autophagy involve Atg5-indpendent autophagy (Shimizu, 2018). Since mKeima assays can be monitored using confocal microscopy, flow cytometry and immunoblotting, the technique is relatively accessible and the large Stokes shift between the fluorophore excitation and emission permits monitoring of GFP labelled structures in conjunction with mKeima constructs (H. An & Harper, 2017; Katayama et al., 2011). Lentiviral expression of mKeima vectors also allows selective autophagy monitoring in many cell types and Mito-mKeima constructs have been used to monitor mitophagy *in vivo* (N. Sun et al., 2015). The adaptability of mKeima reporters and the many ways reporters can be monitored highlights the usefulness of mKeima-based techniques.

There are also several limitations to the mKeima-based assays. mKeima-containing samples must be analyzed in living cells because chemical fixation ablates lysosomal pH differences and reporters must be analyzed relatively quickly to avoid environmental stressors that alter mKeima localization (H. An & Harper, 2017; Katayama et al., 2011). Furthermore, mKeima probes cannot detect early stages of autophagy and using flow cytometry, morphological changes in cells cannot be detected. In summary, with the appropriate experimental considerations, mKeima-based assays provide a valuable tool to monitor many different types of selective autophagy.

.

5.2.2 Monitoring PB Component Degradation Using mKeima Reporters

In this study, the pH-dependent fluorescent protein mKeima was used to develop a novel quantitative assay to determine if KapB expression increases bulk macroautophagy or the selective autophagy of PB proteins. I cloned mKeima fusion proteins to monitor bulk autophagy (mKeima-LC3) or PB selective autophagy (mKeima-DCP1A and mKeima-DDX6). I used DCP1A and DDX6 as my PB reporters because several papers have conclusively linked DCP1A and DDX6 to the maintenance and assembly of PBs (Chiang et al., 2013; Cougot et al., 2012; Tenekeci et al., 2016). We have also observed their disappearance in response to KapB (immunofluorescence for endogenous DDX6 puncta and the GFP-DCP1A reporter both decrease after KapB expression). I obtained a mito-mKeima construct to monitor mitophagy as a form of selective autophagy which I predicted would not respond to KapB expression.

Flow cytometry experiments verified that all mKeima constructs were responsive to upregulators (Torin) or late-stage block (Bafilomycin) of autophagic flux (Figures 3.9, 3.10). As expected, the mKeima-LC3 reporter responded robustly, as LC3 is an essential and ubiquitous component of autophagic machinery (Figure 3.9). Both tagged PB reporters displayed slight yet significant changes after Torin treatment; this is a novel observation for DCP1A and DDX6 and is consistent with previous findings that show that steady state levels of some PB proteins (DCP1A, Pat1B, XRN1) decrease with autophagy induction and accumulate with late-stage autophagy inhibition (Robinson and Corcoran, unpublished) (Figure 3.10). However, the magnitude of the PB reporter response was quite small compared to the other reporters, indicating that DCP1A and DDX6 are not common autophagic substrates. In line with this, no significant differences

were detected in PB reporter construct acidification after KapB expression (Figure 3.11). KapB induces autophagy but using the LC3 and p62 turnover assays we know KapB induced increases in autophagic flux are not as robust as those induced by Torin treatment. Since KapB autophagy induction is not as robust as using Torin and Torin induced small changes in PB-reporter acidification, I believe that this flow-cytometry based assay is not sensitive enough to detect the small changes in autophagic degradation of PB reporters.

Other studies of selective autophagy have monitored mKeima-fusion protein processing as a way to quantitate selective degradation, as the level of processed relative to intact mKeima reflects the rate of turnover (H. An & Harper, 2017). KapB increased detection of processed mKeima-LC3; this confirms previous experiments that KapB increases autophagic flux (Figure 3.12). As expected, KapB expression did not alter levels of processed mito-mKeima. Unfortunately, processed mKeima bands from both PB reporter fusions were too faint to quantify in KapB and control cells, even when excess total protein was immunoblotted (Figure 3.12). Therefore, experiments with PB mKeima reporters were inconclusive.

Using knock-in cell lines, lentiviral transduction of constructs or flow-sorting for high mKeima-construct expressing cells may help mitigate construct expression issues. It is also likely that each protein has a different turnover rate and thus harvest time must be optimized for each construct post-KapB expression. Basal rates of selective autophagy and autophagy in cells vary, therefore using a cell line other than HEK293T cells, which have high rates of basal autophagy, may increase the robustness of responses detected using the mKeima reporters (Musiwaro, Smith, Manifava, Walker, & Ktistakis, 2013).

Furthermore, one must be cautious with extended or high concentration drug treatments as autophagy inducers such as Torin can also increase lysosomal biogenesis thus confounding results that suggest increased lysosomal delivery (Martina et al., 2014). Post optimization, the PB reporters would be useful for determining if selective autophagy receptor knockdown e.g. NDP52 stunts PB reporter turnover or whether KSHV infection changes PB reporter turnover.

Given my results, mKeima-based assays provide a useful tool for when treatments are anticipated to have robust effects on mKeima-constructs. Flow cytometry-based assays are amenable to high throughput experiments upon optimizing timing of construct turnover and expression levels. Microscopy-based mKeima techniques also provide an opportunity to visualize the delivery of diverse cargos to lysosomes and autolysosomes. mKeima assays require optimization, but this optimization does not detract from the inherent value of the technique as it is one of the only ways to directly monitor the selective nature of autophagy.

5.3 PB Disassembly is Regulated by Selective Autophagy Receptor NDP52

As an alternate method to investigate whether KapB engages selective autophagy to facilitate PB disassembly, I knocked down the expression of known receptors of SA (NDP52, OPTN and p62) and monitored PB dynamics via immunofluorescence. The knockdown of NDP52 but not OPTN or p62 reversed KapB induced PB disassembly and increased the number of PBs per cell in control cells (Figures 4.2, 4.3). Rescue of 3'-UTR targeted NDP52 knockdown with RFP-NDP52 restored PB disassembly in a KapB-

specific manner; whereas the UBD, LIR/UBD and Crohn's variant constructs failed to restore KapB-mediated PB disassembly to the same extent (Figures 4.5, 4.6). These results are significant because they identify NDP52 as being required for KapB-mediated PB disassembly. Moreover, these results suggest that PB disassembly relies on NDP52's ability to form a molecular bridge, linking LC3-binding to binding of ubiquitinated cargo. These results support my hypothesis that NDP52 is a selective autophagy receptor for PBs or PB component(s).

5.3.1 Potential Mechanism of PB Granule Disassembly via NDP52

There are several lines of evidence supporting that ribonucleoprotein granule (PBs and other granules) turnover is regulated by selective autophagy. Guo et al., (2014) detected colocalization of GFP-DCP1A with fluorescently labelled p62 and NDP52, suggesting interaction between the two proteins. The selective autophagy receptor VCP also targets SGs to growing phagophores in response to proteotoxic stress (Buchan et al., 2013). In our lab, we observed that steady-state levels of some PB components (e.g. DCP1A) decrease in response to autophagy induction while levels of other proteins like (e.g. Hedls) remain unchanged (Corcoran, unpublished). These results suggest a model that invokes the selective autophagy of key PB proteins, the loss of which induces PB disassembly so that PBs are no longer visible via immunofluorescence. This model of RNA granule disassembly has been observed in *C. elegans,* where the binding of P granule (similar in structure and function to PBs) components to an adaptor protein, SEPA-1, facilitated P granule component targeting to the *C. elegans* "LC3", resulting in P-granule dissolution (Zhao, Tian, & Zhang, 2009). Altogether, these data support our

hypothesis that PB components are targeted for selective degradation, promoting PB disassembly.

The identity of the PB component(s) that interact with NDP52 or the regulation of this interaction is not yet clear. BioGRID is an open access database that contains protein-protein interactions data for humans and other model organism species (Stark et al., 2006). A search for NDP52 interactors on BioGRID identified PB-resident proteins DDX6, MyoVI and LSM4 as possible interacting partners (Stark et al., 2006). DDX6 is an interesting candidate in this regard, as electron microscopy studies of PBs showed that it forms the outer shell of PBs and its removal causes granule disassembly (Cougot et al., 2004). Future work in the lab will use NDP52 co-immunoprecipitation in KapB-expressing cells, followed by mass spectrometry to identify PB proteins that complex with NDP52 specifically after KapB expression.

5.3.2 Potential Molecular Mechanisms Regulating NDP52-Mediated PB Disassembly

Ubiquitination is one mechanism that promotes selective autophagy receptor cargo identification and binding (Shaid, Brandts, Serve, & Dikic, 2013). NDP52 has a UBD in the zinc-finger domain that is crucial for cargo identification and binding. The removal of the ubiquitin binding domain renders NDP52 unable to localize to and bind *Salmonella typhimurium* (Cemma, Kim, & Brumell, 2011; Xie et al., 2015b). The UBD of NDP52 mediates binding to M1-, K63-, K48- and mono-ubiquitinated chains with no clear preference for any particular ubiquitin linkage (Xie et al., 2015). This is unusual, as other sequestosome-like family members, p62 and OPTN display K63-ubiquitin binding preference and hence K63-linkages are believed to target cargo for autophagic over proteasomal degradation (Linares et al., 2013; Richter et al., 2016; Xie et al., 2015).

Although there is very little evidence regarding post translational modifications (PTMs) on PB proteins, Tenekeci et al., (2016) identified that DCP1A, DCP2 and EDC3 are ubiquitinated suggesting that these PB proteins could be marked for turnover by ubiquitination that induces their autophagic degradation. The knockdown of K63-ubiquitination also prevented DCP1A interaction with Hedls and XRN1 and induced PB disassembly (Tenekeci et al., 2016). In this study, PB disassembly correlated to stabilization of several inflammatory ARE-mRNAs, including IL-6 and COX-2, further supporting our hypothesis that PBs are important regulators of ARE-mRNA stabilization (Tenekeci et al., 2016). I predict that whichever PB component is bound by NDP52, this is done in a ubiquitin-dependent manner. Consequently, identifying the ubiquitin status of co-precipitating PB proteins via proteomics experiments or other approaches could help identify which proteins are targeted in KapB-mediated PB disassembly.

In addition to identifying the target cargo, it is also important to understand how KapB modifies NDP52 activity. From the observation that wild-type NDP52 expression only rescues PB disassembly in the context of KapB expression, I believe this implies there is a KapB-specific NDP52 or PB cargo activation step that is not present in the control cells. A key way that selective autophagy receptor activity is modulated is via post-translational modification. In some experiments, I observed a higher mobility band on NDP52 immunoblots that is increased only in cell lysates derived from KapB-expressing cells. In other experiments, KapB expression appears to increase the steady state levels of NDP52. Lu, den Brave, & Jentsch, (2017) suggest that receptor oligomerization is a main regulator of selective autophagy receptor binding. This is further supported by data that shows p62 oligomerization stabilizes its binding to LC3B

and promotes its interaction with K63- and K48-ubiquitin chains (Wurzer et al., 2015). Though NDP52 forms dimers and trimers through its coiled-coil domain, the functional relevance of NDP52 oligomerization has yet to be characterized (Kim, Beom Hong, Hoe Kim, Hoon Kwon, & Kyu Song, 2013). My results are consistent with the possibility that NDP52 oligomerization is important for KapB-mediated PB disassembly. KapB-expressing cells rescued from NDP52 knockdown with a UBD/LIR mutant NDP52 displayed fewer PBs/cell than NDP52 knockdown alone (Figure 4.6). This suggests that another mechanism like oligomerization contributes to the activity of NDP52-mediated PB disassembly. To directly address this, I would like to examine PB dynamics in KapB-expressing cells rescued from NDP52 knockdown with an oligomerization NDP52 mutant and determine the importance of NDP52 receptor oligomerization in PB cargo targeting and degradation.

Post translational modifications (PTMs) including phosphorylation also regulate selective autophagy receptor activity. TANK binding kinase 1 (TBK1) phosphorylates OPTN and p62 to enhance interactions with LC3 orthologs and ubiquitinated cargo; this phosphorylation is essential for efficiency xenophagy and mitophagy (Lazarou et al., 2015; Matsumoto, Wada, Okuno, Kurosawa, & Nukina, 2011; Thurston, Ryzhakov, Bloor, von Muhlinen, & Randow, 2009; Wild et al., 2011). NDP52 has a SKICH domain that is also phosphorylated by TBK1 which is indirectly recruited to the selective autophagy receptor (Fu et al., 2018; Heo, Ordureau, Paulo, Rinehart, & Harper, 2015; Thurston et al., 2009). Although the impacts of this phosphorylation are unknown, TBK1 recruitment to NDP52 promotes its localization to group A streptococcus, suggesting that NDP52 phosphorylation may promote cargo binding (Minowa-Nozawa, Nozawa,

Okamoto-Furuta, Kohda, & Nakagawa, 2017). Since there are no commercially available antibodies available that detect phosphorylated NDP52, the phosphorylation status of NDP52 after KapB expression could be investigated using Phos-Tag gels. If KapB induces NDP52 phosphorylation, these results may suggest that TBK1 is altered by KapB expression providing a potential mechanism of KapB-mediated NDP52 activation.

Much of the research surrounding selective autophagy regulation focuses on PTMs and very little is known about the transcriptional control of selective autophagy receptors. Transcription factor EB (TFEB) is a well characterized transcription factor regulating autophagy, lysosomal biogenesis and exocytosis. There is evidence showing TFEB activation transcriptionally upregulates p62 but it is not known whether NDP52 transcription is also increased (Rusmini et al., 2019). There is also evidence suggesting Nuclear factor E2-related factor 2 (NRF2), a transcription factor activated in response to oxidative stress regulates selective autophagy by inducing the transcription of NDP52 and p62 in addition to bulk autophagy genes (Atg5, Atg7 and Atg12) (A. Jain et al., 2010; Jo et al., 2014; Pajares et al., 2016). Given that NRF-2 is activated in KSHV-infected cells, it would be interesting to determine whether ectopic KapB expression could mediate NRF-2 activation or increase NDP52 transcription (Gjyshi et al., 2015). These experiments would help determine whether KapB is activating NDP52 transcription or altering NDP52 in a post-transcriptional manner.

5.3.3 Alternate Roles of NDP52 in Facilitating PB Disassembly

My data suggests that KapB-mediated PB disassembly relies on NDP52 and is in part dependent on the LIR and UBD domains, thus providing evidence that this phenotype is due to its activity as a selective autophagy receptor and not a result of off-

target effects. Nevertheless, knockdown experiments cannot differentiate with certainty that the selective autophagy receptor activity of NDP52 is the reason for its importance to KapB-mediated PB disassembly. NDP52 also plays important roles in autophagosome maturation and transcriptional control. NDP52 contains a non-canonical LIR that displays preferential binding of LC3 ortholog, LC3C over LC3A and LC3B (Verlhac, Gré, Viret, & Faure, 2015; von Muhlinen et al., 2012). Cargo targeting is mediated through NDP52-LC3C interaction, as was detected during *Salmonella typhimurium* infection (Verlhac et al., 2015; von Muhlinen et al., 2012. Following cargo targeting, autophagosome maturation was mediated in part by the binding of NDP52 to LC3A, LC3B and MyosinVI (Verlhac, Gré, et al., 2015; von Muhlinen et al., 2012). Determining which LC3 ortholog is required for NDP52-mediated PB disassembly after KapB expression may provide insight into differentiating the role of NDP52 as a selective autophagy receptor vs. autophagosome maturation. NDP52 also activates nuclear MyoVI by stabilizing MyoVI binding to RNA polymerase II, which causes enhanced transcription (Fili et al., 2017; Morriswood et al., 2007). The antibody-mediated depletion of NDP52 eliminated this transcriptional response by 50% (Fili et al., 2017; Morriswood et al., 2007). From what is known about PB dynamics, I speculate that decreased cellular mRNA transcripts would not increase the number of PBs per cell to the level that I observed after NDP52 knockdown. This is consistent with the model that KapB induces NDP52 activity as a selective autophagy receptor to mediate PB disassembly (Brengues et al., 2005).

5.3.4 MK2EE-Mediated PB Disassembly Does Not Require NDP52

I also investigated whether NDP52 was required for PB disassembly induced by a constitutively active form of the kinase, MK2 (MK2EE). KapB activates MK2 and previous work showed that MK2EE induces PB disassembly and ARE-mRNA stabilization (Corcoran et al., 2015). I hypothesized that MK2EE-dependent PB disassembly would also be dependent on NDP52. To our surprise, NDP52 knockdown did not reverse MK2-EE mediated PB disassembly or ARE-mRNA stabilization as determined by a luciferase assay (Figures 4.12, 4.13). While it is tempting to conclude that MK2- and KapB-induced PB disassembly is mechanistically different, there are several significant limitations to this experiment. The construct MK2EE is a constitutively active form of MK2 that is not representative of the transient nature of kinase activation in MAPK signalling cascades (Gurgis et al., 2014). MK2 activation also impacts cell cycle regulation by promoting G2/M arrest (Gurgis et al., 2014; Manke et al., 2005). Previous work shows PBs are cleared and become undetectable during late G2 and mitosis (Aizer et al., 2013). It is highly possible that MK2EE induces cell cycle stress thus promoting PB disassembly that is unable to be reversed by NDP52 knockdown. Monitoring PB dynamics using other stimuli that activate MK2 (such as TNF or LPS) may provide a less specific but more physiologically relevant activation of MK2-mediated PB disassembly. Consistent with this, we know that TNF induces PB disassembly (Castle and Corcoran, unpublished).

5.4 KapB Increases Steady-State Levels of Endogenous ARE-mRNAs

Having determined that NPD52 is required for KapB mediated PB disassembly, I also investigated whether KapB-mediated ARE-mRNA stabilization required NDP52.

Using an established luciferase reporter assay that measures firefly luminescence from an ARE-containing Fluc reporter, I showed that KapB-mediated ARE-mRNA stabilization required NDP52 (Figure 4.7) (Corcoran et al., 2011). This reporter assay is an indirect method of assessing ARE-mRNA stabilization; in this case, stabilization is measured by monitoring the luminescence of a Firefly luciferase construct containing an AU-rich element from GM-CSF that is then normalized to the luminescence of the Renilla Luciferase transfection control. Because the assay monitors the functional activity of the translated protein products of the luciferase constructs rather than the transcripts themselves, the luciferase assay tends to have a very robust phenotype. However, it does not identify specific transcripts altered by KapB expression.

To support my data derived from the ARE-mRNA stabilization reporter assay, I used RT-qPCR to investigate if KapB upregulated the steady-state levels of endogenous ARE-mRNAs. I chose to assay the levels of transcripts for IL-6, CXCL8, COX-2, GM-CSF, TNF and IL-1β. All of these transcripts contain AREs, KSHV infection is associated with upregulation of these cytokines or cytokine mRNAs and KapB causes increases the cytokines IL-6 and GM-CSF in several different cell types (Barbara Ensoli & Stürzl, 1998; L. Guo, Louis, & Bohjanen, 2018; King, 2013; Lane et al., 2002; McCormick & Ganem, 2005; Miles et al., 1990; Riva et al., 2010; Sadagopan et al., 2007; Salahuddin et al., 1988). With no pre-treatment, KapB slightly increased the steady-state levels of TNF, GM-CSF and IL-6 relative to vector control (Figure 4.8). With no treatment, Cq values for TNF and GM-CSF were between 32 and 35 in vector and KapB cells; although the minimum information for publication of quantitative real-time PCR experiments (MIQE) guidelines suggest not to disregard Cqs under 40, it will be

important to validate these results with a more sensitive technique like ddPCR (Bustin et al., 2009). That said, KapB-specific increases in IL-6, GM-CSF and TNF were maintained at 6h post LPS with Cq values <30, suggesting qPCR result reliability (Figure 4.8). These data show that certain ARE-mRNA are increased by KapB expression but due to the complex regulation of cytokine mRNAs, these phenotypes require further examination.

Inflammatory responses are temporally regulated and can be highly diverse. This premise is demonstrated during *de novo* KSHV infection where between 5-15 min post infection there is a significant activation of both NF-κβ and AKT signaling (Sadagopan et al., 2007). Moderate activation of NF-κβ is maintained 72h into latency while 4h post infection, AKT activation is drastically reduced (Sadagopan et al., 2007). These results correlated to very different cytokine profiles present at 2h, 4h and 24h post infection, demonstrating the importance of precise timing in the identification and understanding of inflammatory cytokine responses (Sadagopan et al., 2007). Although I completed a time course of LPS treatment (6, 12h), this may not have been enough to properly account for the variability of mRNA half-life which can range from 15 min to 24h (Seko, Cole, Kasprzak, Shapiro, & Ragheb, 2006). Therefore, the times chosen could prevent detection of changes in several mRNAs due to the transient nature of these responses. Since KapB has been expressed for >72h prior to lysis for total RNA, this time course would also not detect transient effects due to initial KapB expression that are not sustained over time. Consequently, the addition of several time points and using an inducible construct to control KapB expression will provide a better understanding of KapB-mediated changes to ARE-mRNA expression.

Besides treatment timing, detecting changes in steady-state levels of mRNAs is also dependent on drug type and concentration. LPS was chosen to stimulate KapB cells as it stimulates TLR4 activation, causing the transcription of inflammatory molecules including many with AREs (Akira & Takeda, 2004; Gruffaz, Vasan, Tan, Ramos da Silva, & Gao, 2017; B. S. Park & Lee, 2013). Indeed, post LPS, increased levels of IL-6, CXCL8, COX-2, GM-CSF, TNF and IL-1β were detected to varying degrees in HUVECs (Figure 4.8). KSHV infection is associated with constitutive upregulation of TLR4 signaling which results in chronic IL-6, IL-1β and IL-18 expression, suggesting stimulation of KapB cells with LPS is physiologically relevant to KSHV infection (Gruffaz et al., 2017). Nonetheless, multiple other TLRs (E.g. TLR2, TLR3) and pattern recognition receptor are important for regulating transcription factor activation during KSHV infection (Jha et al., 2016). LPS also stimulates autophagy by causing reactive oxygen species production; this complicates data analysis as it is difficult to determine whether KapB-mediated increase in ARE-mRNAs are associated with PB disassembly or due to KapB mediated increases in autophagy, as Torin increased CXCL8 and IL-6 and Figure 3.2 (Sul, Park, Son, & Choi, 2017). Therefore, using other different TLR agonists and pro-inflammatory stimuli such as lipoteichoic acid (TLR2 agonist) or poly(I:C) (TLR3 agonist) to stimulate KapB-expressing cells would help to characterize if KapB induced increases in IL-6, GM-CSF and TNF are stimuli-specific and PB or autophagy-related.

In all my experiments, I have measured the steady-state level of a given mRNA transcript, rather than mRNA stability and decay rates. It is possible that by choosing not to determine transcript half-life, I have missed small changes in transcript decay.

Actinomycin D inhibits *de novo* transcription and is commonly used to assay endogenous mRNA decay; this approach could provide valuable insight into KapB-alterations of specific ARE-mRNA decay rates. These experiments would also permit the differentiation between transcriptional effects and mRNA stability effects elicited by KapB–induced PB disassembly. Several studies suggest KapB can impact gene transcription or transcript stabilization. King, 2013 identified that KapB induces STAT-3 phosphorylation and increases steady-state mRNA levels of downstream effector gene CCL5. KapB also increases stabilization of ARE-containing gene PROX-1; the master regulator of lymphatic endothelium differentiation (Yoo et al., 2010). Lastly, KapB was found to bind the transcription factor c-myc altering the expression and activity of angiogenic miRNAs (H.-C. Chang et al., 2016). These studies indicate that KapB may hijack cellular pathways and alter the transcriptional profile of cells. A nuclear-run off assay followed by dot-plot hybridization could be used to detect wither KapB increases specific gene transcription.

By using conditioned media from latently infected cells, I aimed to replicate the cytokine and angiogenic factor-containing milieu that would normally be present during latent infection. KapB expression alone induced slight increases in the levels of IL-6, COX-2, CXCL8 and IL-1β (Figure 4.9). After 6h of conditioned media treatment, KapB-specific increases in IL-6 and COX-2 were detected (Figure 4.9). Because there were some discrepancies in the baseline expression of IL-1β and COX-2 (elevated compared to Figure 4.8) these data were difficult to interpret. The discrepancy may be due to increased KapB transduction efficiency or result from the complex transcriptional and post-transcriptional regulation of IL-1β and COX-2 (Fenton, 1992; Harris et al., 2011; Kang,

Mbonye, DeLong, Wada, & Smith, 2007; Rubartelli, Bajetto, Allavena, Cozzolino, & Sitia, 1993). However, the same experimental limitations discussed above (experiment timing, stimulus choice and assaying steady-state levels of mRNAs instead of decay) may also impact this set of experiments. However, taken together these data suggest that KapB-specific increase in ARE-mRNAs can be induced with several different stimuli.

iSLK.219 cells were originally believed to be endothelial cells but were subsequently discovered to be Caki-1 renal carcinoma epithelial cells (Stürzl et al., 2013). Therefore, conditioned media from these KSHV-infected epithelial cells likely contains a cytokine profile that is distinct from that which would be derived from KSHV-infected EC media. Endothelial cells orchestrate immune cell recruitment and inflammatory responses and consequently, produce a wide variety of adhesion molecules and cytokines relevant to KSHV infection including monocyte chemotactic protein-1 (MCP-1) IL-6, IL-8, TNF (Barbara Ensoli & Stürzl, 1998; Krishnaswamy, Kelley, Yerra, Smith, & Chi, 1999; Makó et al., 2010; Nilsen et al., 1998). The differential cytokine profile in epithelial cells and endothelial cells may explain why the magnitude of KapB specific increases in COX-2 and IL-6 were relatively small. Therefore, repeating conditioned media experiments using supernatant from a primary endothelial model of KSHV infection provides a more representative environment of KSHV infection.

There are several other experiments that would provide better insight into the biological role of KapB-mediated ARE-mRNA stabilization during viral infection. During viral latency, KapB would normally be co-expressed with the other products of the latency locus, including vFLIP, vCyclin, and LANA. All of these KSHV genes can impact the inflammatory nature of the lesion (Purushothaman et al., 2016). Therefore,

experiments with ectopic KapB expression may not adequately represent KapB function during KSHV infection. My experiments support this premise as without stimulation, KapB expression elicits small steady-state increases in some ARE-mRNAs; however, transcriptional upregulation (by LPS or conditioned media) enhances the KapB-mediated phenotype (Figures 4.8, 4.9). Our lab recently created a suite of recombinant KSHV viruses using the BAC16 system that target the kaposin locus (Brulois et al., 2012; MacNeil, Kleer and Corcoran, unpublished). Using RNA-seq or Luminex technology to assess how cytokine and cytokine mRNA levels alter between wild-type KSHV-infected cells and ΔKapB KSHV-infected cells would solidly establish how KapB contributes to the proinflammatory phenotype induced by KSHV latency.

5.4.1 The Impact of NDP52 on Steady-state Levels ARE-mRNA Requires Further Characterization

I sought to determine whether the knock down of selective autophagy receptor NDP52 impacted steady-state levels of ARE-mRNAs that responded to KapB expression. I hypothesized that because NDP52 knockdown reversed PB disassembly, it would also reverse KapB-mediated ARE-mRNA stabilization. Due to time constraints, I conducted this experiment only once. The data showed that NDP52 knockdown does not alter IL-6 or CXCL8 steady-state levels and increased COX-2 levels (Figure 4.10). The only cytokine mRNA that responded as I predicted was GM-CSF, which displayed decreased steady-state levels in KapB-expressing cells that lacked NDP52. This is an interesting observation, in particular because the luciferase reporter ARE-mRNA stabilization assay, which also responded to NDP52 knockdown, incorporates an ARE element derived from the 3'-UTR of GM-CSF into the Fluc reporter.

NDP52 is a negative regulator of NF-κβ signaling because it mediates the degradation of TLR adaptors molecules TRIF and TRAF6 (Inomata, Niida, Shibata, & Into, 2012). Therefore, it is difficult to conclude whether the impact of NDP52 knockdown on cytokine mRNA levels was due to PB disassembly and the concomitant ARE-mRNA stabilization or its regulation of NF-κβ activation. In a study by Inomata et al., (2012), knockdown of NDP52 alone did not increase expression of IL-6 and CXCL8, but in combination with the knockdown of a ubiquitin editing enzyme A20, poly(I:C)-induced increases in IL-6 and CXCL8 transcripts were reduced. Clearly, there are negative regulators of NDP52 that may mask its activity. Yang et al., detected that NDP52 knockdown increased expression of CCL5, IL-6 and CXCL10 in an adenocarcinoma cell line post IL-1β stimulation, thus showing that NDP52-induced changes in mRNA expression are cell-line and stimulus specific (S. Yang et al., 2016). Overall, there is promising evidence indicating NDP52 alters levels of proinflammatory mRNAs, but the precise phenotype and its regulation are not well understood.

5.5 Model of KapB function in KSHV infection

The development of KS results from complex interactions between lytic and latent viral proteins and the immune system (Purushothaman et al., 2016). It is well established that KSHV induced inflammation and angiogenesis plays an important role in KS. Several latent and lytic viral proteins play an important role in inducing these angiogenic and inflammatory phenotypes by altering host cell signaling, causing subsequent activation of several transcription factors that increase the steady-state levels of cytokine mRNAs (Purushothaman et al., 2016). My thesis results, in conjunction with previous reports of KapB activity, lead me to propose a model by which KapB

contributes to the establishment and maintenance of KSHV latent infection and KS-associated inflammation and angiogenesis (see Figure 5.1 for model).

In latently and lytically infected cells, the synergistic activity of vIL-6, vGPCR and vFLIP increase transcription of inflammatory mRNAs, many of which contain AREs. vIL-6 is a lytic gene that directly binds GP130, activating the downstream JAK-STAT, MAPK and AKT pathways resulting in increased activation of transcription factors STAT 1/3 and STAT5. Activation of these transcription factors increases VEGF and angiopoietin-2 expression, promoting angiogenesis and vascular permeability (Osborne, Moore, & Chang, 1999; Purushothaman et al., 2016; Suthaus, Adam, Grötzinger, Scheller, & Rose-John, 2011). As vIL-6 is detected in few cells in the lesion, it is assumed to signal in a paracrine manner (Suthaus et al., 2011). vGPCR is an early lytic gene that also contributes to "KS development in a paracrine fashion" by activating NF-κβ, protein kinase C (PKC), activator protein-1 (AP1) and Nuclear factor of activated T-cells (NFAT), thus causing an increase in VEGF, IL-1β, CXCL8 and TNF levels (Jham et al., 2011; Montaner et al., 2003; Suthaus et al., 2011). vFLIP is a latent gene that activates NF-κβ pathway by directly binding Iκβ kinase, therefore inducing increased TNF, IL-6, IL-10, IL-6 and CXCL8 expression Ballon, Akar, & Cesarman, 2015; Chaudhary, Jasmin, Eby, & Hood, 1999; Field et al., 2003; Guasparri, Keller, & Cesarman, 2004; Grossman, Podgrabinska, Skobe & Ganem, 2006). Some cytokines and immunomodulatory molecules produced by lytic or latently infected KSHV cells are released into the extracellular space stimulating autocrine and paracrine signaling in latently infected and surrounding cells.

The paracrine signaling induced by these molecules and the cell autonomous function of viral proteins expressed during latency (e.g. vFLIP) activate transcription factors like NF-κβ, AP-1 and NFAT to stimulate transcription of inflammatory ARE-mRNAs in the latent cells that comprise the bulk of the lesion (Figure 5.1A). I propose that KapB inhibits the decay of these ARE-mRNAs, enhancing their expression. KapB mediates this effect by inducing the disassembly of PBs using a mechanism that requires the selective autophagy receptor, NDP52 (Figure 5.1B). In my model, activated NDP52 binds a PB component(s) in a ubiquitin-dependent manner while also binding LC3 on the phagophore membrane via a LIR interaction. This molecular bridge targets the PB

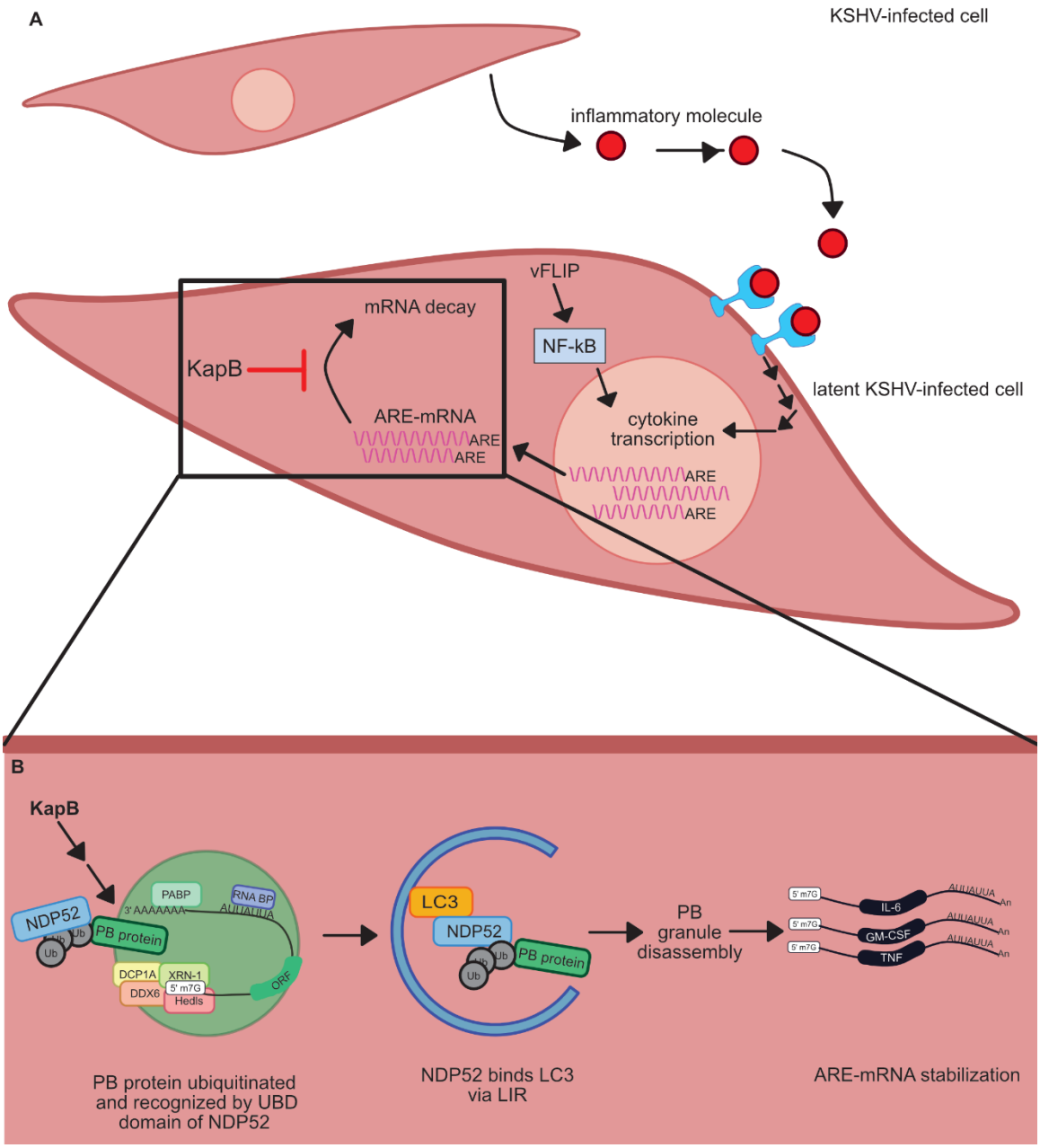

Figure 5.1: Model of KapB-mediated selective PB catabolism in KS lesions.
(A) In latently and lytically infected cells, the synergistic activity of several latent and lytic genes such as vIL-6, vGPCR and vFLIP increase transcription of immunomodulatory mRNAs including many transcripts which contain AREs. ARE-mRNAs are exported to the cytoplasm where KapB inhibits mRNA decay (B) Mechanism of KapB ARE-mRNA decay inhibition. KapB activates selective autophagy receptor NDP52 which binds PB component(s) in a ubiquitin-dependent manner. NDP52 binds LC3 (via LIR interactions) thus targeting the PB component for autophagic degradation. PB component degradation destabilizes the RNA granule causing PB disassembly thus, permitting the stabilization and expression of ARE-mRNA containing transcripts like IL-6, GM-CSF and TNF.

component(s) to autophagic membranes for degradation. When key PB component(s) are lost, this event destabilizes the integrity of the RNP granule, causing PB disassembly. Consequently, ARE-containing inflammatory mRNAs like IL-6, TNF and GM-CSF are not shuttled to PBs for decay; rather, they are stabilized. This is a novel model in which KapB sustains and enhances the transcriptional responses induced by other viral proteins through the selective disassembly of PBs, thereby contributing to the angiogenic and proinflammatory phenotypes important for KS development (Figure 5.1).

5.6 Concluding Remarks

The intricacy of viral infections stems from the complex interactions that occur between the virus and the immune system. KSHV is an excellent example of this complex interplay, whereby viral dysregulation of host cellular pathways alters cellular and immunological homeostasis resulting in tumourigenesis. In my thesis, I sought to better understand the contribution of the latent viral protein Kaposin B to the inflammatory and angiogenic phenotypes detected in the KS lesions. I did so by characterizing the molecular mechanism by which KapB induces the disassembly of post-transcriptional nodes of regulation, PBs. Using a novel assay to monitor the autophagic degradation of PB proteins I determined that PB protein levels are regulated in part by autophagy. I also determined that selective autophagy via NDP52 is a requisite intermediate for PB disassembly and that PB disassembly correlates to increases in certain AU-rich element mRNAs. These results lead me to propose a model of KSHV latency, in which KapB enhances the transcriptional responses induced by other viral proteins and promotes inflammation. While more work is required to fully understand the

complex regulation of selective autophagy receptors and PB component cargo targeting, my thesis provides the groundwork to better understand how viral hijacking of selective autophagy regulation elicits pleiotropic effects.

This study highlights the importance of studying selective autophagy. As our understanding of the wide variety of cargo that is subject to autophagic degradation increases, we can appreciate that the dysregulation of selective autophagy perturbs cellular homeostasis in a myriad of ways, contributing to disease development. While the nonspecific downstream effects of modulating bulk autophagic flux have stunted its clinical usefulness as a therapeutic intervention strategy, the specificity of selective autophagy and its players, the selective autophagy receptors, may provide better therapeutic targets for many diseases. In particular, this study has revealed that therapeutic targeting of NDP52-induced PB catabolism may be a useful strategy to limit pathological inflammation. In summary, my work has uncovered a novel link between selective autophagy and PB dynamics that contributes to the regulation of inflammatory responses thus providing insight into the control and potential treatment of various inflammation-associated diseases.

Bibliography

Ablashi, D. V, Chatlynne, L. G., Whitman, J. E., Cesarman, E., & Cesarman, E. (2002). Spectrum of Kaposi's sarcoma-associated herpesvirus, or human herpesvirus 8, diseases. *Clinical Microbiology Reviews*, *15*(3), 439–464. https://doi.org/10.1128/CMR.15.3.439-464.2002

Aizer, A., Kafri, P., Kalo, A., & Shav-Tal, Y. (2013). The P Body Protein Dcp1a Is Hyper-phosphorylated during Mitosis. *PLoS ONE*, *8*(1), e49783. https://doi.org/10.1371/journal.pone.0049783

Aizer, A., Kalo, A., Kafri, P., Shraga, A., Ben-Yishay, R., Jacob, A., … Shav-Tal, Y. (2014). Quantifying mRNA targeting to P-bodies in living human cells reveals their dual role in mRNA decay and storage. *Journal of Cell Science*, *127*(Pt 20), 4443–4456. https://doi.org/10.1242/jcs.152975

Akira, S., & Takeda, K. (2004). Toll-like receptor signalling. *Nature Reviews Immunology*, *4*(7), 499–511. https://doi.org/10.1038/nri1391

An, H., & Harper, J. W. (2017). Systematic analysis of ribophagy in human cells reveals bystander flux during selective autophagy. *Nature Cell Biology*, *20*(2), 135. https://doi.org/10.1038/s41556-017-0007-x

An, J., Lichtenstein, A. K., Brent, G., Rettig, M. B., Cesarman, E., & Knowles, D. (2002). The Kaposi sarcoma-associated herpesvirus (KSHV) induces cellular interleukin 6 expression: role of the KSHV latency-associated nuclear antigen and the AP1 response element. *Blood*, *99*(2), 649–654. https://doi.org/10.1182/blood.v99.2.649

Anding, A. L., & Baehrecke, E. H. (2017). Developmental Cell Cleaning House: Selective Autophagy of Organelles. https://doi.org/10.1016/j.devcel.2017.02.016

Ayache, J., Bénard, M., Ernoult-Lange, M., Minshall, N., Standart, N., Kress, M., & Weil, D. (2015). P-body assembly requires DDX6 repression complexes rather than decay or Ataxin2/2L complexes. *Molecular Biology of the Cell*, *26*(14), 2579–2595. https://doi.org/10.1091/mbc.E15-03-0136

Bais, C., Van Geelen, A., Eroles, P., Mutlu, A., Chiozzini, C., Dias, S., … Mesri, E. A. (2003). Kaposi's sarcoma associated herpesvirus G protein-coupled receptor immortalizes human endothelial cells by activation of the VEGF receptor-2/ KDR. *Cancer Cell*, *3*(2), 131–143. Retrieved from http://www.ncbi.nlm.nih.gov/pubmed/12620408

Bakheet, T., Williams, B. R. G., & Khabar, K. S. A. (2006). ARED 3.0: the large and diverse AU-rich transcriptome. *Nucleic Acids Research*, *34*(90001), D111–D114. https://doi.org/10.1093/nar/gkj052

Ballestas, M. E., Chatis, P. A., & Kaye, K. M. (1999). Efficient Persistence of Extrachromosomal KSHV DNA Mediated by Latency-Associated Nuclear Antigen. *Science*, *284*(5414), 641–644. https://doi.org/10.1126/science.284.5414.641

Ballon, G., Akar, G., & Cesarman, E. (2015). Systemic Expression of Kaposi Sarcoma Herpesvirus (KSHV) Vflip in Endothelial Cells Leads to a Profound Proinflammatory Phenotype and Myeloid Lineage Remodeling In Vivo. *PLOS Pathogens*, *11*(1), e1004581. https://doi.org/10.1371/journal.ppat.1004581

Barth, S., Glick, D., & Macleod, K. F. (2010). Autophagy: assays and artifacts. *The Journal of Pathology*, *221*(2), 117–124. https://doi.org/10.1002/path.2694

Beckstead, J. H., Wood, G. S., & Fletcher, V. (1985). Evidence for the origin of Kaposi's sarcoma from lymphatic endothelium. *The American Journal of Pathology*, *119*(2), 294–300. Retrieved from http://www.ncbi.nlm.nih.gov/pubmed/2986460

Birgisdottir, Å. B., Lamark, T., & Johansen, T. (2013). The LIR motif - crucial for selective autophagy. *Journal of Cell Science*, *126*(Pt 15), 3237–3247. https://doi.org/10.1242/jcs.126128

Bish, R., Cuevas-Polo, N., Cheng, Z., Hambardzumyan, D., Munschauer, M., Landthaler, M., & Vogel, C. (2015). Comprehensive Protein Interactome Analysis of a Key RNA Helicase: Detection of Novel Stress Granule Proteins. *Biomolecules*, *5*(3), 1441–1466. https://doi.org/10.3390/biom5031441

Blanco, F. F., Sanduja, S., Deane, N. G., Blackshear, P. J., & Dixon, D. a. (2014). Transforming growth factor β regulates P-body formation through induction of the mRNA decay factor tristetraprolin. *Molecular and Cellular Biology*, *34*(2), 180–195. https://doi.org/10.1128/MCB.01020-13

Brengues, M., Teixeira, D., & Parker, R. (2005). Movement of eukaryotic mRNAs between polysomes and cytoplasmic processing bodies. *Science (New York, N.Y.)*, *310*(5747), 486–489. https://doi.org/10.1126/science.1115791

Brulois, K. F., Chang, H., Lee, A. S.-Y., Ensser, A., Wong, L.-Y., Toth, Z., … Jung, J. U. (2012). Construction and Manipulation of a New Kaposi's Sarcoma-Associated Herpesvirus Bacterial Artificial Chromosome Clone. *Journal of Virology*, *86*(18), 9708–9720. https://doi.org/10.1128/jvi.01019-12

Buchan, J. R., Kolaitis, R., Taylor, J. P., & Parker, R. (2013). Eukaryotic Stress Granules Are Cleared by Autophagy and Cdc48 / VCP Function. *Cell*, *153*(7), 1461–1474. https://doi.org/10.1016/j.cell.2013.05.037

Bustin, S. A., Benes, V., Garson, J. A., Hellemans, J., Huggett, J., Kubista, M., … Wittwer, C. T. (2009). The MIQE guidelines: minimum information for publication of quantitative real-time PCR experiments. *Clinical Chemistry*, *55*(4), 611–622. https://doi.org/10.1373/clinchem.2008.112797

Carpenter, A. E., Jones, T. R., Lamprecht, M. R., Clarke, C., Kang, I., Friman, O., … Sabatini, D. M. (2006). CellProfiler: image analysis software for identifying and quantifying cell phenotypes. *Genome Biology*, *7*(10), R100. https://doi.org/10.1186/gb-2006-7-10-r100

Cemma, M., Kim, P. K., & Brumell, J. H. (2011). The ubiquitin-binding adaptor proteins p62/SQSTM1 and NDP52 are recruited independently to bacteria-associated microdomains to target Salmonella to the autophagy pathway. *Autophagy*, *7*(3), 341–345. https://doi.org/10.4161/auto.7.3.14046

Cesarman, E, Nador, R. G., Bai, F., Bohenzky, R. A., Russo, J. J., Moore, P. S., … Knowles, D. M. (1996). Kaposi's sarcoma-associated herpesvirus contains G protein-coupled receptor and cyclin D homologs which are expressed in Kaposi's sarcoma and malignant lymphoma. *Journal of Virology*, *70*(11), 8218–8223. Retrieved from http://www.ncbi.nlm.nih.gov/pubmed/8892957

Cesarman, Ethel, Chang, Y., Moore, P. S., Said, J. W., & Knowles, D. M. (1995). Kaposi's Sarcoma–Associated Herpesvirus-Like DNA Sequences in AIDS-Related Body-Cavity–Based Lymphomas. *New England Journal of Medicine*, *332*(18), 1186–1191. https://doi.org/10.1056/NEJM199505043321802

Cesarman, Ethel, Damania, B., Krown, S. E., Martin, J., Bower, M., & Whitby, D. (2019). Kaposi sarcoma. *Nature Reviews Disease Primers*, *5*(1), 9. https://doi.org/10.1038/s41572-019-0060-9

Chakraborty, S., Veettil, M. V., & Chandran, B. (2012). Kaposi's sarcoma associated herpesvirus entry into target cells. *Frontiers in Microbiology*, *3*(JAN), 1–13. https://doi.org/10.3389/fmicb.2012.00006

Chang, H.-C., Hsieh, T.-H., Lee, Y.-W., Tsai, C.-F., Tsai, Y.-N., Cheng, C.-C., & Wang, H.-W. (2016). c-Myc and viral cofactor Kaposin B co-operate to elicit angiogenesis through modulating miRNome traits of endothelial cells. *BMC Systems Biology*, *10*(S1), S1. https://doi.org/10.1186/s12918-015-0242-3

Chang, P.-J., Shedd, D., Gradoville, L., Cho, M.-S., Chen, L.-W., Chang, J., & Miller, G. (2002). Open reading frame 50 protein of Kaposi's sarcoma-associated herpesvirus directly activates the viral PAN and K12 genes by binding to related response elements. *Journal of Virology*, *76*(7), 3168–3178. https://doi.org/10.1128/jvi.76.7.3168-3178.2002

Chang, Y., Cesarman, E., Pessin, M. S., Lee, F., Culpepper, J., Knowles, D. M., & Moore, P. S. (1994). Identification of herpesvirus-like DNA sequences in AIDS-associated Kaposi's sarcoma. *Science (New York, N.Y.)*, *266*(5192), 1865–1869. Retrieved from http://www.ncbi.nlm.nih.gov/pubmed/7997879

Chang, Y., & Moore, P. S. (1996). Kaposi's Sarcoma (KS)-associated herpesvirus and its role in KS. *Infectious Agents and Disease*, *5*(4), 215–222. Retrieved from http://www.ncbi.nlm.nih.gov/pubmed/8884366

Chaudhary, P. M., Jasmin, A., Eby, M. T., & Hood, L. (1999). Modulation of the NF-κB pathway by virally encoded Death Effector Domains-containing proteins. *Oncogene*, *18*(42), 5738–5746. https://doi.org/10.1038/sj.onc.1202976

Chiang, P. Y., Shen, Y. F., Su, Y. L., Kao, C. H., Lin, N. Y., Hsu, P. H., … Chang, C. J. (2013). Phosphorylation of mRNA Decapping Protein Dcp1a by the ERK Signaling Pathway during Early Differentiation of 3T3-L1 Preadipocytes. *PLoS ONE*, *8*(4). https://doi.org/10.1371/journal.pone.0061697

Chung, Y.-H., Means, R. E., Choi, J.-K., Lee, B.-S., & Jung, J. U. (2002). Kaposi's sarcoma-associated herpesvirus OX2 glycoprotein activates myeloid-lineage cells to induce inflammatory cytokine production. *Journal of Virology*, *76*(10), 4688–4698. https://doi.org/10.1128/jvi.76.10.4688-4698.2002

Corcoran, J. A., Johnston, B. P., & McCormick, C. (2015). Viral activation of MK2-hsp27-p115RhoGEF-RhoA signaling axis causes cytoskeletal rearrangements, p-body disruption and ARE-mRNA stabilization. *PLoS Pathogens*, *11*(1), e1004597. https://doi.org/10.1371/journal.ppat.1004597

Corcoran, J. A., Khaperskyy, D. A., Johnston, B. P., King, C. A., Cyr, D. P., Olsthoorn, A. V., & McCormick, C. (2012). Kaposi's Sarcoma-Associated Herpesvirus G-Protein-Coupled Receptor Prevents AU-Rich-Element-Mediated mRNA Decay. *Journal of Virology*, *86*(16), 8859–8871. https://doi.org/10.1128/JVI.00597-12

Corcoran, J. A., Khaperskyy, D. A., & McCormick, C. (2011). Assays for monitoring viral manipulation of host ARE-mRNA turnover. *Methods*, *55*(2), 172–181. https://doi.org/10.1016/j.ymeth.2011.08.005

Cougot, N., Babajko, S., & Séraphin, B. (2004). Cytoplasmic foci are sites of mRNA decay in human cells. *The Journal of Cell Biology*, *165*(1), 31–40. https://doi.org/10.1083/jcb.200309008

Cougot, N., Cavalier, A., Thomas, D., & Gillet, R. (2012). The Dual Organization of P-bodies Revealed by Immunoelectron Microscopy and Electron Tomography. *Journal of Molecular Biology*, *420*(1–2), 17–28. https://doi.org/10.1016/j.jmb.2012.03.027

Decker, C. J., & Parker, R. (2012). P-Bodies and Stress Granules : Possible Roles in the Control of Translation and mRNA Degradation, 1–16. https://doi.org/10.1101/cshperspect.a012286

Decker, C. J., Teixeira, D., & Parker, R. (2007). Edc3p and a glutamine/asparagine-rich domain of Lsm4p function in processing body assembly in Saccharomyces cerevisiae. *The Journal of Cell Biology*, *179*(3), 437–449. https://doi.org/10.1083/jcb.200704147

Decker, L. L., Shankar, P., Khan, G., Freeman, R. B., Dezube, B. J., Lieberman, J., & Thorley-Lawson, D. A. (1996). The Kaposi sarcoma-associated herpesvirus (KSHV) is present as an intact latent genome in KS tissue but replicates in the peripheral blood mononuclear cells of KS patients. *The Journal of Experimental Medicine*, *184*(1), 283–288. https://doi.org/10.1084/jem.184.1.283

Dikic, I., & Elazar, Z. (2018). Mechanism and medical implications of mammalian autophagy. *Nature Reviews Molecular Cell Biology*, *19*(6), 349–364. https://doi.org/10.1038/s41580-018-0003-4

Dolman, N. J., Chambers, K. M., Mandavilli, B., Batchelor, R. H., & Janes, M. S. (2013). Tools and techniques to measure mitophagy using fluorescence microscopy. *Autophagy*, *9*(11), 1653–1662. https://doi.org/10.4161/auto.24001

Duprez, R., Lacoste, V., Briere, J., Couppie, P., Frances, C., Sainte-Marie, D., … Gessain, A. (2007). Evidence for a Multiclonal Origin of Multicentric Advanced Lesions of Kaposi Sarcoma. *JNCI Journal of the National Cancer Institute*, *99*(14), 1086–1094. https://doi.org/10.1093/jnci/djm045

Ellinghaus, D., Zhang, H., Zeissig, S., Lipinski, S., Till, A., Jiang, T., … Franke, A. (2013). Association between variants of PRDM1 and NDP52 and Crohn's disease, based on exome sequencing and functional studies. *Gastroenterology*, *145*(2), 339–347. https://doi.org/10.1053/j.gastro.2013.04.040

Engel, K., Schultz, H., Martin, F., Kotlyarov, A., Plath, K., Hahn, M., … Gaestel, M. (1995). Constitutive activation of mitogen-activated protein kinase-activated protein kinase 2 by mutation of phosphorylation sites and an A-helix motif. *The Journal of Biological Chemistry*, *270*(45), 27213–27221. https://doi.org/10.1074/jbc.270.45.27213

Ensoli, B, & Stürzl, M. (1998). Kaposi's sarcoma: a result of the interplay among inflammatory cytokines, angiogenic factors and viral agents. *Cytokine & Growth Factor Reviews*, *9*(1), 63–83. Retrieved from http://www.ncbi.nlm.nih.gov/pubmed/9720757

Ensoli, Barbara, Nakamura, S., Salahuddin, S. Z., Biberfeld, P., Larsson, L., Beaver, B., … Gallo, R. C. (2010). AIDS-Kaposi's Sarcoma-Derived Cells Express Cytokines with Autocrine and Paracrine Growth Effects. *Science*, *243*(4888), 223–226.

Ensoli, Barbara, & Stürzl, M. (1998). Kaposi's sarcoma: a result of the interplay among inflammatory cytokines, angiogenic factors and viral agents. *Cytokine & Growth Factor Reviews*, *9*(1), 63–83. https://doi.org/10.1016/S1359-6101(97)00037-3

Eulalio, A., Behm-Ansmant, I., & Izaurralde, E. (2007). P bodies: at the crossroads of post-transcriptional pathways. *Nature Reviews Molecular Cell Biology*, *8*(1), 9–22. https://doi.org/10.1038/nrm2080

Eulalio, A., Behm-Ansmant, I., Schweizer, D., & Izaurralde, E. (2007). P-body formation is a consequence, not the cause, of RNA-mediated gene silencing. *Molecular and Cellular Biology*, *27*(11), 3970–3981. https://doi.org/10.1128/MCB.00128-07

Fenger-Grøn, M., Fillman, C., Norrild, B., & Lykke-Andersen, J. (2005). Multiple processing body factors and the ARE binding protein TTP activate mRNA decapping. *Molecular Cell*, *20*(6), 905–915. https://doi.org/10.1016/j.molcel.2005.10.031

Fenton, M. J. (1992). Review: Transcriptional and post-transcriptional regulation of interleukin 1 gene expression. *International Journal of Immunopharmacology*, *14*(3), 401–411. https://doi.org/10.1016/0192-0561(92)90170-P

Field, N., Low, W., Daniels, M., Howell, S., Daviet, L., Boshoff, C., & Collins, M. (2003). KSHV vFLIP binds to IKK-γ to activate IKK. *Journal of Cell Science*, *116*(18), 3721–3728. https://doi.org/10.1242/JCS.00691

Fili, N., Hari-Gupta, Y., Dos Santos, Á., Cook, A., Poland, S., Ameer-Beg, S. M., … Toseland, C. P. (2017). NDP52 activates nuclear myosin VI to enhance RNA polymerase II transcription. *Nature Communications*, *8*(1), 1871. https://doi.org/10.1038/s41467-017-02050-w

Franks, T. M., & Lykke-Andersen, J. (2007). TTP and BRF proteins nucleate processing body formation to silence mRNAs with AU-rich elements. *Genes and Development*, *21*(6), 719–735. https://doi.org/10.1101/gad.1494707

Franks, T. M., & Lykke-Andersen, J. (2008). The control of mRNA decapping and P-body formation. *Molecular Cell*, *32*(5), 605–615. https://doi.org/10.1016/j.molcel.2008.11.001

Fu, T., Liu, J., Wang, Y., Xie, X., Hu, S., & Pan, L. (2018). Mechanistic insights into the interactions of NAP1 with the SKICH domains of NDP52 and TAX1BP1. *Proceedings of the National Academy of Sciences of the United States of America*, *115*(50), E11651–E11660. https://doi.org/10.1073/pnas.1811421115

Fujimura, K., Kano, F., & Murata, M. (2008). Identification of PCBP2, a facilitator of IRES-mediated translation, as a novel constituent of stress granules and processing bodies. *RNA (New York, N.Y.)*, *14*(3), 425–431. https://doi.org/10.1261/rna.780708

Gallouzi, I. E., Brennan, C. M., Stenberg, M. G., Swanson, M. S., Eversole, A., Maizels, N., & Steitz, J. A. (2000). HuR binding to cytoplasmic mRNA is perturbed by heat shock. *Proceedings of the National Academy of Sciences of the United States of America*, *97*(7), 3073–3078. https://doi.org/10.1073/pnas.97.7.3073

Galluzzi, L., Baehrecke, E. H., Ballabio, A., Boya, P., Bravo-San Pedro, J. M., Cecconi, F., … Kroemer, G. (2017). Molecular definitions of autophagy and related processes. *The EMBO Journal*, *36*(13), 1811–1836. https://doi.org/10.15252/embj.201796697

Galluzzi, L., Bravo-San Pedro, J. M., Levine, B., Green, D. R., & Kroemer, G. (2017). Pharmacological modulation of autophagy: therapeutic potential and persisting obstacles. *Nature Reviews. Drug Discovery*, *16*(7), 487–511. https://doi.org/10.1038/nrd.2017.22

Ganem, D. (2010). KSHV and the pathogenesis of Kaposi sarcoma: listening to human biology and medicine. *The Journal of Clinical Investigation*, *120*(4), 939–949. https://doi.org/10.1172/JCI40567

Garcia, M. C., Ray, D. M., Lackford, B., Rubino, M., Olden, K., & Roberts, J. D. (2009). Arachidonic Acid Stimulates Cell Adhesion through a Novel p38 MAPK-RhoA Signaling Pathway That Involves Heat Shock Protein 27. *Journal of Biological Chemistry*, *284*(31), 20936–20945. https://doi.org/10.1074/jbc.M109.020271

Georgakopoulos, N. D., Wells, G., & Campanella, M. (2017). The pharmacological regulation of cellular mitophagy. *Nature Chemical Biology*, *13*(2), 136–146. https://doi.org/10.1038/nchembio.2287

Gjyshi, O., Roy, A., Dutta, S., Veettil, M. V., Dutta, D., & Chandran, B. (2015). Activated Nrf2 Interacts with Kaposi's Sarcoma-Associated Herpesvirus Latency Protein LANA-1 and Host Protein KAP1 To Mediate Global Lytic Gene Repression. *Journal of Virology*, *89*(15), 7874–7892. https://doi.org/10.1128/JVI.00895-15

Glick, D., Barth, S., & Macleod, K. F. (2010). Autophagy: cellular and molecular mechanisms. *INVITED REVIEW Journal of Pathology J Pathol*, *221*(February), 3–12. https://doi.org/10.1002/path.2697

Gradoville, L., Gerlach, J., Grogan, E., Shedd, D., Nikiforow, S., Metroka, C., & Miller, G. (2000). Kaposi's sarcoma-associated herpesvirus open reading frame 50/Rta protein activates the entire viral lytic cycle in the HH-B2 primary effusion lymphoma cell line. *Journal of Virology*, *74*(13), 6207–6212. https://doi.org/10.1128/jvi.74.13.6207-6212.2000

Grossmann, C., Podgrabinska, S., Skobe, M., & Ganem, D. (2006). Activation of NF-kappaB by the latent vFLIP gene of Kaposi's sarcoma-associated herpesvirus is required for the spindle shape of virus-infected endothelial cells and contributes to their proinflammatory phenotype. *Journal of Virology*, *80*(14), 7179–7185. https://doi.org/10.1128/JVI.01603-05

Gruffaz, M., Vasan, K., Tan, B., Ramos da Silva, S., & Gao, S.-J. (2017). TLR4-Mediated Inflammation Promotes KSHV-Induced Cellular Transformation and Tumorigenesis by Activating the STAT3 Pathway. *Cancer Research*, *77*(24), 7094–7108. https://doi.org/10.1158/0008-5472.CAN-17-2321

Guasparri, I., Keller, S. A., & Cesarman, E. (2004). KSHV vFLIP Is Essential for the Survival of Infected Lymphoma Cells. *The Journal of Experimental Medicine*, *199*(7), 993–1003. https://doi.org/10.1084/jem.20031467

Guo, H.-G., Sadowska, M., Reid, W., Tschachler, E., Hayward, G., & Reitz, M. (2003). Kaposi's Sarcoma-Like Tumors in a Human Herpesvirus 8 ORF74 Transgenic Mouse. *Journal of Virology*, *77*(4), 2631–2639. https://doi.org/10.1128/JVI.77.4.2631-2639.2003

Guo, H., Chitiprolu, M., Gagnon, D., Meng, L., Perez-Iratxeta, C., Lagace, D., & Gibbings, D. (2014). Autophagy supports genomic stability by degrading retrotransposon RNA. *Nature Communications*, *5*, 5276. https://doi.org/10.1038/ncomms6276

Guo, L., Louis, I. V.-S., & Bohjanen, P. R. (2018). Post-transcriptional regulation of cytokine expression and signaling. *Current Trends in Immunology*, *19*, 33–40. Retrieved from http://www.ncbi.nlm.nih.gov/pubmed/30568341

Gurgis, F. M. S., Ziaziaris, W., & Munoz, L. (2014). Mitogen-Activated Protein Kinase-Activated Protein Kinase 2 in Neuroinflammation, Heat Shock Protein 27 Phosphorylation, and Cell Cycle: Role and Targeting. *Molecular Pharmacology*, *85*(2), 345–356. https://doi.org/10.1124/mol.113.090365

Gurkar, A. U., Chu, K., Raj, L., Bouley, R., Lee, S.-H., Kim, Y.-B., … Lee, S. W. (2013). Identification of ROCK1 kinase as a critical regulator of Beclin1-mediated autophagy during metabolic stress. *Nature Communications*, *4*, 2189. https://doi.org/10.1038/ncomms3189

Gustafson, E. A., & Wessel, G. M. (2010). DEAD-box helicases: posttranslational regulation and function. *Biochemical and Biophysical Research Communications*, *395*(1), 1–6. https://doi.org/10.1016/j.bbrc.2010.02.172

Hara-Kuge, S., & Fujiki, Y. (2008). The peroxin Pex14p is involved in LC3-dependent degradation of mammalian peroxisomes. *Experimental Cell Research*, *314*(19), 3531–3541. https://doi.org/10.1016/j.yexcr.2008.09.015

Hardy, S. D., Shinde, A., Wang, W.-H., Wendt, M. K., & Geahlen, R. L. (2017). Regulation of epithelial-mesenchymal transition and metastasis by TGF-β, P-bodies, and autophagy. *Oncotarget*, *8*(61), 103302–103314. https://doi.org/10.18632/oncotarget.21871

Harris, J., Hartman, M., Roche, C., Zeng, S. G., O'Shea, A., Sharp, F. A., … Kornfeld, H. (2011). Autophagy controls IL-1B secretion by targeting Pro-IL-1B for degradation. *Journal of Biological Chemistry*, *286*(11), 9587–9597. https://doi.org/10.1074/jbc.M110.202911

Heo, J.-M., Ordureau, A., Paulo, J. A., Rinehart, J., & Harper, J. W. (2015). The PINK1-PARKIN Mitochondrial Ubiquitylation Pathway Drives a Program of OPTN/NDP52 Recruitment and TBK1 Activation to Promote Mitophagy. *Molecular Cell*, *60*(1), 7–20. https://doi.org/10.1016/j.molcel.2015.08.016

Horvathova, I., Voigt, F., Kotrys, A. V., Zhan, Y., Artus-Revel, C. G., Eglinger, J., … Chao, J. A. (2017). The Dynamics of mRNA Turnover Revealed by Single-Molecule Imaging in Single Cells. *Molecular Cell*, *68*(3), 615-625.e9. https://doi.org/10.1016/j.molcel.2017.09.030

Hu, G., McQuiston, T., Bernard, A., Park, Y.-D., Qiu, J., Vural, A., … Williamson, P. R. (2015). A conserved mechanism of TOR-dependent RCK-mediated mRNA degradation regulates autophagy. *Nature Cell Biology*, *17*(7), 930–942. https://doi.org/10.1038/ncb3189

Hubstenberger, A., Courel, M., Bénard, M., Souquere, S., Ernoult-Lange, M., Chouaib, R., … Weil, D. (2017). P-Body Purification Reveals the Condensation of Repressed mRNA Regulons. *Molecular Cell*, *68*(1), 144-157.e5. https://doi.org/10.1016/j.molcel.2017.09.003

Ichimura, Y., Kumanomidou, T., Sou, Y., Mizushima, T., Ezaki, J., Ueno, T., … Komatsu, M. (2008). Structural basis for sorting mechanism of p62 in selective autophagy. *The Journal of Biological Chemistry*, *283*(33), 22847–22857. https://doi.org/10.1074/jbc.M802182200

Inomata, M., Niida, S., Shibata, K., & Into, T. (2012). Regulation of Toll-like receptor signaling by NDP52-mediated selective autophagy is normally inactivated by A20. *Cellular and Molecular Life Sciences : CMLS*, *69*(6), 963–979. https://doi.org/10.1007/s00018-011-0819-y

Jain, A., Lamark, T., Sjøttem, E., Bowitz Larsen, K., Atesoh Awuh, J., Øvervatn, A., … Johansen, T. (2010). *p62/SQSTM1* Is a Target Gene for Transcription Factor NRF2 and Creates a Positive Feedback Loop by Inducing Antioxidant Response Element-driven Gene Transcription. *Journal of Biological Chemistry*, *285*(29), 22576–22591. https://doi.org/10.1074/jbc.M110.118976

Jain, S., & Parker, R. (2013). The Discovery and Analysis of P Bodies (pp. 23–43). Springer, New York, NY. https://doi.org/10.1007/978-1-4614-5107-5_3

Jha, H., Banerjee, S., & Robertson, E. (2016). The Role of Gammaherpesviruses in Cancer Pathogenesis. *Pathogens*, *5*(1), 18. https://doi.org/10.3390/pathogens5010018

Jham, B. C., Ma, T., Hu, J., Chaisuparat, R., Friedman, E. R., Pandolfi, P. P., … Montaner, S. (2011). Amplification of the angiogenic signal through the activation of the TSC/mTOR/HIF axis by the KSHV vGPCR in Kaposi's sarcoma. *PLoS ONE*, *6*(4). https://doi.org/10.1371/journal.pone.0019103

Ji, C. H., & Kwon, Y. T. (2017). Crosstalk and Interplay between the Ubiquitin-Proteasome System and Autophagy. *Molecules and Cells*, *40*(7), 441–449. https://doi.org/10.14348/molcells.2017.0115

Jo, C., Gundemir, S., Pritchard, S., Jin, Y. N., Rahman, I., & Johnson, G. V. W. (2014). Nrf2 reduces levels of phosphorylated tau protein by inducing autophagy adaptor protein NDP52. *Nature Communications*, *5*, 3496. https://doi.org/10.1038/ncomms4496

Jones, T., Ramos da Silva, S., Bedolla, R., Ye, F., Zhou, F., & Gao, S. (2014). Viral Cyclin promotes KSHV-induced cellular transformation and tumorigenesis by overriding contact inhibition. *Cell Cycle*, *13*(5), 845–858. https://doi.org/10.4161/cc.27758

Kabeya, Y. (2000). LC3, a mammalian homologue of yeast Apg8p, is localized in autophagosome membranes after processing. *The EMBO Journal*, *19*(21), 5720–5728. https://doi.org/10.1093/emboj/19.21.5720

Kahn, H. J., Bailey, D., & Marks, A. (2002). Monoclonal Antibody D2-40, a New Marker of Lymphatic Endothelium, Reacts with Kaposi's Sarcoma and a Subset of Angiosarcomas. *Modern Pathology*, *15*(4), 434–440. https://doi.org/10.1038/modpathol.3880543

Kang, Y.-J., Mbonye, U. R., DeLong, C. J., Wada, M., & Smith, W. L. (2007). Regulation of Intracellular Cyclooxygenase Levels by Gene Transcription and Protein Degradation. *Progress in Lipid Research*, *46*(2), 108. https://doi.org/10.1016/J.PLIPRES.2007.01.001

Katayama, H., Kogure, T., Mizushima, N., Yoshimori, T., & Miyawaki, A. (2011). Chemistry & Biology Article A Sensitive and Quantitative Technique for Detecting Autophagic Events Based on Lysosomal Delivery. https://doi.org/10.1016/j.chembiol.2011.05.013

Katayama, H., Yamamoto, A., Mizushima, N., Yoshimori, T., & Miyawaki, A. (2008). GFP-like proteins stably accumulate in lysosomes. *Cell Structure and Function*, *33*(1), 1–12. Retrieved from http://www.ncbi.nlm.nih.gov/pubmed/18256512

Kaur, J., & Debnath, J. (2015). Autophagy at the crossroads of catabolism and anabolism. *Nature Reviews Molecular Cell Biology*, *16*(8), 461–472. https://doi.org/10.1038/nrm4024

Kedersha, N., Stoecklin, G., Ayodele, M., Yacono, P., Lykke-Andersen, J., Fritzler, M. J., … Anderson, P. (2005a). Stress granules and processing bodies are dynamically linked sites of mRNP remodeling. *The Journal of Cell Biology*, *169*(6), 871–884. https://doi.org/10.1083/jcb.200502088

Kedersha, N., Stoecklin, G., Ayodele, M., Yacono, P., Lykke-Andersen, J., Fritzler, M. J., … Anderson, P. (2005b). Stress granules and processing bodies are dynamically linked sites of mRNP remodeling. *The Journal of Cell Biology*, *169*(6), 871–884. https://doi.org/10.1083/jcb.200502088

Khaminets, A., Behl, C., & Dikic, I. (2016). Ubiquitin-Dependent And Independent Signals In Selective Autophagy. *Trends in Cell Biology*, *26*(1), 6–16. https://doi.org/10.1016/j.tcb.2015.08.010

Kim, B.-W., Beom Hong, S., Hoe Kim, J., Hoon Kwon, D., & Kyu Song, H. (2013). Structural basis for recognition of autophagic receptor NDP52 by the sugar receptor galectin-8. *Nature Communications*, *4*(1), 1613. https://doi.org/10.1038/ncomms2606

Kimura, S., Noda, T., & Yoshimori, T. (2007). Dissection of the Autophagosome Maturation Process by a Novel Reporter Protein, Tandem Fluorescent-Tagged LC3. *Autophagy*, *3*(5), 452–460. https://doi.org/10.4161/auto.4451

King, C. A. (2013). Kaposi's sarcoma-associated herpesvirus kaposin B induces unique monophosphorylation of STAT3 at serine 727 and MK2-mediated inactivation of the STAT3 transcriptional repressor TRIM28. *Journal of Virology*, *87*(15), 8779–8791. https://doi.org/10.1128/JVI.02976-12

Klepp, O., Dahl, O., & Stenwig, J. T. (1978). Association of Kaposi's sarcoma and prior immunosuppressive therapy. A 5-year material of Kaposi's sarcoma in Norway. *Cancer*, *42*(6), 2626–2630. https://doi.org/10.1002/1097-0142(197812)42:6<2626::AID-CNCR2820420618>3.0.CO;2-7

Klionsky, D. J., Abdalla, F. C., Abeliovich, H., Abraham, R. T., Acevedo-Arozena, A., Adeli, K., … Zuckerbraun, B. (2012). Guidelines for the use and interpretation of assays for monitoring autophagy. *Autophagy*, *8*(4), 445–544. https://doi.org/10.4161/auto.19496

Kogure, T., Karasawa, S., Araki, T., Saito, K., Kinjo, M., & Miyawaki, A. (2006). A fluorescent variant of a protein from the stony coral Montipora facilitates dual-color single-laser fluorescence cross-correlation spectroscopy. *Nature Biotechnology*, *24*(5), 577–581. https://doi.org/10.1038/nbt1207

Krishnaswamy, G., Kelley, J., Yerra, L., Smith, J. K., & Chi, D. S. (1999). Human Endothelium as a Source of Multifunctional Cytokines: Molecular Regulation and Possible Role in Human Disease. *Journal of Interferon & Cytokine Research*, *19*(2), 91–104. https://doi.org/10.1089/107999099314234

Kuma, A., Matsui, M., & Mizushima, N. (2007). LC3, an Autophagosome Marker, Can be Incorporated into Protein Aggregates Independent of Autophagy: Caution in the Interpretation of LC3 Localization. *Autophagy*, *3*(4), 323–328. https://doi.org/10.4161/auto.4012

Kwon, K.-Y., Viollet, B., & Yoo, O. J. (2011). CCCP induces autophagy in an AMPK-independent manner. *Biochemical and Biophysical Research Communications*, *416*(3–4), 343–348. https://doi.org/10.1016/j.bbrc.2011.11.038

Lane, B. R., Liu, J., Bock, P. J., Schols, D., Coffey, M. J., Strieter, R. M., … Markovitz, D. M. (2002). Interleukin-8 and growth-regulated oncogene alpha mediate angiogenesis in Kaposi's sarcoma. *Journal of Virology*, *76*(22), 11570–11583. https://doi.org/10.1128/jvi.76.22.11570-11583.2002

Lazarou, M., Sliter, D. A., Kane, L. A., Sarraf, S. A., Wang, C., Burman, J. L., … Youle, R. J. (2015). The ubiquitin kinase PINK1 recruits autophagy receptors to induce mitophagy. *Nature*, *524*(7565), 309–314. https://doi.org/10.1038/nature14893

Leung, T., Chen, X. Q., Manser, E., & Lim, L. (1996). The p160 RhoA-binding kinase ROK alpha is a member of a kinase family and is involved in the reorganization of the cytoskeleton. *Molecular and Cellular Biology*, *16*(10), 5313–5327. Retrieved from http://www.ncbi.nlm.nih.gov/pubmed/8816443

Li, H., Komatsu, T., Dezube, B. J., & Kaye, K. M. (2002). The Kaposi's Sarcoma-Associated Herpesvirus K12 Transcript from a Primary Effusion Lymphoma Contains Complex Repeat Elements, Is Spliced, and Initiates from a Novel Promoter. *Journal of Virology*, *76*(23), 11880. https://doi.org/10.1128/JVI.76.23.11880-11888.2002

Linares, J. F., Duran, A., Yajima, T., Pasparakis, M., Moscat, J., & Diaz-Meco, M. T. (2013). K63 Polyubiquitination and Activation of mTOR by the p62-TRAF6 Complex in Nutrient-Activated Cells. *Molecular Cell*, *51*(3), 283–296. https://doi.org/10.1016/j.molcel.2013.06.020

Liu, X., Cao, H., Li, J., Wang, B., Zhang, P., Dong Zhang, X., … Zhan, Z. (2017). Autophagy induced by DAMPs facilitates the inflammation response in lungs undergoing ischemia-reperfusion injury through promoting TRAF6 ubiquitination. *Cell Death and Differentiation*, *24*(4), 683–693. https://doi.org/10.1038/cdd.2017.1

Lu, K., den Brave, F., & Jentsch, S. (2017). Receptor oligomerization guides pathway choice between proteasomal and autophagic degradation. *Nature Cell Biology*, *19*(6), 732–739. https://doi.org/10.1038/ncb3531

Lukac, D. M., Renne, R., Kirshner, J. R., & Ganem, D. (1998). Reactivation of Kaposi's Sarcoma-Associated Herpesvirus Infection from Latency by Expression of the ORF 50 Transactivator, a Homolog of the EBV R Protein. *Virology*, *252*(2), 304–312. https://doi.org/10.1006/viro.1998.9486

Lukac, D. M., & Yuan, Y. (2007). *Reactivation and lytic replication of KSHV*. *Human Herpesviruses: Biology, Therapy, and Immunoprophylaxis*. Cambridge University Press. Retrieved from http://www.ncbi.nlm.nih.gov/pubmed/21348086

Luo, Y., Na, Z., & Slavoff, S. A. (2018). P-Bodies: Composition, Properties, and Functions. *Biochemistry*, *57*(17), 2424–2431. https://doi.org/10.1021/acs.biochem.7b01162

Makó, V., Czú Cz, J., Ka Weiszhár, Z., Herczenik, E., Matkó, J., Prohászka, Z., & Cervenak, L. (2010). Proinflammatory Activation Pattern of Human Umbilical Vein Endothelial Cells Induced by IL-1b, TNF-a, and LPS. https://doi.org/10.1002/cyto.a.20952

Manke, I. A., Nguyen, A., Lim, D., Stewart, M. Q., Elia, A. E. H., & Yaffe, M. B. (2005). MAPKAP Kinase-2 Is a Cell Cycle Checkpoint Kinase that Regulates the G2/M Transition and S Phase Progression in Response to UV Irradiation. *Molecular Cell*, *17*(1), 37–48. https://doi.org/10.1016/j.molcel.2004.11.021

Marnef, A., Maldonado, M., Bugaut, A., Balasubramanian, S., Kress, M., Weil, D., & Standart, N. (2010). Distinct functions of maternal and somatic Pat1 protein paralogs. *RNA (New York, N.Y.)*, *16*(11), 2094–2107. https://doi.org/10.1261/rna.2295410

Martina, J. A., Diab, H. I., Lishu, L., Jeong-A, L., Patange, S., Raben, N., & Puertollano, R. (2014). The nutrient-responsive transcription factor TFE3 promotes autophagy, lysosomal biogenesis, and clearance of cellular debris. *Science Signaling*, *7*(309), ra9. https://doi.org/10.1126/scisignal.2004754

Matsumoto, G., Wada, K., Okuno, M., Kurosawa, M., & Nukina, N. (2011). Serine 403 Phosphorylation of p62/SQSTM1 Regulates Selective Autophagic Clearance of Ubiquitinated Proteins. *Molecular Cell*, *44*(2), 279–289. https://doi.org/10.1016/j.molcel.2011.07.039

Mauthe, M., Orhon, I., Rocchi, C., Zhou, X., Luhr, M., Hijlkema, K.-J., … Reggiori, F. (2018). Chloroquine inhibits autophagic flux by decreasing autophagosome-lysosome fusion. *Autophagy*, *14*(8), 1435–1455. https://doi.org/10.1080/15548627.2018.1474314

McCormick, C., & Ganem, D. (2005). The Kaposin B Protein of KSHV Activates the p38/MK2 Pathway and Stabilizes Cytokine mRNAs. *Science*, *307*(5710), 739–741. https://doi.org/10.1126/science.1105779

McCormick, C., & Ganem, D. (2006). Phosphorylation and function of the kaposin B direct repeats of Kaposi's sarcoma-associated herpesvirus. *Journal of Virology*, *80*(12), 6165–6170. https://doi.org/10.1128/JVI.02331-05

Mesri, E. A., Cesarman, E., & Boshoff, C. (2010). Kaposi's sarcoma and its associated herpesvirus. *Nature Reviews. Cancer*, *10*(10), 707–719. https://doi.org/10.1038/nrc2888

Miles, S. A., Rezai, A. R., Salazar-González, J. F., Vander Meyden, M., Stevens, R. H., Logan, D. M., … Kishimoto, T. (1990). AIDS Kaposi sarcoma-derived cells produce and respond to interleukin 6. *Proceedings of the National Academy of Sciences of the United States of America*, *87*(11), 4068–4072. https://doi.org/10.1073/pnas.87.11.4068

Minowa-Nozawa, A., Nozawa, T., Okamoto-Furuta, K., Kohda, H., & Nakagawa, I. (2017). Rab35 GTPase recruits NDP52 to autophagy targets. *The EMBO Journal*, *36*(18), 2790–2807. https://doi.org/10.15252/embj.201796463

Mizushima, N., Yoshimori, T., & Levine, B. (2010). Methods in Mammalian Autophagy Research. *Cell*, *140*(3), 313–326. https://doi.org/10.1016/j.cell.2010.01.028

Montaner, S., Sodhi, A., Molinolo, A., Bugge, T. H., Sawai, E. T., He, Y., … Gutkind, J. S. (2003). Endothelial infection with KSHV genes in vivo reveals that vGPCR initiates Kaposi's sarcomagenesis and can promote the tumorigenic potential of viral latent genes. *Cancer Cell*, *3*(1), 23–36. https://doi.org/10.1016/S1535-6108(02)00237-4

Morriswood, B., Ryzhakov, G., Puri, C., Arden, S. D., Roberts, R., Dendrou, C., … Buss, F. (2007). T6BP and NDP52 are myosin VI binding partners with potential roles in cytokine signalling and cell adhesion. *Journal of Cell Science*, *120*(Pt 15), 2574–2585. https://doi.org/10.1242/jcs.007005

Musiwaro, P., Smith, M., Manifava, M., Walker, S. A., & Ktistakis, N. T. (2013). Characteristics and requirements of basal autophagy in HEK 293 cells. https://doi.org/10.4161/auto.25455

Myoung, J., & Ganem, D. (2011). iSLK cell. *Journal of Virological Methods*, *174*(1–2), 12–21. https://doi.org/10.1016/j.jviromet.2011.03.012

Nezich, C. L., Wang, C., Fogel, A. I., & Youle, R. J. (2015). MiT/TFE transcription factors are activated during mitophagy downstream of Parkin and Atg5. *The Journal of Cell Biology*, *210*(3), 435–450. https://doi.org/10.1083/jcb.201501002

Nicholas, J., Ruvolo, V. R., Burns, W. H., Sandford, G., Wan, X., Ciufo, D., … Reitz, M. S. (1997). Kaposi's sarcoma-associated human herpesvirus-8 encodes homologues of macrophage inflammatory protein-1 and interleukin-6. *Nature Medicine*, *3*(3), 287–292. https://doi.org/10.1038/nm0397-287

Nilsen, E. M., Johansen, F.-E., Jahnsen, F. L., Lundin, K. E. A., Scholz, T., Brandtzaeg, P., & Haraldsen, G. (1998). Cytokine profiles of cultured microvascular endothelial cells from the human intestine. *Gut*, *42*(5), 635–642. https://doi.org/10.1136/GUT.42.5.635

Noda, N. N., Kumeta, H., Nakatogawa, H., Satoo, K., Adachi, W., Ishii, J., … Inagaki, F. (2008). Structural basis of target recognition by Atg8/LC3 during selective autophagy. *Genes to Cells*, *13*(12), 1211–1218. https://doi.org/10.1111/j.1365-2443.2008.01238.x

Noda, N. N., Ohsumi, Y., & Inagaki, F. (2010). Atg8-family interacting motif crucial for selective autophagy. *FEBS Letters*, *584*(7), 1379–1385. https://doi.org/10.1016/j.febslet.2010.01.018

Olsvik, H. L., Lamark, T., Takagi, K., Larsen, K. B., Evjen, G., Øvervatn, A., … Johansen, T. (2015). FYCO1 Contains a C-terminally Extended, LC3A/B-preferring LC3-interacting Region (LIR) Motif Required for Efficient Maturation of Autophagosomes during Basal Autophagy. *Journal of Biological Chemistry*, *290*(49), 29361–29374. https://doi.org/10.1074/jbc.M115.686915

Osborne, J., Moore, P. S., & Chang, Y. (1999). KSHV-encoded viral IL-6 activates multiple human IL-6 signaling pathways. *Human Immunology*, *60*(10), 921–927. Retrieved from http://www.ncbi.nlm.nih.gov/pubmed/10566591

Ozgur, S., Chekulaeva, M., & Stoecklin, G. (2010). Human Pat1b Connects Deadenylation with mRNA Decapping and Controls the Assembly of Processing Bodies. *Molecular and Cellular Biology*, *30*(17), 4308–4323. https://doi.org/10.1128/MCB.00429-10

Padman, B. S., Nguyen, T. N., Uoselis, L., Skulsuppaisarn, M., Nguyen, L. K., & Lazarou, M. (2019). LC3/GABARAPs drive ubiquitin-independent recruitment of Optineurin and NDP52 to amplify mitophagy. *Nature Communications*, *10*(1), 1–13. https://doi.org/10.1038/s41467-019-08335-6

Pajares, M., Jiménez-Moreno, N., García-Yagüe, Á. J., Escoll, M., de Ceballos, M. L., Van Leuven, F., … Cuadrado, A. (2016). Transcription factor NFE2L2/NRF2 is a regulator of macroautophagy genes. *Autophagy*, *12*(10), 1902–1916. https://doi.org/10.1080/15548627.2016.1208889

Palanisamy, V., Jakymiw, A., Van Tubergen, E. A., D'Silva, N. J., & Kirkwood, K. L. (2012). Control of Cytokine mRNA Expression by RNA-binding Proteins and microRNAs. *Journal of Dental Research*, *91*(7), 651–658. https://doi.org/10.1177/0022034512437372

Palanisamy, V., Park, N. J., Wang, J., & Wong, D. T. (2008). AUF1 and HuR proteins stabilize interleukin-8 mRNA in human saliva. *Journal of Dental Research*, *87*(8), 772–776. https://doi.org/87/8/772 [pii]

Pankiv, S., Clausen, T. H., Lamark, T., Brech, A., Bruun, J.-A., Outzen, H., … Johansen, T. (2007). p62/SQSTM1 Binds Directly to Atg8/LC3 to Facilitate Degradation of Ubiquitinated Protein Aggregates by Autophagy. *Journal of Biological Chemistry*, *282*(33), 24131–24145. https://doi.org/10.1074/jbc.M702824200

Park, B. S., & Lee, J.-O. (2013). Recognition of lipopolysaccharide pattern by TLR4 complexes. *Experimental & Molecular Medicine*, *45*(12), e66–e66. https://doi.org/10.1038/emm.2013.97

Park, J. W., Lee, S. Y., Yang, J. Y., Rho, H. W., Park, B. H., Lim, S. N., … Kim, H. R. (1997). Effect of carbonyl cyanide m-chlorophenylhydrazone (CCCP) on the dimerization of lipoprotein lipase. *Biochimica et Biophysica Acta*, *1344*(2), 132–138. https://doi.org/10.1016/s0005-2760(96)00146-4

Parker, R., & Sheth, U. (2007a). P bodies and the control of mRNA translation and degradation. *Molecular Cell*, *25*(5), 635–646. https://doi.org/10.1016/j.molcel.2007.02.011

Parker, R., & Sheth, U. (2007b). P Bodies and the Control of mRNA Translation and Degradation. *Molecular Cell*, *25*(5), 635–646. https://doi.org/10.1016/j.molcel.2007.02.011

Parker, R., & Sheth, U. (2007c). P Bodies and the Control of mRNA Translation and Degradation. *Molecular Cell*, *25*(5), 635–646. https://doi.org/10.1016/J.MOLCEL.2007.02.011

Pearce, M., Matsumura, S., & Wilson, A. C. (2005). Transcripts encoding K12, v-FLIP, v-cyclin, and the microRNA cluster of Kaposi's sarcoma-associated herpesvirus originate from a common promoter. *Journal of Virology*, *79*(22), 14457–14464. https://doi.org/10.1128/JVI.79.22.14457-14464.2005

Penefsky, H. S. (1985). Mechanism of inhibition of mitochondrial adenosine triphosphatase by dicyclohexylcarbodiimide and oligomycin: relationship to ATP synthesis. *Proceedings of the National Academy of Sciences of the United States of America*, *82*(6), 1589–1593. https://doi.org/10.1073/pnas.82.6.1589

Petherick, K. J., Williams, A. C., Lane, J. D., Ordóñez-Morán, P., Huelsken, J., Collard, T. J., … Greenhough, A. (2013). Autolysosomal β-catenin degradation regulates Wnt-autophagy-p62 crosstalk. *The EMBO Journal*, *32*(13), 1903–1916. https://doi.org/10.1038/emboj.2013.123

Phospholipids, O. F., & Energy, F. O. R. (1973). Partial Resolution of the Enzymes Catalyzing Oxidative Phosphorylation, *248*(10), 676–684.

Purushothaman, P., Uppal, T., Sarkar, R., & Verma, S. (2016). KSHV-Mediated Angiogenesis in Tumor Progression. *Viruses*, *8*(12), 198. https://doi.org/10.3390/v8070198

Pyakurel, P., Pak, F., Mwakigonja, A. R., Kaaya, E., Heiden, T., & Biberfeld, P. (2006). Lymphatic and vascular origin of Kaposi's sarcoma spindle cells during tumor development. *International Journal of Cancer*, *119*(6), 1262–1267. https://doi.org/10.1002/ijc.21969

Qin, J., Li, W., Gao, S.-J., & Lu, C. (2017). KSHV microRNAs: Tricks of the Devil. *Trends in Microbiology*, *25*(8), 648–661. https://doi.org/10.1016/j.tim.2017.02.002

Rahman, H., Qasim, M., Oellerich, M., & Asif, A. R. (2014). Crosstalk between Edc4 and mammalian target of rapamycin complex 1 (mTORC1) signaling in mRNA decapping. *International Journal of Molecular Sciences*, *15*(12), 23179–23195. https://doi.org/10.3390/ijms151223179

Renne, R., Zhong, W., Herndier, B., McGrath, M., Abbey, N., Kedes, D., & Ganem, D. (1996). Lytic growth of Kaposi's sarcoma-associated herpesvirus (human herpesvirus 8) in culture. *Nature Medicine*, *2*(3), 342–346. https://doi.org/10.1038/nm0396-342

Richter, B., Sliter, D. A., Herhaus, L., Stolz, A., Wang, C., Beli, P., … Dikic, I. (2016). Phosphorylation of OPTN by TBK1 enhances its binding to Ub chains and promotes selective autophagy of damaged mitochondria. *Proceedings of the National Academy of Sciences of the United States of America*, *113*(15), 4039–4044. https://doi.org/10.1073/pnas.1523926113

Riva, G., Barozzi, P., Torelli, G., & Luppi, M. (2010). Immunological and Inflammatory Features of Kaposi's Sarcom and Other Kaposi's Sarcoma-Associated Herpesvirus/Human Herpesvirus 8-Associated Neoplasias. *AIDS Reviews*, *9*, 25–39.

Rock, K. L., Gramm, C., Rothstein, L., Clark, K., Stein, R., Dick, L., … Goldberg, A. L. (1994). Inhibitors of the proteasome block the degradation of most cell proteins and the generation of peptides presented on MHC class I molecules. *Cell*, *78*(5), 761–771. https://doi.org/10.1016/S0092-8674(94)90462-6

Rogov, V., Dötsch, V., Johansen, T., & Kirkin, V. (2014). Interactions between Autophagy Receptors and Ubiquitin-like Proteins Form the Molecular Basis for Selective Autophagy. *Molecular Cell*, *53*(2), 167–178. https://doi.org/10.1016/j.molcel.2013.12.014

Rogov, V., & Kirkin, V. (2014). Selective Autophagy: Role of Ubiquitin and Ubiquitin-Like Proteins in Targeting Protein Aggregates, Organelles, and Pathogens. *Autophagy: Cancer, Other Pathologies, Inflammation, Immunity, Infection, and Aging*, 59–88. https://doi.org/10.1016/B978-0-12-405877-4.00004-4

Rubartelli, A., Bajetto, A., Allavena, G., Cozzolino, F., & Sitia, R. (1993). Post-translational regulation of interleukin 1 beta secretion. *Cytokine*, *5*(2), 117–124. Retrieved from http://www.ncbi.nlm.nih.gov/pubmed/8334227

Rusmini, P., Cortese, K., Crippa, V., Cristofani, R., Cicardi, M. E., Ferrari, V., … Poletti, A. (2019). Trehalose induces autophagy via lysosomal-mediated TFEB activation in models of motoneuron degeneration. *Autophagy*, *15*(4), 631–651. https://doi.org/10.1080/15548627.2018.1535292

Russo, J. J., Bohenzky, R. A., Chien, M. C., Chen, J., Yan, M., Maddalena, D., … Moore, P. S. (1996). Nucleotide sequence of the Kaposi sarcoma-associated herpesvirus (HHV8). *Proceedings of the National Academy of Sciences of the United States of America*, *93*(25), 14862–14867. https://doi.org/10.1073/pnas.93.25.14862

Sadagopan, S., Sharma-Walia, N., Veettil, M. V., Raghu, H., Sivakumar, R., Bottero, V., & Chandran, B. (2007). Kaposi's Sarcoma-Associated Herpesvirus Induces Sustained NF-κB Activation during De Novo Infection of Primary Human Dermal Microvascular Endothelial Cells That Is Essential for Viral Gene Expression. *Journal of Virology*, *81*(8), 3949–3968. https://doi.org/10.1128/JVI.02333-06

Sadler, R., Wu, L., Forghani, B., Renne, R., Zhong, W., Herndier, B., & Ganem, D. (1999). A Complex Translational Program Generates Multiple Novel Proteins from the Latently Expressed Kaposin (K12) Locus of Kaposi's Sarcoma-Associated Herpesvirus. *Journal of Virology*, *73*(7).

Salahuddin, S., Nakamura, S., Biberfeld, P., Kaplan, M., Markham, P., Larsson, L., & Gallo, R. (1988). Angiogenic properties of Kaposi's sarcoma-derived cells after long-term culture in vitro. *Science*, *242*(4877), 430–433. https://doi.org/10.1126/science.2459779

Seko, Y., Cole, S., Kasprzak, W., Shapiro, B. A., & Ragheb, J. A. (2006). The role of cytokine mRNA stability in the pathogenesis of autoimmune disease. *Autoimmunity Reviews*, *5*(5), 299–305. https://doi.org/10.1016/J.AUTREV.2005.10.013

Shaid, S., Brandts, C. H., Serve, H., & Dikic, I. (2013). Ubiquitination and selective autophagy. *Cell Death & Differentiation*, *20*(1), 21–30. https://doi.org/10.1038/cdd.2012.72

Shen, L., Qi, Z., Zhu, Y., Song, X., Xuan, C., Ben, P., … Yin, Z. (2016). Phosphorylated heat shock protein 27 promotes lipid clearance in hepatic cells through interacting with STAT3 and activating autophagy. *Cellular Signalling*, *28*(8), 1086–1098. https://doi.org/10.1016/J.CELLSIG.2016.05.008

Sheth, U., & Parker, R. (2003). Decapping and decay of messenger RNA occur in cytoplasmic processing bodies. *Science (New York, N.Y.)*, *300*(5620), 805–808. https://doi.org/10.1126/science.1082320

Shimizu, S. (2018). Biological Roles of Alternative Autophagy. *Molecules and Cells*, *41*(1), 50–54. https://doi.org/10.14348/molcells.2018.2215

Sin, W. C., Chen, X. Q., Leung, T., & Lim, L. (1998). RhoA-binding kinase alpha translocation is facilitated by the collapse of the vimentin intermediate filament network. *Molecular and Cellular Biology*, *18*(11), 6325–6339. https://doi.org/10.1128/MCB.18.11.6325

Soulier, J., Grollet, L., Oksenhendler, E., Cacoub, P., Cazals-Hatem, D., Babinet, P., … Degos, L. (1995). Kaposi's sarcoma-associated herpesvirus-like DNA sequences in multicentric Castleman's disease. *Blood*, *86*(4), 1276–1280. Retrieved from http://www.ncbi.nlm.nih.gov/pubmed/7632932

Stark, C., Breitkreutz, B.-J., Reguly, T., Boucher, L., Breitkreutz, A., & Tyers, M. (2006). BioGRID: a general repository for interaction datasets. *Nucleic Acids Research*, *34*(Database issue), D535-9. https://doi.org/10.1093/nar/gkj109

Staskus, K. A., Zhong, W., Gebhard, K., Herndier, B., Wang, H., Renne, R., … Haase, A. T. (1997). Kaposi's sarcoma-associated herpesvirus gene expression in endothelial (spindle) tumor cells. *Journal of Virology*, *71*(1), 715–719. Retrieved from http://www.ncbi.nlm.nih.gov/pubmed/8985403

Stoecklin, G., & Kedersha, N. (2013). Relationship of GW/P-bodies with stress granules. *Advances in Experimental Medicine and Biology*, *768*, 197–211. https://doi.org/10.1007/978-1-4614-5107-5_12

Stürzl, M., Gaus, D., Dirks, W. G., Ganem, D., & Jochmann, R. (2013). Kaposi's sarcoma-derived cell line SLK is not of endothelial origin, but is a contaminant from a known renal carcinoma cell line. *International Journal of Cancer*, *132*(8), 1954–1958. https://doi.org/10.1002/ijc.27849

Sul, O.-J., Park, H.-J., Son, H.-J., & Choi, H.-S. (2017). Lipopolysaccharide (LPS)-Induced Autophagy Is Responsible for Enhanced Osteoclastogenesis. *Molecules and Cells*, *40*(11), 880–887. https://doi.org/10.14348/molcells.2017.0230

Sun, N., Dombi, E., Bohr, V. A., Nilsen, H., Tavernarakis, N., Poulton, J., … Spangler, R. D. (2017). Detection of Mitophagy in Human Cells, C.Elegans, and Mice. *Journal of Visualized Experiments*, *1*(129), 1–9. https://doi.org/10.3791/56301

Sun, N., Yun, J., Liu, J., Malide, D., Liu, C., Rovira, I. I., … Finkel, T. (2015). Measuring In Vivo Mitophagy. *Molecular Cell*, *60*(4), 685–696. https://doi.org/10.1016/j.molcel.2015.10.009

Sun, R., Lin, S.-F., Gradoville, L., Yuan, Y., Zhu, F., & Miller, G. (1998). A viral gene that activates lytic cycle expression of Kaposi's sarcoma-associated herpesvirus. *Proceedings of the National Academy of Sciences*, *95*(18), 10866–10871. https://doi.org/10.1073/pnas.95.18.10866

Suthaus, J., Adam, N., Grötzinger, J., Scheller, J., & Rose-John, S. (2011). Viral Interleukin-6: Structure, pathophysiology and strategies of neutralization. *European Journal of Cell Biology*, *90*(6–7), 495–504. https://doi.org/10.1016/j.ejcb.2010.10.016

Tenekeci, U., Poppe, M., Beuerlein, K., Busch, J., Schmitz, M. L., & Kracht Correspondence, M. (2016). K63-Ubiquitylation and TRAF6 Pathways Regulate Mammalian P-Body Formation and mRNA Decapping. *Molecular Cell*, *62*, 943–957. https://doi.org/10.1016/j.molcel.2016.05.017

Thoreen, C. C., Kang, S. A., Won Chang, J., Liu, Q., Zhang, J., Gao, Y., … Gray, N. S. (2009). An ATP-competitive Mammalian Target of Rapamycin Inhibitor Reveals Rapamycin-resistant Functions of mTORC1. https://doi.org/10.1074/jbc.M900301200

Thurston, T. L. M., Ryzhakov, G., Bloor, S., von Muhlinen, N., & Randow, F. (2009). The TBK1 adaptor and autophagy receptor NDP52 restricts the proliferation of ubiquitin-coated bacteria. *Nature Immunology*, *10*(11), 1215–1221. https://doi.org/10.1038/ni.1800

Till, A., Lipinski, S., Ellinghaus, D., Mayr, G., Subramani, S., Rosenstiel, P., & Franke, A. (2013). Autophagy receptor CALCOCO2/NDP52 takes center stage in Crohn disease. *Autophagy*, *9*(8), 1256–1257. https://doi.org/10.4161/auto.25483

Tsubuki, S., Saito, Y., Tomioka, M., Ito, H., & Kawashima, S. (1996). Differential Inhibition of Calpain and Proteasome Activities by Peptidyl Aldehydes of Di-Leucine and Tri-Leucine. *Journal of Biochemistry*, *119*(3), 572–576. https://doi.org/10.1093/oxfordjournals.jbchem.a021280

van Dijk, E., Cougot, N., Meyer, S., Babajko, S., Wahle, E., & Séraphin, B. (2002). Human Dcp2: a catalytically active mRNA decapping enzyme located in specific cytoplasmic structures. *The EMBO Journal*, *21*(24), 6915–6924. https://doi.org/10.1093/emboj/cdf678

Van Dross, R., Yao, S., Asad, S., Westlake, G., Mays, D. J., Barquero, L., … Browning, P. J. (2005). Constitutively Active K-cyclin/cdk6 Kinase in Kaposi Sarcoma–Associated Herpesvirus–Infected Cells. *JNCI: Journal of the National Cancer Institute*, *97*(9), 656–666. https://doi.org/10.1093/jnci/dji113

Verlhac, P., Gré, I. P., Viret, C., & Faure, M. (2015). Autophagy Receptor NDP52 Regulates Pathogen-Containing Autophagosome Maturation. *Cell Host & Microbe*, *17*, 515–525. https://doi.org/10.1016/j.chom.2015.02.008

Verlhac, P., Gregoire, I. P., Azocar, O., Petkova, D. S., Baguet, J., Viret, C., & Faure, M. (2015). Autophagy receptor NDP52 regulates pathogen-containing autophagosome maturation. *Cell Host and Microbe*, *17*(4), 515–525. https://doi.org/10.1016/j.chom.2015.02.008

Vieira, J., & O'Hearn, P. M. (2004). Use of the red fluorescent protein as a marker of Kaposi's sarcoma-associated herpesvirus lytic gene expression. *Virology*, *325*(2), 225–240. https://doi.org/10.1016/j.virol.2004.03.049

Villa, E., Proïcs, E., Rubio-Patiño, C., Obba, S., Zunino, B., Bossowski, J. P., … Ricci, J. E. (2017). Parkin-Independent Mitophagy Controls Chemotherapeutic Response in Cancer Cells. *Cell Reports*, *20*(12), 2846–2859. https://doi.org/10.1016/j.celrep.2017.08.087

Violot, S., Carpentier, P., Blanchoin, L., & Bourgeois, D. (2009). Reverse pH-Dependence of Chromophore Protonation Explains the Large Stokes Shift of the Red Fluorescent Protein mKeima. *Journal of the American Chemical Society*, *131*(30), 10356–10357. https://doi.org/10.1021/ja903695n

von Muhlinen, N., Akutsu, M., Ravenhill, B. J., Foeglein, Á., Bloor, S., Rutherford, T. J., … Randow, F. (2012). LC3C, Bound Selectively by a Noncanonical LIR Motif in NDP52, Is Required for Antibacterial Autophagy. *Molecular Cell*, *48*(3), 329–342. https://doi.org/10.1016/j.molcel.2012.08.024

von Muhlinen, N., Akutsu, M., Ravenhill, B. J., Foeglein, Á., Bloor, S., Rutherford, T. J., … Randow, F. (2012). LC3C, bound selectively by a noncanonical LIR motif in NDP52, is required for antibacterial autophagy. *Molecular Cell*, *48*(3), 329–342. https://doi.org/10.1016/j.molcel.2012.08.024

Wang, H.-W., Trotter, M. W. B., Lagos, D., Bourboulia, D., Henderson, S., Mäkinen, T., … Boshoff, C. (2004). Kaposi sarcoma herpesvirus–induced cellular reprogramming contributes to the lymphatic endothelial gene expression in Kaposi sarcoma. *Nature Genetics*, *36*(7), 687–693. https://doi.org/10.1038/ng1384

Wei, Y., An, Z., Zou, Z., Sumpter, R., Su, M., Zang, X., … Levine, B. (2015). The stress-responsive kinases MAPKAPK2/MAPKAPK3 activate starvation-induced autophagy through Beclin 1 phosphorylation. *ELife*, *4*. https://doi.org/10.7554/eLife.05289

Wen, K. W., & Damania, B. (2010). Kaposi sarcoma-associated herpesvirus (KSHV): molecular biology and oncogenesis. *Cancer Letters*, *289*(2), 140–150. https://doi.org/10.1016/j.canlet.2009.07.004

Wilczynska, A., Aigueperse, C., Kress, M., Dautry, F., & Weil, D. (2005). The translational regulator CPEB1 provides a link between dcp1 bodies and stress granules. *Journal of Cell Science*, *118*(5), 981–992. https://doi.org/10.1242/jcs.01692

Wild, P., Farhan, H., McEwan, D. G., Wagner, S., Rogov, V. V, Brady, N. R., … Dikic, I. (2011). Phosphorylation of the autophagy receptor optineurin restricts Salmonella growth. *Science (New York, N.Y.)*, *333*(6039), 228–233. https://doi.org/10.1126/science.1205405

Wurzer, B., Zaffagnini, G., Fracchiolla, D., Turco, E., Abert, C., Romanov, J., & Martens, S. (2015). Oligomerization of p62 allows for selection of ubiquitinated cargo and isolation membrane during selective autophagy. *ELife*, *4*, e08941. https://doi.org/10.7554/eLife.08941

Xie, X., Li, F., Wang, Y., Wang, Y., Lin, Z., Cheng, X., … Pan, L. (2015a). Molecular basis of ubiquitin recognition by the autophagy receptor CALCOCO2. *Autophagy*, *11*(10), 1775–1789. https://doi.org/10.1080/15548627.2015.1082025

Yamamoto, A., Tagawa, Y., Yoshimori, T., Moriyama, Y., Masaki, R., & Tashiro, Y. (1998). Bafilomycin A1 prevents maturation of autophagic vacuoles by inhibiting fusion between autophagosomes and lysosomes in rat hepatoma cell line, H-4-II-E cells. *Cell Structure and Function*, *23*(1), 33–42. Retrieved from http://www.ncbi.nlm.nih.gov/pubmed/9639028

Yang, S., Imamura, Y., Jenkins, R. W., Cañadas, I., Kitajima, S., Aref, A., … Barbie, D. A. (2016). Autophagy Inhibition Dysregulates TBK1 Signaling and Promotes Pancreatic Inflammation. *Cancer Immunology Research*, *4*(6), 520–530. https://doi.org/10.1158/2326-6066.CIR-15-0235

Yang, T.-Y., Chen, S.-C., Leach, M. W., Manfra, D., Homey, B., Wiekowski, M., … Lira, S. A. (2000). Transgenic Expression of the Chemokine Receptor Encoded by Human Herpesvirus 8 Induces an Angioproliferative Disease Resembling Kaposi's Sarcoma. *Journal of Experimental Medicine*, *191*(3), 445–454. https://doi.org/10.1084/jem.191.3.445

Yang, Z., Jakymiw, A., Wood, M. R., Eystathioy, T., Rubin, R. L., Fritzler, M. J., & Chan, E. K. L. (2004). GW182 is critical for the stability of GW bodies expressed during the cell cycle and cell proliferation. *Journal of Cell Science*, *117*(23), 5567–5578. https://doi.org/10.1242/jcs.01477

Yoo, J., Kang, J., Lee, H. N., Aguilar, B., Kafka, D., Lee, S., … Hong, Y.-K. K. (2010). Kaposin-B enhances the PROX1 mRNA stability during lymphatic reprogramming of vascular endothelial cells by Kaposi's sarcoma herpes virus. *PLoS Pathogens*, *6*(8), 37–38. https://doi.org/10.1371/journal.ppat.1001046

Yoon, J.-H., Choi, E.-J., & Parker, R. (2010). Dcp2 phosphorylation by Ste20 modulates stress granule assembly and mRNA decay in Saccharomyces cerevisiae. *The Journal of Cell Biology*, *189*(5), 813–827. https://doi.org/10.1083/jcb.200912019

Yoshii, S. R., & Mizushima, N. (2017). Monitoring and measuring autophagy. *International Journal of Molecular Sciences*, *18*(9), 1–13. https://doi.org/10.3390/ijms18091865

Zaffagnini, G., & Martens, S. (2016). Mechanisms of Selective Autophagy. *Journal of Molecular Biology*, *428*(9), 1714–1724. https://doi.org/10.1016/j.jmb.2016.02.004

Zhao, Y., Tian, E., & Zhang, H. (2009). Selective autophagic degradation of maternally-loaded germline P granule components in somatic cells during *C. elegans* embryogenesis. *Autophagy*, *5*(5), 717–719. https://doi.org/10.4161/auto.5.5.8552